



**UCGE Reports
Number 20291**

Department of Geomatics Engineering

**Precise Point Positioning Using Dual-Frequency
GPS and GLONASS Measurements**

(URL: <http://www.geomatics.ucalgary.ca/research/publications>)

by

Changsheng Cai

August 2009



UNIVERSITY OF CALGARY

Precise Point Positioning Using Dual-Frequency GPS and GLONASS Measurements

by

Changsheng Cai

A THESIS

SUBMITTED TO THE FACULTY OF GRADUATE STUDIES
IN PARTIAL FULFILMENT OF THE REQUIREMENTS FOR THE
DEGREE OF MASTER SCIENCE

DEPARTMENT OF GEOMATICS ENGINEERING

CALGARY, ALBERTA

AUGUST, 2009

© Changsheng Cai 2009

Abstract

This thesis presents a comprehensive study on Precise Point Positioning (PPP) using combined GPS/GLONASS dual frequency code and carrier phase observations. The existing PPP technique is implemented using only GPS measurements, which will be restricted from use in some situations such as in urban canyons and open-pit mine areas due to insufficient satellite number. In addition, the positioning accuracy and convergence time of PPP need to be further improved. A good strategy is to integrate GPS and GLONASS.

In this research, a combined GPS/GLONASS traditional PPP model and a combined GPS/GLONASS UofC PPP model are developed, including their functional and stochastic models. The combined GPS and GLONASS PPP models have been implemented in a new version of the P³ software package. The performance of the combined GPS and GLONASS PPP is assessed using static data from IGS tracking network and kinematic data from an experiment. Numerical results indicate that the positioning accuracy and convergence time have a significant improvement after adding GLONASS observations. A further improvement can be expected when a full GLONASS constellation is completed in the near future. The stability of the GPS-GLONASS system time difference is investigated in the thesis. Recommendations for future work are also addressed.

Acknowledgements

First of all, I would like to express my great gratitude to my supervisor, Dr. Yang Gao, for his academic guidance, financial support and encouragement during the period of my graduate study.

I would like to express my thanks to my friends for their all kinds of help: Wenyao Tao, Min Wang, Feng Xu, Junbo Shi, Wei Cao, Gang Chen, Fang Wang, Zhizhao Liu, Kongzhe Chen, Maya Nand Jha, Feng Tang, Shuang Du, Ala'a Kassab, Hamid Assilzadeh, Debo Sun, and Hang Liu. Special thanks are sent to Dr. Yufeng Zhang for his unselfish knowledge sharing, fruitful discussion and beneficial suggestion.

I would like to express my sincere gratitude to my friends Allan Sorensen and Doris Sorensen for their generous help during my graduate study.

I would like to thank Dr. Naser El-Sheimy, Dr. Susan Skone from the Department of Geomatics Engineering, and Dr. Frank Cheng from the Department of Mechanical and Manufacturing Engineering for serving on my examine committee.

I would like to extend my thanks to all faculty and staff members in the Department of Geomatics Engineering for their support.

Many thanks are also sent to Geoide for travel funds, the Department of Geomatics Engineering for the Special Award, the University of Calgary for the Graduate Research Scholarship (GRS), and the Institute of Navigation (ION) for the student paper sponsorship.

Finally, thanks would be given to my family for their unconditional love and support all the years.

Table of Contents

Abstract	ii
Acknowledgements	iii
Table of Contents	iv
List of Tables	vi
List of Figures and Illustrations	vii
List of Symbols	x
List of Abbreviations	xii
CHAPTER ONE: INTRODUCTION	1
1.1 Background	1
1.2 Research Objective	4
1.3 Thesis Outline	5
CHAPTER TWO: GPS AND GLONASS SYSTEMS	7
2.1 GPS System	7
2.2 GLONASS System	9
2.3 GPS and GLONASS Modernizations	11
2.3.1 Modernization of GPS	11
2.3.2 Modernization of GLONASS	14
2.4 Comparisons between GPS and GLONASS	15
2.4.1 Differences between GPS and GLONASS	15
2.4.2 Time System	17
2.4.2.1 GLONASS Time	17
2.4.2.2 GPS Time	18
2.4.2.3 Time Transformation	18
2.4.3 Coordinate System	19
2.4.3.1 GLONASS Coordinate System	19
2.4.3.2 GPS Coordinate System	21
2.4.3.3 Transformation between PZ-90 and WGS-84	21
CHAPTER THREE: ERROR SOURCES AND HANDLING STRATEGIES IN PPP ...	23
3.1 Introduction	23
3.2 Conventional Error Sources	24
3.2.1 Satellite Orbit and Clock Errors	24
3.2.1.1 IGS Organization	25
3.2.1.2 GPS Precise Products	27
3.2.1.3 GLONASS Precise Products	28
3.2.2 Ionospheric Delay	31
3.2.3 Tropospheric Delay	34
3.2.4 Receiver Clock Offset	37
3.2.5 Multipath and Measurement noise	37
3.3 Special Error Sources	39
3.3.1 Satellite and Receiver Antenna Phase Center Offsets	39
3.3.2 Phase Wind Up	41
3.3.3 Relativistic Effect	43

3.3.4 Earth Tide	44
3.3.5 Ocean Tide Loading	45
3.3.6 Atmosphere Loading	46
3.3.7 Sagnac Effect.....	47
CHAPTER FOUR: COMBINED GPS AND GLONASS PPP MODELS.....	49
4.1 Introduction.....	49
4.2 Kalman Filter Estimation.....	50
4.3 GPS PPP Observation Model	52
4.3.1 Traditional Model.....	53
4.3.2 UofC Model.....	55
4.4 Combined GPS and GLONASS PPP Models.....	57
4.4.1 Combined GPS/GLONASS Traditional Model	57
4.4.2 Combined GPS/GLONASS UofC Model	63
4.5 Stochastic Modeling	66
4.5.1 Stochastic Model of Measurements.....	66
4.5.1.1 Traditional Model	66
4.5.1.2 UofC Model	68
4.5.2 Stochastic Model of Parameters	70
CHAPTER FIVE: RESULTS AND ANALYSIS.....	73
5.1 Software Development	73
5.2 Data Description	77
5.3 Parameter Estimation Results and Analysis	78
5.4 Performance Comparison between GPS-only and GPS/GLONASS PPP	92
5.5 Kinematic Positioning Results and Analysis	100
5.5.1 Data Description.....	100
5.5.2 Positioning Results and Discussion.....	103
CHAPTER SIX: STABILITY ANALYSIS OF GPS-GLONASS SYSTEM TIME DIFFERENCE	110
6.1 Introduction.....	110
6.2 Estimation of System Time Difference	110
6.3 Stability of GPS-GLONASS System Time Difference	112
CHAPTER SEVEN: CONCLUSIONS AND RECOMMENDATIONS.....	119
7.1 Conclusions.....	119
7.2 Recommendations for Future Work	123
APPENDIX A PROCESSING RESULTS OF PPP AT IGS STATIONS	125
APPENDIX B TROPOSPHERIC MAPPING FUNCTIONS	128
REFERENCES	132

List of Tables

Table 2-1 Comparisons between GPS and GLONASS	16
Table 2-2 Geodetic Constants and Parameters of PZ-90 Ellipsoid	20
Table 3-1 Accuracy of Coordinates and Velocity of GLONASS Satellites	25
Table 3-2 GPS Precise Satellite Orbit and Clock Products	27
Table 3-3 GLONASS Precise Satellite Orbit and Clock Products	30
Table 3-4 GPS Satellite Antenna Phase Center Offsets in the Satellite Fixed Reference Frame (m)	40
Table 3-5 GLONASS Satellite Antenna Phase Center Offsets in the Satellite Fixed Reference Frame as of Feb.15, 2009 (m).....	41
Table 5-1 GPS/GLONASS Stations	77
Table 5-2 Statistics of Position Results (m).....	80
Table 5-3 RMS Statistics of Observation Residuals in Each Elevation Bin (m).....	88
Table 5-4 Average RMS of 36 Samples (m)	98
Table 5-5 Average Convergence Time of 36 Samples (Epochs).....	100
Table 5-6 RMS Statistics of Kinematic PPP Positioning Errors (m).....	106
Table 5-7 RMS Statistics of Positioning Errors with Different Clock Products (m).....	109
Table 6-1 GPS/GLONASS Stations	113
Table 6-2 Statistics of Estimated System Time Difference (ns).....	118
Table B-1 Tropospheric Mapping Functions	128

List of Figures and Illustrations

Figure 2-1 GPS Constellation with Six Orbital Planes	8
Figure 2-2 GLONASS Constellation with Three Orbital Planes.....	10
Figure 2-3 Modernized GPS Signal Spectra.....	13
Figure 2-4 Projected Number of Available GLONASS Signals	15
Figure 3-1 Organization of the International GNSS Service (IGS).....	26
Figure 3-2 GPS/GLONASS Stations in the IGS Tracking Network	26
Figure 3-3 Satellite Antenna Phase Center Offset	39
Figure 4-1 Kalman Filter Operation Illustration.....	52
Figure 5-1 Main Screen of P ³ Software Package.....	74
Figure 5-2 Processing Result Graphs.....	75
Figure 5-3 Basic Procedure of Combined GPS/GLONASS PPP Processing.....	76
Figure 5-4 GPS/GLONASS Stations in the IGS Tracking Network	77
Figure 5-5 GPS Only vs. GPS/GLONASS Positioning Errors.....	79
Figure 5-6 Satellite Number Used and DOP.....	81
Figure 5-7 Observation Residuals at a Certain Epoch	82
Figure 5-8 Satellite Sky Plot at a Certain Epoch	83
Figure 5-9 Code Observation Residuals in GPS/GLONASS Processing.....	84
Figure 5-10 Phase Observation Residuals in GPS/GLONASS Processing	85
Figure 5-11 Elevation Dependence of Code Observation Residuals.....	86
Figure 5-12 Elevation Dependence of Phase Observation Residuals.....	87
Figure 5-13 Satellite Elevation Angles in GPS/GLONASS Processing.....	88
Figure 5-14 Ambiguity Estimates in GPS/GLONASS Processing	89
Figure 5-15 Receiver Clock Offset Estimates	90
Figure 5-16 Zenith Wet Tropospheric Delay Estimates	90

Figure 5-17 Estimated GPS-GLONASS System Time Difference	91
Figure 5-18 Processing Results at CONZ.....	93
Figure 5-19 Processing Results at RCMN	94
Figure 5-20 Processing Results at UNBJ.....	95
Figure 5-21 RMS Statistics of East Position Errors of 36 Samples.....	97
Figure 5-22 RMS Statistics of North Position Errors of 36 Samples	98
Figure 5-23 RMS Statistics of Height Errors of 36 Samples.....	98
Figure 5-24 Convergence Time in East Component of 36 Samples.....	99
Figure 5-25 Convergence Time in North Component of 36 Samples	99
Figure 5-26 Convergence Time in Height Component of 36 Samples.....	100
Figure 5-27 Equipments in the Kinematic GPS/GLONASS Experiment	101
Figure 5-28 Trajectory Plotted with P ³ Software Package	102
Figure 5-29 Trajectory Produced by GrafNav TM Software Package	102
Figure 5-30 PPP Positioning Errors with Respect to Differential Solutions	104
Figure 5-31 Satellite Number Used and PDOP in the Kinematic Test.....	104
Figure 5-32 Kinematic PPP Positioning Errors	106
Figure 5-33 GPS Positioning Errors with Different Orbit and Clock Products.....	108
Figure 5-34 GPS Positioning Errors with Different Sampling Clock Products.....	109
Figure 6-1 Estimated System Time Difference for 30 IGS Stations	115
Figure 6-2 Estimated System Time Difference of LEICA GRX1200GGPRO Receivers.....	115
Figure 6-3 Estimated System Time Difference of TPS E_GGD Receivers	116
Figure 6-4 Estimated System Time Difference of JPS LEGACY Receivers	116
Figure 6-5 Estimated System Time Difference of JPS E_GGD Receivers	117
Figure A-1 Processing Results at ANKR.....	125
Figure A-2 Processing Results at LHAZ	126

Figure A-3 Processing Results at NTUS 127

List of Symbols

Symbol	Definition
Δd_{dry}	Zenith dry tropospheric delay component
Δd_{wet}	Zenith wet tropospheric delay component
M_{dry}	Dry tropospheric delay mapping function
M_{wet}	Wet tropospheric delay mapping function
x_k	State vector at epoch k
z_k	Measurement vector at epoch k
H_k	Design matrix at epoch k
w_k	Process noise
v_k	Measurement noise
P_i	Measured pseudorange on Li (m)
Φ_i	Measured carrier phase on Li (m)
ρ	True geometric range (m)
c	Speed of light (m/s)
dt	Receiver clock error (s)
dT	Satellite clock error (s)
d_{orb}	Satellite orbit error (m)
d_{trop}	Tropospheric delay (m)
d_{ion/L_i}	Ionospheric delay on Li (m)

λ_i	Wavelength on Li (m/cycle)
N_i	Integer phase ambiguity on Li (cycle)
d_{mult/P_i}	Multipath effect in the measured pseudorange on Li (m)
d_{mult/Φ_i}	Multipath effect in the measured carrier phase on Li (m)
\mathcal{E}	Measurement noise (m)
$\sigma_{P_i}^2$	Variance of P code observation on Li
$\sigma_{\Phi_i}^2$	Variance of carrier phase observation on Li
q	Spectral density
Q	Process noise matrix
q_ϕ	Spectral density of positions in latitude direction
q_λ	Spectral density of positions in longitude direction
q_h	Spectral density of positions in height direction
R_m	Earth radius in meridian direction
R_n	Earth radius in prime meridian direction
h	Station height above ellipsoid
Δt	Time increment
ϕ	Latitude of station

List of Abbreviations

Abbreviation	Definition
AIUB	Astronomical Institute at the University of Berne
AS	Anti-Spoofing
BKG	Bundesamt für Kartographie und Geodäsie
CS	Central Synchronizer
C/A	Coarse /Acquisition
CDMA	Code Division Multiple Access
DOP	Dilution of Precision
ECEF	Earth Centered Earth Fixed
ELS	Early/Late Slope
ESA	European Space Agency
ESOC	European Space Operations Center
FDMA	Frequency Division Multiple Access
FOC	Full Operational Capability
GIM	Global Ionospheric Model
GLONASS	Russian Global Navigation Satellite System
GNSS	Global Navigation Satellite System
GPS	Global Positioning System
IAC	Information Analytical Center
ICD	Interface Control Document
IERS	International Earth Rotation Service
ITRF	International Terrestrial Reference Frame

IGS	International GNSS Service
IRM	IERS Reference Meridian
IGEX	International GLONASS Experiment
IGLOS	International GLONASS Service Pilot Project
JPL	Jet Propulsion Laboratory
MCS	Master Control Station
MCC	Russian Mission Control Center
NRCan	Natural Resources Canada
PCV	Phase Center Variation
PPP	Precise point positioning
PPS	Precise Positioning Service
PRN	Pseudo Random Noise
RINEX	Receiver Independent Exchange Format
RMS	Root Mean Square
SA	Selective Availability
SNR	Signal to Noise Ratio
SPS	Standard Positioning Service
STD	Standard Deviation
TEC	Total Electron Content
UTC	Coordinated Universal Time
WGS72	World Geodetic System 1972
WGS84	World Geodetic System 1984
ZWD	Zenith Wet Delay

Chapter One: Introduction

1.1 Background

Precise point positioning (PPP) with decimetre to centimetre level accuracies has become possible since the advent of precise satellite ephemerides and clock corrections from IGS (International GNSS Service) and several other organizations. PPP is a stand-alone precise geodetic point positioning approach that uses un-differenced dual-frequency pseudorange and carrier phase observations along with precise GPS satellite orbit and clock products. PPP has been receiving increased interests within GPS positioning and navigation community since its advent for a number of reasons: simple field operation, cost-effective, high-accuracy positioning results and no base stations required. Based on the processing of dual-frequency measurements from a single GPS receiver, position solutions with centimetre or decimetre level accuracies can be attained in static and kinematic modes on a global scale. Such an accuracy level currently can only be achieved through a differential positioning method by processing observations collected simultaneously from at least two receivers.

Over the past ten years, a number of researchers and engineers have developed the PPP technique and its applications. The PPP method for a static application was first introduced by Zumberge et al. (1997). A traditional PPP observation model that uses ionosphere-free linear combinations between code observations as well as between carrier phase observations was presented (Zumberge et.al, 1997). Kouba and Héroux introduced the PPP technique using the traditional observation model in detail. A centimetre-level positioning accuracy was achieved in a static mode using un-differenced

code and carrier phase observations from dual-frequency receivers (Kouba and Héroux, 2001). A UofC PPP observation model was proposed by Gao and Shen (2001, 2002), which uses ionosphere-free code and carrier phase observation combinations instead of code and code observation combinations. Several researchers have expanded PPP applications from static modes to kinematic modes as well as from post-mission to real-time processing. Among them, Gao et al. (2003,2004) presented kinematic positioning results at a sub-decimetre level and static positioning results at a centimetre level using a real-time PPP method with precise satellite orbit and clock products from the Internet. Such an accuracy level was also achieved by Chen (2004) using real-time orbit and clock products. In addition, single-frequency PPP approaches have been developed at decimetre-level accuracy (Chen and Gao, 2005; Gao et al., 2006; Le and Tiberius, 2007; Chen and Gao, 2008).

In recent years, PPP has become a valuable tool for some geodetic applications. Several software packages capable of PPP processing have been developed, including the GIPSY-OASIS (GOA II) software package developed at the Jet Propulsion Laboratory (JPL), the Bernese GPS software package (BSW) developed at the Astronomical Institute at the University of Berne (AIUB), and the P³ software package developed at the University of Calgary. The development of these software packages further promotes the applications of the PPP technology.

Although the PPP approach has indicated considerable advantages for a variety of applications in terms of its operational flexibility and cost-effectiveness, it requires a long initialization time before a position solution reaches its optimal precision. Normally it will take about 20 to 30 minutes for the position solution to converge to a decimetre level.

The convergence time is quite dependent on many factors such as the number and geometry of visible satellites, user environment and dynamics, observation quality and sampling rate (Bisnath and Gao, 2008). In addition, currently PPP is only capable of providing centimetre-level accuracy in a static mode and decimetre-level accuracy in a kinematic mode. The further improvement of the positioning accuracy is still needed in some applications. Since more visible satellites and observations are available, a combined use of GPS and GLONASS in the PPP is expected to improve the positioning accuracy, reliability and convergence time. The benefits of the integration of the GPS and GLONASS have been obvious especially for applications such as urban canyons and open-pit mining operations (Tsujii et al., 2000).

Since the International GLONASS Experiment (IGEX-98) and the follow-on GLONASS Service Pilot Project (IGLOS) were carried out, GLONASS precise orbit and clock data has been becoming available. This provides a basis for developing a combined GPS and GLONASS PPP system. The other issues involved in the combined GPS and GLONASS PPP include the incomplete GLONASS satellite constellation and the interoperability. Fortunately, the Russian government has approved a long-term plan to reconstitute a GLONASS constellation of 24 satellites. The Russian GNSS system will be restored by the end of 2009 according to a presentation by the head of the Information Analysis Center (Inside GNSS, 2008a). Besides, Russia is moving to add Code Division Multiple Access (CDMA) signals to the Frequency Division Multiple Access (FDMA) format in order to facilitate the combined use of GPS and GLONASS. The CDMA signals will be implemented on the next-generation GLONASS-K satellites with the first launch in late 2010 (Inside GNSS, 2008b).

In this thesis, the combined GPS and GLONASS PPP models are developed. The performance of the combined GPS and GLONASS PPP is assessed in both static and kinematic modes in terms of the positioning accuracy and convergence time through a comparison with GPS-only PPP. A new version of the P³ software package is developed to enable the processing of the combined GPS/GLONASS observations.

1.2 Research Objective

The main objective of the thesis is to develop models and algorithms for the combined GPS and GLONASS PPP using dual-frequency un-differenced code and carrier phase observations and to assess the performance of the combined GPS and GLONASS PPP. To achieve this objective, the following tasks are accomplished:

1. Conduct the comparisons between the GPS and GLONASS systems.
2. Investigate the error sources and their mitigation strategies in PPP for both GPS and GLONASS systems.
3. Develop the functional models and the corresponding stochastic models of the combined GPS and GLONASS PPP. Assess the performance of the combined GPS and GLONASS PPP in terms of the positioning accuracy and convergence time.
4. Analyze the stability of GPS-GLONASS system time difference.
5. Implement the combined GPS and GLONASS PPP algorithm in a new version of P³ software package.

1.3 Thesis Outline

This thesis is organized as follows:

Chapter 1 describes a background of the PPP, including the concept, development and current status. The research objectives are given in this chapter.

Chapter 2 introduces GPS and GLONASS systems. The modernizations of GPS and GLONASS as well as their recent progress are described. A comprehensive comparison between GPS and GLONASS systems is given in this chapter.

Chapter 3 describes the error sources involved in the combined GPS and GLONASS PPP. The errors are categorized into conventional errors and special errors to PPP. Their mitigating strategies are also discussed.

Chapter 4 introduces the Kalman filter estimation method. Observation models of the GPS PPP, including the traditional model and the UofC model, are described. The combined GPS and GLONASS PPP models with functional and stochastic models are presented in this chapter.

Chapter 5 introduces the development of a new version of P³ software package. The static and kinematic processing results of the combined GPS and GLONASS PPP and their analysis are provided. The performance of the combined GPS and GLONASS PPP is assessed in terms of the converged positioning accuracy and convergence time in this chapter.

Chapter 6 investigates the stability of the GPS-GLONASS system time difference. This system time difference is estimated using data collected from various types of receivers and the estimation results are provided and analyzed in this chapter.

Chapter 7 summarizes the conclusions obtained from this research and recommendations for future work.

Chapter Two: GPS and GLONASS Systems

This chapter starts with a brief introduction to GPS and GLONASS systems. Then the modernization plan and current status for both GPS and GLONASS are described. Finally, a comprehensive comparison between GPS and GLONASS systems is made with an emphasis on their time references and coordinate systems. This comparison contributes to building the combined GPS and GLONASS PPP models to be presented in a later chapter.

2.1 GPS System

Global Positioning System (GPS) is a global satellite-based navigation and positioning system, which is developed by the United States Department of Defense. GPS consists of three main segments: Space, Control and User. The Space Segment nominally consists of 24 satellites orbiting at an altitude of approximately 20,200 km above the Earth's surface. These satellites transmit microwave signals to allow GPS users to determine their location, velocity and time in real time or post mission. The GPS satellites are distributed in six orbital planes with nominally four satellites in each plane (see Figure 2-1). The six orbital planes have approximately 55 degrees inclination with respect to the equatorial plane. For such a constellation design, four to ten GPS satellites are visible anywhere in the world. With more satellites in orbit, the visibility of the satellites will be improved. The current GPS constellation consists of 31 Block II/IIA/IIR/IIR-M satellites.

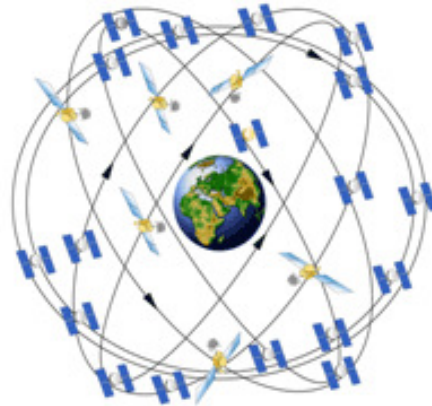


**Figure 2-1 GPS Constellation with Six Orbital Planes
(Space-based PNT, 2009)**

GPS satellites are initially designed to transmit carrier signals on two L-band frequencies: L1=1575.42 MHz and L2=1227.60 MHz. Three categories of pseudo-random noise (PRN) ranging codes are designed, including the Coarse / Acquisition (C/A) code with a 1.023 MHz chip rate and a period of one millisecond, the precision (P) code with a 10.23 MHz chip rate and a period of seven days, and the Y-code used as a substitute for P-code when the anti-spoofing (A-S) mode is activated. The C/A code and P code on both L1 and L2 are available for Block IIR-M satellites, while the coarse acquisition code on L2 is not available for Block II/IIA/IIR satellites. The C/A code unrestricted to civil users is commonly used in the Standard Positioning Service (SPS) that provides a positioning accuracy of 13 m (95 percent) in the horizontal components and 22 m (95 percent) in the vertical component as well as time transfer with an accuracy within 40 ns (95 percent) (USNO,2008). Unlike the C/A code, the P code is only made available to U.S. military, selected allied militaries and governments for Precise Positioning Service (PPS) with a positioning accuracy of around 10 m (95 percent). In

addition to ranging signals, each satellite transmits navigation message data containing its orbital elements, clock corrections, system time, status messages, and other parameters.

The GPS Control Segment consists of twelve Monitor Stations, four Ground Antennas, and one Master Control Station (MCS). The task of the Monitor Stations is to track all visible satellites and collect observation data. Then the MCS processes this data to determine satellites' orbits and update the navigation message. The updated navigation message is transmitted to each satellite via the Ground Antennas. The User Segment consists of GPS receivers and antennas that are capable of providing position, velocity and time information.

For a position determination, the time when the signal was transmitted from the satellite is compared with the time when the signal was received in the receiver. According to this time difference, the distance between a receiver and a satellite may be determined. Since the satellites' position coordinates can be acquired using broadcast ephemerides in the navigation message, the users' position may be calculated by trilateration. Nominally three satellites can determine the users' position on the Earth's surface but actually at least four satellites are required due to an additional estimation of the receiver clock offset.

2.2 GLONASS System

The Russian Global Navigation Satellite System (GLONASS) has a constellation of 24 satellites, which continuously transmit signals on two carrier frequencies. The satellite signals can be received by users anywhere on the Earth's surface to determine their position and velocity using code pseudorange and carrier phase measurements.

The first GLONASS satellites were launched into orbit in 1982. Afterwards a GLONASS experiment was carried out to test the whole GLONASS system. The performance of the GLONASS satellites was also improved gradually. Although the preliminary plans were scheduled to 1991 for a complete operational system, the deployment of the full constellation with 24 satellites was not completed until early 1996.

The GLONASS Space Segment includes 24 satellites distributed on three orbital planes. Each satellite can be identified by its slot number. The three orbital planes are separated 120 degrees (see Figure 2-2). The satellites on the same orbit plane are separated by 45 degrees. The satellite orbits are closely circular with an inclination of about 64.8 degrees, a semi-axis of 25,440 km and a period of 11h 15m 44s.

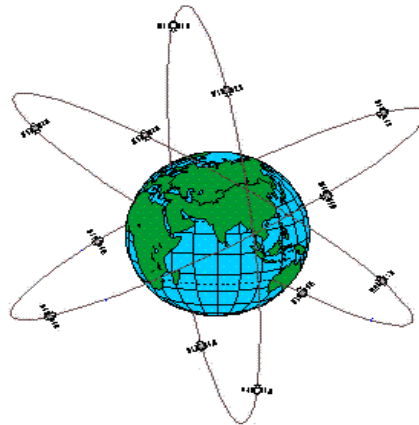


Figure 2-2 GLONASS Constellation with Three Orbital Planes
(Zheng, 2009)

The GLONASS Ground Control Segment is located in the former Soviet Union territory. Similarly to the GPS, the GLONASS has its own coordinate system and time reference. The GLONASS coordinate system is referred to as the PZ-90 and the time scale is based on UTC (SU). Differently from GPS, the GLONASS time scale is not continuous and must be adjusted for periodic leap seconds.

All satellites transmit signals on two frequency bands simultaneously for the user to correct the ionospheric delay error with dual-frequency measurements. As the GLONASS uses the FDMA (Frequency Division Multiple Access) technique, each satellite is allocated a particular frequency within each frequency band, which is determined by the frequency channel number. Thus users' receivers can identify the satellite according to these different frequencies. However, not all satellites have different frequencies. Two satellites occupying antipodal locations in the same orbit plane transmit signals in exactly the same frequency, with a few exceptions.

The GLONASS satellites modulate their navigation message to the carrier frequency. Two modulations are adopted for ranging: the Coarse Acquisition code with a chip length of 586.7 m and the Precision code with a chip length of 58.67 m. The satellites also transmit information such as their ephemerides, almanac and time correction parameters. The broadcast ephemerides are predicted in a period of twenty-four hours and uploaded from the Ground Control Center. Each satellite transmits a new set of ephemerides every thirty minutes. The almanac is updated approximately once per day (Tripod, 2007). The precise ephemerides are also called post-processed ephemerides, which are available from IGS or other organizations. The final IGS GLONASS precise orbit has an accuracy of 15 cm with a latency of two weeks.

2.3 GPS and GLONASS Modernizations

2.3.1 Modernization of GPS

GPS reached Full Operational Capability with its realization of the original design goals in 1995. In 1998 the U.S. initiated a GPS modernization plan because of some

weaknesses of the existing GPS system such as unavailable C/A code on L2 for civil users and P code susceptible to interference and jamming (Royal Observatory of Belgium, 2004). Modernizing the existing GPS system is also for the purpose of competing with the emerging Galileo satellite navigation system. The modernization program includes adding ground stations, adding a second civil signal (L2C), adding a third civil frequency (L5), adding new military signals (M-code) with increased signal power, improving the accuracy and availability of position solutions for all users, and adding a fourth civil signal (L1C).

L2C is a new civil signal broadcast on the L2 frequency band and transmitted by all Block IIR-M satellites as well as later designed satellites. The L2C signal aims to improve the positioning accuracy and act as a redundant signal. The immediate effect of two civil signals on each satellite is to allow removing the ionospheric delay error, which is usually treated as the largest error source and mitigated by applying a global ionospheric correction model in single point positioning. M-code is a new military signal designed to provide better jamming resistance than the Y code signal. Unlike the P(Y) code, M-code signal can directly be locked without the need of locking first onto the C/A code. L5 is a third civil frequency (1176.45 MHz) to be carried on the GPS Block IIF satellites, which is designed to meet the demand for life safety with improved signal structure, higher transmission power, wider bandwidth, longer spreading codes and enhanced performance (Gakstatter, 2006). L1C is a modernized civil signal at L1 frequency with increased robust navigation performance in a challenged tracking environment, which is designed to enable the greater interoperability with Galileo L1 for

civil use. It will be available with the first Block III launch. Figure 2-3 depicts the modernization process of the GPS signals.

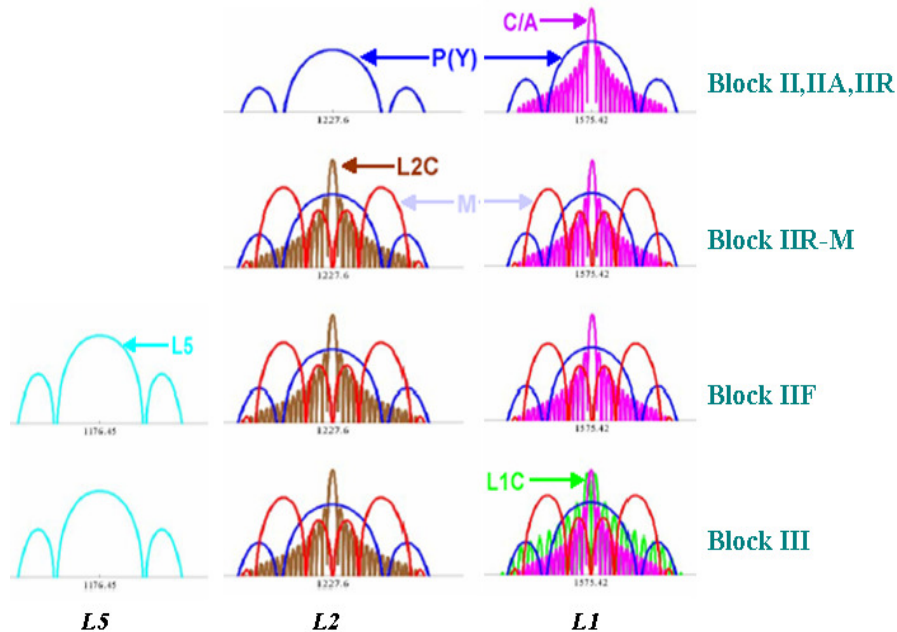


Figure 2-3 Modernized GPS Signal Spectra (Stansell, 2006)

The first step of the GPS modernization was realized by removing the Selective Availability (SA) on May 2, 2000, which improves the stand-alone positioning accuracy to about 20 m. The first modernized GPS Block IIR satellite (IIR-M) with a second civil signal (L2C) was launched on September 26, 2005. Currently in a total of 31 GPS operational satellites, six satellites belong to the modernized Block IIR-M satellites. The last two Block IIR-M satellites will be launched in August 2009. The first launch of GPS Block IIF satellites with the full L5 capability is scheduled in November 2009. More Block IIF satellites will be launched in 2010 (UNAVCO, 2009). The next-generation modernization project, GPS Block III with L1C, is scheduled to launch in 2013.

2.3.2 Modernization of GLONASS

GLONASS reached its Full Operational Capability (FOC) with 24 satellites in January 1996. Unfortunately, the GLONASS constellation dropped to seven satellites in November 2001 due to insufficient funds (Zinoviev, 2005). However, Russian government approved a Federal GLONASS Program for the period of 2002-2011 to rebuild and modernize GLONASS on August 20, 2001 (Gibbons, 2006). The Federal GLONASS Program is directly funded from the Federal Budget with annual corrections. According to this program, a full constellation of 24 satellites with FOC will become available. In addition, the GLONASS performance comparable with that of GPS will be reached by 2010. The modernization plan involves adding a second civil code to the GLONASS-M satellites, adding a third civil frequency to the next-generation GLONASS-K satellites, updating the ground control segment and improving orbit determination and time synchronization accuracy. The modernization plan also includes supporting the design and manufacture of GLONASS, GLONASS/GPS, and GLONASS/GPS/Galileo equipments for military and civil users (Gibbons, 2008).

GLONASS-M satellite is a modernized version of the GLONASS spacecraft with some new features, such as increasing the design-lifetime to seven years, adding a second civil modulation on the L2 frequency band, improving navigation performance, updating navigation radio signals and increasing stability of navigation signals (Bartenev et al., 2006). GLONASS-K satellites are the next-generation satellites with an addition of a third civil signal frequency and a service life up to 10-12 years. In addition, The Code Division Multiple Access (CDMA) signals will be implemented on GLONASS-K satellites (Gibbons, 2008). The GLONASS-K represents a radical change in GLONASS

spacecraft design, adopting a non pressured and modular spacecraft bus design (Kaplan and Hegarty, 2006).

GLONASS has been on the way to its modernization. The first GLONASS-M satellite was launched in 2003. Currently the number of total satellites in the constellation reaches 20 and most of them are GLONASS-M satellites (IAC, 2009). The first GLONASS-K satellite will be expected to launch in late 2010. The number of the available GLONASS signals can be seen in Figure 2-4.

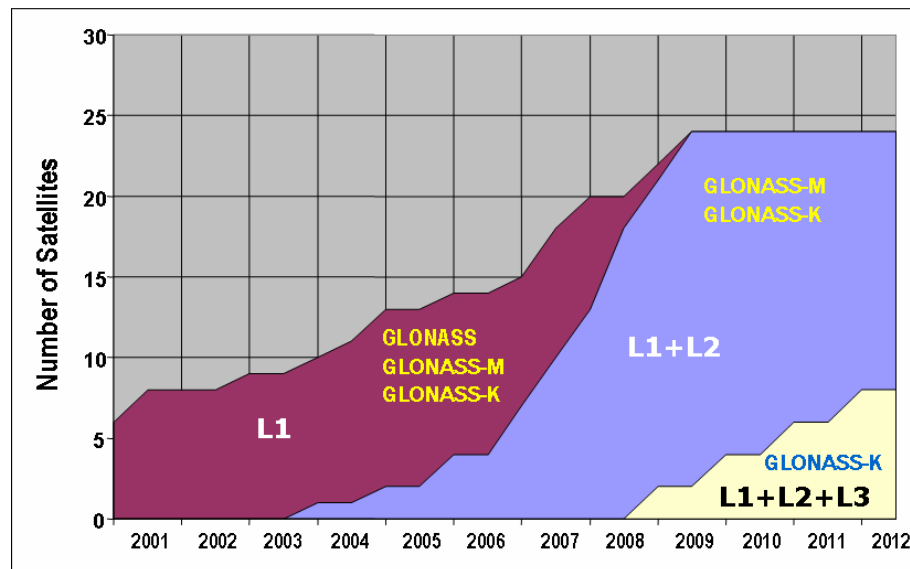


Figure 2-4 Projected Number of Available GLONASS Signals
(Averin, 2006)

2.4 Comparisons between GPS and GLONASS

2.4.1 Differences between GPS and GLONASS

Although GPS and GLONASS are very similar satellite navigation systems, there are a number of differences between both systems. Firstly, GPS and GLONASS satellites

transmit signals on both L1 and L2 frequencies. The signal frequencies are the same for all GPS satellites whereas they are different for different GLONASS satellites.

Table 2-1 Comparisons between GPS and GLONASS (Roßbach, 2000)

		GLONASS	GPS
Constellation	Number of satellites	24	24
	Number of orbital planes	3	6
	Semi-major axis	25510km	26580km
	Orbital height	19130km	20200km
	Orbital period	11h 15.8 min	11h 58 min
	Inclination	64.8°	55°
Signal Characteristics	Distinguishing satellites	FDMA	CDMA
	Carrier frequencies	1602+k*0.5625 MHz 1246+k*0.4375 MHz	1575.42 MHz 1227.60 MHz
	Code frequency(MHz)	C/A code : 0.511 P code : 5.11	C/A code:1.023 P code:10.23
	Broadcast ephemerides	Position, velocity, acceleration	Keplerian elements
Reference Standards	Reference system	PZ-90	WGS-84
	System time	GLONASS Time	GPS Time

Secondly, GPS satellite coordinates are computed in the World Geodetic System datum of WGS-84 while GLONASS has a coordinate system datum of PZ-90. Thirdly, GPS satellite time is based on a continuous GPS system time whereas GLONASS satellite time is based on a discontinuous GLONASS system time due to being periodically adjusted by leap seconds. In addition, the code rate of GLONASS C/A and P codes is half

of that of the corresponding GPS codes. GPS ephemerides parameters are Keplerian but GLONASS ephemerides parameters are given in Earth-Centered Earth-Fixed XYZ coordinates (Chamberlain, 1991). The greater orbital inclination of GLONASS will offer better satellite coverage in high latitude regions. Comparisons in detail between GPS and GLONASS are summarized in Table 2-1 in terms of orbital parameters, signal characteristics and reference standards.

2.4.2 Time System

Both GPS and GLONASS have their own independent time systems, which are connected to different realizations of UTC (Coordinated Universal Time). Therefore, the transformation from GLONASS time into GPS time can't be performed easily. Despite this, the difference between the two time scales must be taken into account in the combined GPS/GLONASS data processing.

2.4.2.1 GLONASS Time

GLONASS and GLONASS-M satellite clocks have a daily stability better than $5 \cdot 10^{-13}$ and $1 \cdot 10^{-13}$, respectively. The mutual synchronization accuracy of the satellite time scales is not worse than 20 nanoseconds (1σ) for GLONASS satellites and 8 nanoseconds (1σ) for GLONASS-M satellites. The GLONASS system time is maintained by the GLONASS Central Synchronizer (CS) time by means of a set of hydrogen clocks whose daily stability is not worse than $1 \cdot 5 \cdot 10^{-14}$. The difference between the GLONASS time and the National Reference Time UTC (SU) is less than 1 millisecond and is contained in the navigation message according to the GLONASS ICD.

The GLONASS time scale is periodically corrected an integer number of seconds simultaneously with the UTC corrections. Therefore there is no integer-second difference between the GLONASS time and the UTC (SU) due to the leap second corrections but a constant difference of three hours exists (GLONASS ICD, 2002).

2.4.2.2 GPS Time

The GPS system time maintained by the GPS Master Control Station begins from January 6, 1980. It is different from the UTC as leap seconds are introduced into the latter time scale. Besides this, a further difference between the GPS system time and the UTC in the order of nanoseconds exists due to the fact that the GPS system time and the UTC are maintained by different master clocks (Roßbach, 2000). Usually the GPS system time has a difference of less than 100 ns with the UTC (USNO) maintained by the US Naval Observatory. GPS users are informed about this difference by means of a set of UTC parameters in the GPS navigation message (Roßbach, 2000).

2.4.2.3 Time Transformation

There is a difference of leap seconds between GLONASS and GPS times. The GLONASS time could be transformed into the GPS time using the following formula (Kang et al., 2002).

$$t_{GPS} = t_{GLONASS} + \tau_c + \tau_u + \tau_g \quad (2.4.1)$$

where

$$\tau_c = t_{UTC(SU)} - t_{GLONASS}$$

$$\tau_u = t_{UTC} - t_{UTC(SU)}$$

$$\tau_g = t_{GPS} - t_{UTC}$$

UTC is obtained using data from about 230 atomic clocks in 60 world-wide laboratories (BIPM, 1995). UTC (USNO) and UTC (SU) are two local UTCs. The UTC (USNO) is kept by an ensemble of cesium standards and hydrogen masers with a difference to the UTC in the order of some nanoseconds. The UTC (SU) is kept by an ensemble of hydrogen masers as one of the most stable atomic time scales in the world (Lewandowski et al., 1996). Its difference to the UTC is in the order of some microseconds. As a result, the difference between the UTC (USNO) and the UTC (SU) is also in the order of some microseconds. As the data collected from the local timing centers can't be compared in real-time, the difference between the UTC (USNO) and the UTC (SU) and thus the difference between GPS and GLONASS time scales can't be directly obtained in real-time. This is the major issue involved when combined GPS/GLONASS data is used for some real-time applications (Roßbach, 2000).

2.4.3 Coordinate System

2.4.3.1 GLONASS Coordinate System

GLONASS broadcast ephemerides describe satellite positions in the PZ-90 Earth-Centered Earth-Fixed reference frame defined as follows (GLONASS ICD, 2002):

1. Origin is located at the center of the Earth's body.
2. Z-axis is directed to the Conventional Terrestrial Pole as recommended by the International Earth Rotation Service (IERS).

3. X-axis is directed to the point of intersection of the Earth's equatorial plane and the zero meridian established by BIH (Bureau International de l'Heure).
4. Y-axis completes a right-handed coordinate system.

Table 2-2 Geodetic Constants and Parameters of PZ-90 Ellipsoid (GLONASS ICD, 2002)

Earth rotation rate	7.292115×10^{-5} radian/s
Gravitational constant	$398\,600.44 \times 10^9$ m ³ /s ²
Gravitational constant of atmosphere(fM_a)	0.35×10^9 m ³ /s ²
Speed of light	299 792 458 m/s
Semi-major axis	6 378 136 m
Flattening	1/298.257 839 303
Equatorial acceleration of gravity	978 032.8 mgal
Correction to acceleration of gravity at sea-level due to atmosphere	-0.9 mgal
Second zonal harmonic of the geopotential(J_2^0)	1082625.7×10^{-9}
Fourth zonal harmonic of the geopotential(J_4^0)	-2370.9×10^{-9}
Normal potential at surface of common terrestrial ellipsoid (U_0)	$62\,636\,861.074$ M ² /s ²

Geodetic coordinates of a point (M) in the PZ-90 coordinate system refers to the ellipsoid whose parameters are given in Table 2-2. The geodetic latitude of the point is defined as an angle between the normal to the ellipsoid surface and the equatorial plane. The geodetic longitude of the point is defined as an angle between the initial (zero) meridian plane and the meridian plane passing through the point (M). The geodetic height of the point is defined as a distance from the ellipsoid surface to the point (M) along the normal.

2.4.3.2 GPS Coordinate System

GPS originally adopted a coordinate frame known as World Geodetic System 1972 (WGS72) and then the reference frame was changed to the World Geodetic System 1984 (WGS84). The reference frame being used by GPS is defined as follows (GPS ICD, 2000):

1. Origin is Earth's center of mass.
2. Z-axis is the direction of the IERS (International Earth Rotation Service) Reference Pole (IRP).
3. X-axis is the intersection of the IERS Reference Meridian (IRM) and the plane passing through the origin and normal to the Z-axis.
4. Y-axis completes a right-handed Earth-Centered Earth-fixed orthogonal coordinate system.

2.4.3.3 Transformation between PZ-90 and WGS-84

For a combined use of GLONASS and GPS, transformation parameters between PZ-90 and WGS-84 must be first obtained if broadcast ephemerides are used. The PZ-90 and WGS-84 have slightly different definitions as described above. But even with the same definition they still differ in the realization of the coordinate systems. Rossbach et al. (1996) obtained a set of transformation parameters using stations with known relative coordinates for both systems. Misra et al. (1996) used a set of GLONASS satellite coordinates in both PZ-90 and WGS-84 to obtain transformation parameters. Both methods received comparable results. Once a set of transformation parameters are determined, the transformation of station coordinates may be carried out using the Seven-

Parameter Helmert transformation model. Alternatively, GPS and GLONASS satellite positions may be computed in the same reference frame and then the stations' coordinates obtained will also be in that reference frame (Habrich, 1999). As the broadcast ephemerides with different reference frames are used in the combined GPS/GLONASS single point positioning, the coordinate transformation must be made. However, in the combined GPS and GLONASS PPP, the coordinate transformation is not needed due to the identical coordinate reference adopted in the precise GPS/GLONASS orbit products.

Chapter Three: Error Sources and Handling Strategies in PPP

3.1 Introduction

A key issue for precise point positioning to achieve high-accuracy positioning results is how to mitigate all potential errors involved in the space segment, signal propagation, ground environment and receiver segment. In the differential GPS positioning, the reason that millimetre-level accuracy can be achieved is because some errors can be fully or partially removed by differencing observations between two stations. However, this differential technique can't be used in PPP due to the fact that only observations from a single receiver are available. Therefore, all errors must be handled in PPP in order to achieve centimetre-level accuracy.

The potential error sources are classified into two groups in this chapter. One includes the conventional error sources that usually need to be handled in GPS positioning, such as the satellite orbit and clock errors, ionospheric delay error, tropospheric delay error, receiver clock offset, multipath, and measurement noise. The other includes the special error sources that need to be mitigated specifically to PPP, such as the satellite and receiver antenna phase center offsets, phase wind up, relativistic effect, Earth tide, ocean tide loading, atmosphere loading, and Sagnac effect. Most of these errors can be mitigated to some extent through modeling. The receiver clock offset and tropospheric delay error may be estimated as unknown parameters while the ionospheric delay error can be mitigated by constructing the ionosphere-free observation combinations.

3.2 Conventional Error Sources

3.2.1 Satellite Orbit and Clock Errors

A satellite orbit error may be defined as a discrepancy between the true satellite position and its computation value. This discrepancy is usually expressed in three orbit components: along-track, cross-track and radial. The satellite orbit error has a direct effect on single point positioning. First of all, the positioning accuracy in the height component is relatively poor mainly due to no satellites observed below the horizon. In addition, the positioning accuracy in the east (longitude) component is slightly weaker than that in the north (latitude) component due to the design of satellite orbits and the motion of satellites (Rizos, 1999). A satellite clock error may be described by the clock bias, drift and drift rate.

The satellite orbit and clock offset information are contained in the satellite ephemerides, which may be classified into broadcast ephemerides and precise ephemerides. This GPS broadcast ephemerides (also called predicted ephemerides) which consist of a set of Keplerian elements are available to GPS users at the time of observation with an accuracy of about 1.6 m for satellites' positions and 7 ns for clock corrections (IGS, 2008). The GLONASS broadcast ephemerides which are given in the form of coordinates, velocities and accelerations are also immediately available during the data collection. The accuracy of GLONASS broadcast ephemerides is given in Table 3-1. The precise ephemerides are also called post-processed ephemerides, which are not available in real-time due to a delay caused by the process of the data collection, transmission, computation and distribution to users. The GPS precise ephemerides are estimated using the data collected at globally distributed reference stations whose

coordinates are precisely predetermined. These reference stations equipped with high-performance dual-frequency GPS receivers collect observations uninterrupted. These observations are then transmitted to a data processing center where sophisticated algorithms are used to conduct the computation to generate the precise satellite orbit and clock products. Finally, these precise data products are distributed to users via Internet or geostationary communication satellites.

Table 3-1 Accuracy of Coordinates and Velocity of GLONASS Satellites (GLONASS ICD, 2002)

	Coordinates(m)		Velocity(cm/s)	
	GLONASS	GLONASS-M	GLONASS	GLONASS-M
Along track	20	7	0.05	0.03
Cross track	10	7	0.1	0.03
Radial	5	1.5	0.3	0.2

3.2.1.1 IGS Organization

International GNSS Service (IGS) is a main source of precise satellite orbit and clock products. It is an international civilian GNSS organization that provides GPS and GLONASS observation data and high-precision GPS and GLONASS orbit and clock products to support Earth science research and multidisciplinary applications. IGS consists of four global data centers, six regional data centers, seventeen operational data centers, ten analysis centers and a number of regional associate analysis centers. Figure 3-1 illustrates the IGS organization structure. The IGS has built a global GPS tracking network with more than 300 continuously operating GPS stations and nearly 100 GPS/GLONASS stations, which can be seen from Figure 3-2. Through the tracking network, the IGS collects, archives, and distributes GPS or GLONASS observation data to all kinds of users for scientific and engineering applications and studies.

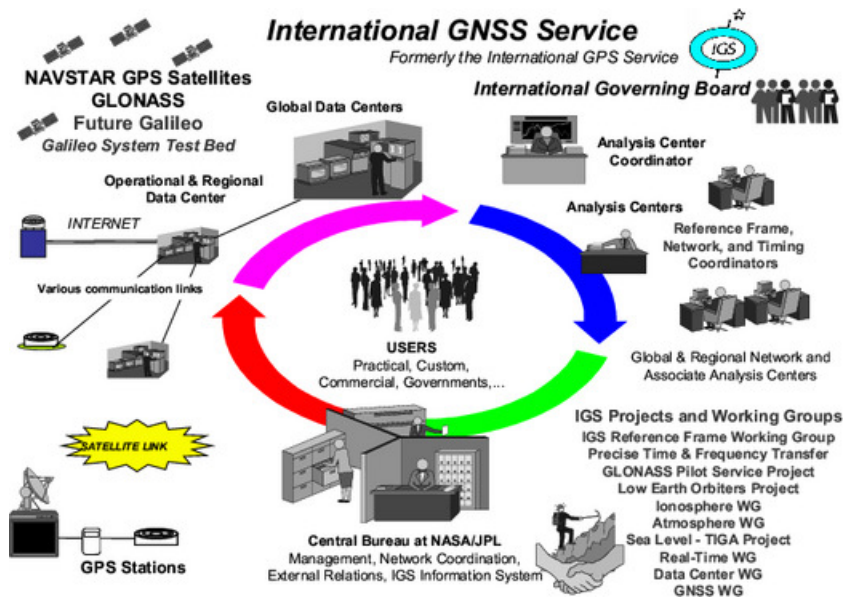
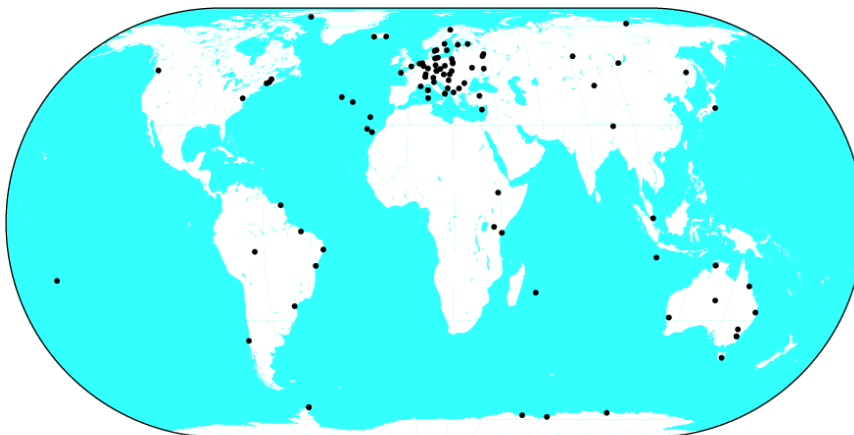


Figure 3-1 Organization of the International GNSS Service (IGS)
(IGS, 2009a)



IGS 2009 Feb 5 16:50:55

Figure 3-2 GPS/GLONASS Stations in the IGS Tracking Network
(IGS, 2009b)

3.2.1.2 GPS Precise Products

The products that IGS provides include precise satellite ephemerides, satellite and station clocks information, and geocentric coordinates of IGS tracking stations, Earth rotation parameters, and atmospheric parameters. Since 1994 the IGS has been providing precise GPS satellite orbit and clock correction products to the scientific community with increased accuracy and timeliness (Kouba and Héroux, 2001). Today, a series of IGS products with different accuracies and latencies are available to GNSS users, including ultra-rapid, rapid, and final precise products. There is a trade-off between accuracy and timeliness for these products. From the IGS ultra-rapid to IGS final products, the accuracy is increasing but the latency becomes longer.

**Table 3-2 GPS Precise Satellite Orbit and Clock Products
(IGS, 2008; Chen, 2004)**

Orbit/clock		Accuracy	Latency	Updates	Sample Interval
Broadcast	orbit	~160cm	real time	--	daily
	clock	~70ns			
Ultra-Rapid (predicted half)	orbit	~10cm	real time	four times daily	15 min
	clock	~5ns			
Ultra-Rapid (observed half)	orbit	<5cm	3 hours	four times daily	15 min
	clock	~0.2ns			
IGS Rapid	orbit	<5cm	17 hours	daily	15 min
	clock	0.1ns			5 min
IGS Final	orbit	<5cm	~13 days	weekly	15 min
	clock	<0.1ns			5 min
JPL Near Real- Time (NRT)	orbit	~22cm	2~3 min	15 min	5 min
	clock	~0.7ns			
JPL Real-Time (IGDG)	orbit	~18cm	~4 sec	1 sec	~28 sec
	clock	~1ns			1 sec
NRCan Real- Time(GPS·C)	orbit	~10cm	~5 sec	2 sec	~20 sec
	clock	~1ns			2 sec

In addition to the IGS, other organizations such as Jet Propulsion Laboratory (JPL) and Natural Resources Canada (NRCan) also provide GPS precise products to

users. JPL can provide the near real-time precise satellite orbit and clock products and the real-time Internet-based Global Differential GPS corrections (Heflin, 2000; Muellerschoen et al., 2000). NRCAN has begun to provide GPS precise products by broadcasting GPS • C corrections through satellites and Internet since 2004 (Chen, 2004; CDGPS, 2009). Table 3-2 summarizes the precise GPS satellite orbit and clock products from IGS, JPL and NRCAN.

3.2.1.3 GLONASS Precise Products

The International GLONASS Experiment (IGEX-98) is a global GLONASS observation and analysis campaign for geodetic and geodynamics applications, which was carried out between October 19, 1998 and April 19, 1999. Its main objectives are to collect GLONASS datasets using globally distributed dual-frequency GPS/GLONASS receivers and determine the precise GLONASS satellite orbits. The IGEX-98 has a global observation network consisting of 52 stations equipped with 19 dual-frequency and 13 single-frequency receivers. After the IGEX-98 campaign, an infrastructure comparable to that of the IGS was established (Habrich, 1999). The IGEX-98 generated the precise orbits of all the operational GLONASS satellites (Weber et al., 2005).

The International GLONASS Service Pilot Project (IGLOS) is a follow-on project of the IGEX-98 with the major purpose to integrate the GLONASS satellite system into the operation of IGS. The IGLOS Pilot Project has a global network consisting of about 50 tracking stations with dual-frequency GPS/GLONASS receivers. GLONASS data is collected continuously and archived in the RINEX format at the IGS Global Data Centers (Weber et al., 2005). The GPS and GLONASS observations are

processed simultaneously and thus the generated precise orbit products for both systems are in the same reference frame (Weber and Fragner, 2002).

Currently four IGS analysis centers routinely can provide GLONASS precise orbit products, including CODE (University Berne, Switzerland), IAC (Information - Analytical Center), ESA/ESOC (European Space Operations Center, Germany) and BKG (Bundesamt für Kartographie und Geodäsie, Germany).

CODE provides final, rapid and predicted rapid GLONASS orbit products (Weber et al., 2005; Schaer et al., 2004). The CODE orbits are expressed in the IGB00 reference frame, which is a realization of the ITRF2000 (Bruyninx, 2007). IAC is a department of MCC (Russian Mission Control Center) that routinely monitors the GLONASS performance. IAC initiated a routine orbit and clock determination using IGS tracking network data in 2004. As one of 4 IGS analysis centers, it has routinely provided GLONASS post-mission orbit and clock products since 2005. These products include the final orbit and clock data with a delay of 5 days and the rapid orbit and clock data with a delay of 1 day (Oleynik et al., 2006).

ESOC began to process and analyze GNSS data for a precise orbit determination in 1991. ESA/ESOC first uses its GPSOBS/BAHN software to compute the precise GPS orbit and clock parameters and then aligns its GLONASS solution to the ITRF2000 reference frame using the precise GPS orbit data and tight constraints on the coordinates of seven observing stations (Romero et al., 2004). BKG has begun to process and analyze the combined GPS/GLONASS observations from global tracking stations since the IGEX-98 began. Similarly to ESA/ESOC, BKG first computes GPS orbits, clock estimation and Earth orientation parameters and then utilizes the Bernese software to

produce precise GLONASS orbit and station coordinates on a daily basis using double-differenced phase observations (Habrich et al., 2004). It provides GLONASS precise orbit data, receiver-specific estimates of a system time difference between GPS and GLONASS, and the station coordinates.

Similarly to the IGS final GPS orbits, the independent GLONASS orbits from the four organizations have been combined to generate the IGS final GLONASS orbits with an accuracy of 10-15cm (Weber et al., 2005).

Table 3-3 GLONASS Precise Satellite Orbit and Clock Products (IGS,2008; Oleynik et al.,2006; Hesselbarth and Wanninger,2008)

Orbit/clock		Accuracy	Latency	Updates	Sample Interval
IGS Final	orbit	15 cm	two weeks	weekly	15 min
IAC Rapid	orbit	--	1 day	--	15 min
	clock	--			5 min
IAC Final	orbit	~15 cm	5 days	--	15 min
	clock	~1.5 ns			5 min
ESOC Final	orbit	--	--	--	15 min
	clock	--			5 min

Currently only two data analysis centers, namely IAC and ESA/ESOC, provide post-mission GLONASS clock data. But their direct comparison can hardly be made due to different reference time scales used and different inter-frequency biases applied to the GLONASS code measurements. The agreement between the IAC and ESOC post-mission GLONASS clock values is at the level of 1.5ns (Oleynik et al., 2006). With only two contributing centers, IGS does not provide precise GLONASS satellite clock corrections. A summary of GLONASS precise orbit and clock products is given in Table 3-3.

3.2.2 Ionospheric Delay

The ionosphere is the region of the atmosphere layer at a height of about 50 to 1000 km above the Earth's surface. In this layer, the Sun's ultraviolet light ionizes atoms and molecules. As a result, the electrons and ions are produced from the neutral atmospheric particles during the process of photoionization (Liao, 2000). The free electrons in the ionosphere layer exert severe influences on the propagation of microwave signals, including refraction, reflection and absorption. When GPS or GLONASS signals travel through the ionosphere, the signals' transmitting speed changes, and therefore the measured range between a user and a satellite is corrupted by the ionospheric delay. The ionosphere delay error that can reach tens of metres at zenith has become the dominant error source since the removal of GPS Selective Availability (SA). To achieve a higher accuracy in the satellite positioning and navigation, the ionospheric effect must be taken into account.

The refractive index is one of the most important parameters to characterize the ionosphere. The ionosphere is a dispersive medium, and its refractive index is therefore a function of the frequency. As a result, the ionosphere layer will cause different delays for the GPS or GLONASS L1 and L2 frequencies. The first-order approximation of the phase refractive index may be written as (Seeber, 1993):

$$n_p = 1 - \frac{40.3 \cdot N_e}{f^2} \quad (3.2.1)$$

where N_e is the total electron density (el/m³); f is the radio wave frequency (Hz).

In the same way, the first-order group refractive index can be expressed by the following formula:

$$n_g = 1 + \frac{40.3 \cdot N_e}{f^2} \quad (3.2.2)$$

The propagation speed may be expressed as a function of the refractive index in the following:

$$v = \frac{c}{n} \quad (3.2.3)$$

where c is the speed of light.

The group delay of the ionosphere can be expressed in the unit of length as follows (Liao, 2000):

$$\Delta g = \int (n_g - 1) dl \quad (3.2.4)$$

From Equation (3.2.2), Equation (3.2.4) can be rewritten as:

$$\Delta g = \frac{40.3}{f^2} \int N_e dl = \frac{40.3}{f^2} \cdot TEC \quad (3.2.5)$$

where TEC (Total Electron Content) is the total number of electrons along the path between a station and a satellite. Similarly, the carrier phase advance may be written as:

$$\Delta \Phi = \int (n_p - 1) dl = -\frac{40.3}{f^2} \int N_e dl = -\frac{40.3}{f^2} \cdot TEC \quad (3.2.6)$$

As can be seen from the sign of group delay and phase advance, the phase pseudoranges are measured shorter than the true geometric range between the satellite and the receiver whereas the code pseudoranges are measured longer than the true geometric range. Therefore the carrier phase pseudoranges are considered “advanced” while the code pseudoranges are considered “delayed”.

For single frequency GPS users, a Klobuchar ionosphere model, which uses a sinusoidal curve to fit the average diurnal variation of the ionosphere, is commonly used to correct the ionospheric error. The parameters of the Klobuchar model are broadcast through the navigation message. A drawback of the Klobuchar model is that it can only compensate 50-60% of the total ionosphere effect (Klobuchar, 1996). Chen and Gao (2005) compared the Klobuchar model with the global ionospheric model (GIM) provided by IGS and the ionospheric delay estimation model in which the zenith ionospheric delay is estimated using code and phase observations (Schaer et al., 1998; Beran et al., 2003). The results indicate that the ionospheric estimation model and GIM offer better performance than the Klobuchar model.

For dual frequency GPS users, the ionosphere effect can be mitigated through linear combination of measurements on L1 and L2 according to the dispersive property of ionosphere. In precise point positioning, the ionosphere-free observation combinations are usually applied for mitigating the influence of the ionospheric error. The following two equations represent the traditional ionosphere-free observation combinations (Kouba and Héroux, 2001).

$$P_{IF} = \frac{f_{L1}^2}{(f_{L1}^2 - f_{L2}^2)} P_{L1} - \frac{f_{L2}^2}{(f_{L1}^2 - f_{L2}^2)} P_{L2} \quad (3.2.7)$$

$$\phi_{IF} = \frac{f_{L1}^2}{(f_{L1}^2 - f_{L2}^2)} \phi_{L1} - \frac{f_{L2}^2}{(f_{L1}^2 - f_{L2}^2)} \phi_{L2} \quad (3.2.8)$$

where P_{IF} and ϕ_{IF} are the ionosphere-free code and phase observations, respectively; ϕ_{L1} and ϕ_{L2} are the carrier phase observations at L1 and L2 in the unit of length,

respectively; P_{L1} and P_{L2} are the code observations at L1 and L2, respectively; f_{L1} and f_{L2} are the carrier frequencies at L1 and L2, respectively.

3.2.3 Tropospheric Delay

The troposphere is the atmosphere layer from the Earth's surface up to about 40 km (Hofmann, 2001). Unlike the ionosphere, it is a non-dispersive medium and therefore its effect can't be eliminated by the observation combination from L1 and L2 data. The magnitude of the tropospheric delay depends on many factors such as the satellite elevation angle, the altitude of the station, atmospheric pressure, temperature, and water vapor pressure. It is usually divided into dry and wet components. The former is caused by the higher portion of the troposphere and accounts for about 90% of the total tropospheric delay whereas the latter is caused by the lower portion of the troposphere and accounts for about 10% of the total tropospheric delay. Besides, the dry tropospheric delay can be easily modeled, but the wet tropospheric delay is difficult to be modeled due to the irregular variation of the liquid water and water vapor over space and time in the troposphere (Misra and Enge, 2001). Although the wet tropospheric component represents approximately 10% of the total tropospheric effect, it causes the main difficulty in eliminating the tropospheric effect through modeling.

The average total tropospheric delay at zenith is about 2.5 m (Abdel-salam, 2005). The dry and wet tropospheric delays are usually modeled at zenith and then scaled by a mapping function to the satellite elevation, as shown in the following equation:

$$\Delta d_{trop} = \Delta d_{dry} \cdot M_{dry} + \Delta d_{wet} \cdot M_{wet} \quad (3.2.9)$$

where Δd_{dry} is the zenith dry component; Δd_{wet} is the zenith wet component; M_{dry} is the dry mapping function; M_{wet} is the wet mapping function.

There exist many tropospheric models. Among them the Saastamoinen and Hopfield models are most commonly used (Mekik, 1997). The Hopfield model is built by a large number of meteorological radiosonde balloon profiles and is made at different locations over quite a number of years. In the Hopfield model, the troposphere delay is modeled with a constant lapse rate of temperature and a height integral which is a linear function of the pressure measured on the Earth surface. The dry and wet tropospheric delay at zenith can be given as (Mekik, 1997):

Dry zenith delay:

$$\Delta d_{dry} = 10^{-6} \cdot k_1 \cdot \frac{P_s}{T_s} \cdot \int_{h_s}^{h_d} \left[\frac{h_d - h}{h_d - h_s} \right]^4 \cdot dh = 10^{-6} \cdot k_1 \cdot \frac{P_s}{T_s} \cdot \frac{h_d - h_s}{5} \quad (3.2.10)$$

$$h_d - h_s = 148.98 \cdot (T_s - 4.12) \quad (3.2.11)$$

Wet zenith delay:

$$\Delta d_{wet} = 10^{-6} (k_3 + 273(k_2 - k_1)) \cdot \frac{e_s}{T_s} \cdot \int_{h_s}^{h_w} \left[\frac{h_w - h}{h_w - h_s} \right]^4 \cdot dh \quad (3.2.12)$$

$$= 10^{-6} \cdot (k_3 + 273(k_2 - k_1)) \cdot \frac{e_s}{T_s} \cdot \frac{h_w - h_s}{5}$$

$$h_w - h_s = 11km \quad (3.2.13)$$

where h_d and h_w are the heights of the dry and wet troposphere above the geoid, respectively (m); e_s is the surface partial water vapor pressure (mbar); T_s is the surface

temperature (K); P_s is the surface pressure (mbar); h_s is the surface height above the geoid (m); k_1, k_2 and k_3 are the constants.

There are many mapping functions in use. The Niell mapping function is one of them and commonly used to compute the tropospheric delay from the zenith to an arbitrary elevation angle. It is an empirical function that is dependent on the latitude of the station and time with different forms for wet and dry tropospheric delays. The Niell mapping function can be written as (Shrestha, 2003):

$$m_{dry}(\mathcal{E}) = \frac{\frac{1}{1 + \frac{a_{dry}}{1 + \frac{b_{dry}}{1 + c_{dry}}}}}{\sin \mathcal{E} + \frac{a_{dry}}{\sin \mathcal{E} + \frac{b_{dry}}{\sin \mathcal{E} + c_{dry}}}} + \left[\frac{1}{\sin \mathcal{E} - \frac{\frac{1}{1 + \frac{a_{ht}}{1 + \frac{b_{ht}}{1 + c_{ht}}}}}{\sin \mathcal{E} + \frac{a_{ht}}{\sin \mathcal{E} + \frac{b_{ht}}{\sin \mathcal{E} + c_{ht}}}}}{1} \right] \times \frac{H}{1000} \quad (3.2.14)$$

$$m_{wet}(\mathcal{E}) = \frac{\frac{1}{1 + \frac{a_{wet}}{1 + \frac{b_{wet}}{1 + c_{wet}}}}}{\sin \mathcal{E} + \frac{a_{wet}}{\sin \mathcal{E} + \frac{b_{wet}}{\sin \mathcal{E} + c_{wet}}}} \quad (3.2.15)$$

where, \mathcal{E} is the satellite elevation angle; H is the station height above sea level; $a_{dry}, b_{dry}, c_{dry}, a_{ht}, b_{ht}, c_{ht}, a_{wet}, b_{wet}, c_{wet}$ are the coefficients dependent on the station latitude.

Other mapping functions are given in Appendix B.

In precise point positioning, the dry tropospheric delay error is corrected through a tropospheric model while the wet component is estimated as an unknown parameter along with the three-dimension coordinates, receiver clock offset, and ambiguities.

3.2.4 Receiver Clock Offset

The receiver clock is usually equipped with quartz crystal oscillators because of the advantages of small size, little power consumption, and low price. Due to the relatively poor stability of the quartz clock, the receiver clock drifts in a short period of time, which will cause a rapid change of the receiver clock offset over time. Therefore, the receiver clock offset is usually estimated as an unknown parameter along with three coordinate components in precise point positioning. Alternatively, the receiver clock offset may be removed if observations between satellites are differenced.

3.2.5 Multipath and Measurement noise

A multipath error is caused by the signals reflected from objects in the vicinity of a station. It corrupts the direct line-of-sight signals from the GPS or GLONASS satellites and thus degrades the accuracy of code and carrier phase measurements (Weill, 2003). Despite the rapid development of the receiver technology, the multipath still remains a main error source in the positioning and navigation. Theoretically the maximum multipath error is approximately half the code chip length: 150 m for C/A code and 15 m for P(Y) code. The multipath effect on the phase observation does not exceed one-quarter of its wavelength, about 5-6 cm for L1 and L2 (Shen, 2002).

Several receiver-based methods of multipath mitigation have been developed in the past few years. The existing approaches can be classified into three categories (Yang et al., 2004). The first category is based on the radio frequency signals, which includes using a choke-ring antenna and using multiple GPS antennas. The second category is based on the available baseband signals, which includes the narrow correlator technology, double delta correlator, early/late slope technique (ELS), and early1/ early2(E1/E2) tracking. The third category is based on final code and carrier phase measurements after receiver baseband processing, which includes processing the previous day's measurements as corrections for the next day's measurements, analyzing the Signal to Noise Ratio (SNR) of the measurements, and estimating the multipath error with a proper model.

Several measures can be taken to mitigate the multipath effect. First of all, an effective measure is to simply set up an antenna in an area free of nearby reflectors. When the receiver has to be placed in a reflective environment, a good quality antenna that is multipath resistant can be used. Secondly, an antenna with a ground plane or choke-ring assembly and a receiver that can filter out multipath signal disturbance can be taken to reduce the effect of multipath error. Thirdly, a mask elevation angle can be set to avoid observing low elevation satellites whose signals are susceptible to multipath.

The measurement noise caused by the antenna, receiver oscillator and other components is generally small in magnitude. It has some characteristics such as low correlation between observations and Gaussian distribution. The measurement noise is usually at a decimetre level for code observations and a few millimetres for carrier phase observations. Its effect can be mitigated using high-quality hardware equipments.

3.3 Special Error Sources

3.3.1 Satellite and Receiver Antenna Phase Center Offsets

The satellite antenna phase center offset caused by the separation between the satellite's mass center and the phase center of the satellite antenna must be taken into account in PPP. The reason is that the precise satellite orbit and clock products refer to the satellite's mass center due to the fact that the force models of modeling satellite orbit are made to the mass center while the code and carrier phase observations used in PPP refer to the antenna phase center. The phase center offsets for most satellites are in the body z coordinate direction towards the Earth and in the body x coordinate direction which is on the plane containing the Sun (Kouba and Héroux, 2001). Figure 3-3 shows the satellite antenna phase center offset.

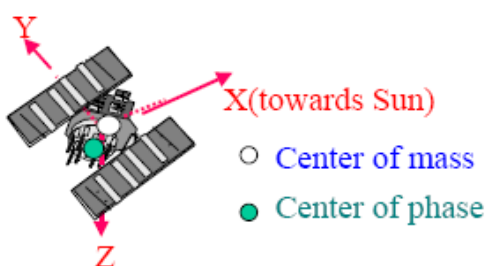


Figure 3-3 Satellite Antenna Phase Center Offset
(Kouba and Héroux, 2001)

Not all types of satellites need to consider the satellite antenna phase center offset. GPS Block IIR satellites and the later designed satellites do not need to apply the phase center offset correction due to the consistency of two centers. This offset for Block II/IIA satellites is a constant value which is given in Table 3-4. The correction may be made through the following equation (Leick, 2004):

$$X_{phase} = X_{mass} + [e_x \ e_y \ e_z]^{-1} [x_{offset} \ y_{offset} \ z_{offset}]^T \quad (3.3.1)$$

where e_x is the satellite-Sun unit vector in Earth Centered Earth Fixed (ECEF); e_z is the satellite unit vector toward the Earth in ECEF; e_y is the third vector to complete the right hand system; x_{offset} , y_{offset} , z_{offset} are the offsets in the satellite fixed coordinates system; X_{phase} , X_{mass} are the satellite coordinates referring to the antenna phase center and satellite mass center, respectively.

**Table 3-4 GPS Satellite Antenna Phase Center Offsets in the Satellite Fixed Reference Frame (m)
(Kouba and Héroux, 2001)**

	X_{offset}	Y_{offset}	Z_{offset}
Block II/IIA	0.279	0	1.023
Block IIR	0	0	0

Similarly to GPS, the GLONASS satellite antenna phase center offset must also be considered in PPP due to the separation between the satellite mass center and the antenna phase center. Given in Table 3-5 is the GLONASS satellite antenna phase center offsets in the satellite fixed reference frame.

Since the electrical phase center of a receiver antenna that the measurements refer to is different from the center of the physical mark, the receiver antenna phase center offset needs to be taken into account in PPP. For any given GNSS receiver antenna, its phase center varies with the changing direction of the received satellite signal. The magnitude of the variation usually depends on the satellite elevation angle. The inherent azimuth has a very small effect on the phase center variation, which is usually caused by the local environment around the antenna site. Antenna calibrations may be divided into

two parts (Czopek and Mader, 2002). One is the calibration for an average phase center offset with respect to a physical feature of the antenna. The other is the calibration for the phase center variation (PCV) with the elevation angle or possibly azimuth. Both parts must be conducted in the antenna calibrations.

Table 3-5 GLONASS Satellite Antenna Phase Center Offsets in the Satellite Fixed Reference Frame as of Feb.15, 2009 (m) (IGS, 2009)

PRN	# GC	X	Y	Z
01	796	0	0	1.9444
02	794	-0.545	0	2.3000
03	727	-0.545	0	2.3000
04	795	0	0	2.0061
05	711	0	0	1.9141
06	701	-0.545	0	2.1947
07	712	-0.545	0	2.3232
08	729	-0.545	0	2.3000
09	722	-0.545	0	2.3000
10	717	-0.545	0	2.3000
11	723	-0.545	0	2.3000
13	721	-0.545	0	2.3000
14	715	-0.545	0	2.3000
15	716	-0.545	0	2.3000
17	718	-0.545	0	2.3000
18	724	-0.545	0	2.3000
19	720	-0.545	0	2.3000
20	719	-0.545	0	2.3000
21	725	-0.545	0	2.3000
22	798	-0.545	0	2.3000
23	714	-0.545	0	2.2772
24	713	-0.545	0	2.3253

3.3.2 Phase Wind Up

As the navigation signals transmitted on L1 and L2 by each GPS or GLONASS satellite are right-hand circularly polarized, the carrier phase observations from a receiver are dependent on the mutual orientation of the satellite and receiver antennas. A relative

rotation of satellite and receiver antennas may change the observed carrier phase up to one cycle. This effect is called “phase wind up”(Wu et al.,1993). A receiver antenna is usually oriented towards a fixed direction in a static mode while the satellite antenna usually rotates slowly due to the continuous reorientation of its solar panels towards the Sun. The satellite antenna can rotate up to one revolution within less than half an hour during the period of eclipsing due to the fact that the satellite antenna is undergoing a rapid rotation in order to reorient its solar panels towards the Sun (Kouba and Héroux, 2001).

The effect of the phase wind up is negligible for the differential positioning spanning up to several hundred kilometres while it is quite significant for the precise point positioning since this effect can reach up to one half of the wavelength (Kouba and Héroux, 2001).The correction of the phase wind up may be made through the following equations (Wu at al., 1993):

$$D = x - k(k \cdot x) + k \times y \quad (3.3.2)$$

$$D' = \bar{x} - k(k \cdot \bar{x}) - k \times \bar{y} \quad (3.3.3)$$

$$\Delta\phi = \text{sign}(k \cdot (D' \times D)) \cos^{-1}(D' \cdot D / |D'| |D|) \quad (3.3.4)$$

where

- k is the satellite to receiver unit vector;
- x, y, z are the local receiver unit vectors;
- $\bar{x}, \bar{y}, \bar{z}$ are the satellite body coordinate unit vectors;
- $\Delta\phi$ is the phase wind up correction;
- D, D' are the effective dipole vectors of the satellite and receiver.

3.3.3 Relativistic Effect

The principle of the satellite positioning is established on the basis of measuring the signal's travelling time from a satellite to a receiver. The relativity is caused by the gravitational potential and the moving velocity difference of a satellite clock and a receiver clock. It affects the measured time and therefore the relativity correction must be applied in PPP. The satellite clocks are subject to two relativistic effects: special relativity and general relativity. According to the theory of the special relativity, the satellite clock traveling at a constant speed appears slower than the clock on the ground due to the time dilation effect of their relative motion (Tao, 2008). This relativistic effect correction can be applied as follows (GPS ICD, 2000):

$$\Delta t_r = -\frac{2\vec{R}\cdot\vec{V}}{c^2} \quad (3.3.5)$$

where Δt_r is the relativity correction; \vec{R} is the instantaneous position vector of the satellite; \vec{V} is the instantaneous velocity vector of the satellite; c is the speed of light.

According to the general relativity, a satellite clock appears to run faster than the one on the ground due to their difference in gravitational potential. This correction for this effect is given by the following equation (Rothacher and Beutler, 2002):

$$\Delta t_p = \frac{2GM}{c^2} \ln\left(\frac{r^s + r_r + r_r^s}{r^s + r_r - r_r^s}\right) \quad (3.3.6)$$

where,

Δt_p is a gravity delay error;

G is a gravitational constant;

- M is the mass of the Earth;
- r^s is a distance between the satellite and the Earth center;
- r_r is a distance between the receiver and the Earth center;
- r_r^s is a distance from the receiver to the satellite.

3.3.4 Earth Tide

Since the Earth is not a rigid body, it responds as an elastic body to external forces exerted by celestial bodies. Earth tides are caused by the gravitational force imposed by the Sun and Moon. It will cause periodic deformation on the Earth and lead to vertical and horizontal site displacement, which can be represented by spherical harmonics of degree and order characterized by the Love number and the Shida number. The effect of the Earth tides that is dependent on station latitude, tide frequency, and sidereal time can reach about 30 cm in the height component and 5 cm in the horizontal plane (Kouba and Héroux, 2001). The displacement caused by the solid Earth tide may be divided into a permanent part and a periodic part. The periodic part can be largely averaged out in the static positioning of an entire day while the permanent part that can reach 12 cm in the middle latitude region remains (Kouba and Héroux, 2001). Even with a long observing time, neglecting the Earth tide correction will result in a positioning error of up to 12.5 cm in the height component and 5 cm in the horizontal plane in point positioning. The equation including both the permanent and periodical displacement corrections is given in the following (IERS, 1989):

$$\Delta\vec{r} = \sum_{j=2}^3 \frac{GM_j}{GM} \frac{r^4}{R_j^3} \left\{ \left[3l_2 (\hat{R}_j \cdot \hat{r}) \right] \hat{R}_j + \left[3 \left(\frac{h_2}{2} - l_2 \right) (\hat{R}_j \cdot \hat{r})^2 - \frac{h_2}{2} \right] \hat{r} \right\} + \left[-0.025m \cdot \sin\phi \cdot \cos\phi \cdot \sin(\theta_g + \lambda) \right] \cdot \hat{r} \quad (3.3.7)$$

where

$\Delta\vec{r}$ is a site displacement vector in Cartesian coordinate system;

GM is gravitational parameters of the Earth;

GM_j is gravitational parameters of the Moon ($j = 2$) and the Sun ($j = 3$);

r is geocentric state vectors of the station;

R_j is geocentric state vectors of the Moon ($j = 2$) and the Sun ($j = 3$);

\hat{r} is geocentric unit state vectors of the station;

\hat{R}_j is geocentric unit state vectors of the Moon ($j = 2$) and the Sun ($j = 3$);

l_2 is the nominal second degree Love number(0.609);

h_2 is the nominal Shida dimensionless number(0.085);

ϕ is the site latitude;

λ is the site longitude;

θ_g is the Greenwich Mean Sidereal Time.

3.3.5 Ocean Tide Loading

Similarly to the solid Earth tides, the redistribution of seawater under the gravitational force imposes a load on the sea floor and adjacent land, which causes the deformation of the sea floor and a surface displacement of an adjacent land. The pure ocean tide may be measured using tide gauges as well as altimeters and observed at the

beach for its rising and falling with respect to a benchmark (Witchayangkoon, 2000).

The ocean loading consists of the diurnal and semi diurnal period components with an order of magnitude smaller than solid Earth tides. Its effect must be taken into account in centimetre-level precise kinematic point positioning or precise static point positioning near the sea over the time interval shorter than 24 h, while its effect is negligible when the station is far away from ocean coast lines (Kouba and Héroux, 2001). The model of ocean loading is given as follows (IERS, 1996):

$$\Delta c = \sum_j f_j A_{cj} \cos(\omega_j t + \chi_j + u_j - \phi_{cj}) \quad (3.3.8)$$

where

Δc is a displacement caused by ocean loading;

j represents 11 tidal waves ($M_2, S_2, N_2, K_2, K_1, O_1, P_1, Q_1, M_f, M_m, S_{sa}$);

f_j depends on the longitude of lunar node (at 1-3 mm precision $f_j=1$);

u_j depends on the longitude of lunar node (at 1-3 mm precision $u_j=0$);

ω_j is an angular velocity at time $t=0h$;

χ_j is an astronomical argument at time $t=0h$;

A_{cj} is a station specific amplitude;

ϕ_{cj} is a station specific phase.

3.3.6 Atmosphere Loading

The atmosphere loading is caused by the spatial and temporal variations of atmospheric mass. It has an indirect impact on the ocean and Earth tides, which causes

the deformation of the Earth's surface (Witchayangkoon, 2000). As a result, the displacement caused by the atmosphere loading can reach up to 20 mm in the vertical component and 3 mm in the horizontal component (Petrov and Boy, 2004). This displacement is a function of geographic location with a larger value in middle latitude regions in comparison with high latitude regions (IERS, 1996). A number of models of the atmosphere loading displacement varying from simple to complex are available. Among them, a simple model is given as follows (Rabbel and Schuh, 1986):

$$\Delta r = -0.35p - 0.55p' \quad (3.3.9)$$

where Δr is the atmosphere loading displacement in the unit of millimetre; p is the site pressure difference from the standard value(101.3 KPA); p' is the pressure anomaly within 2000 km from the station.

3.3.7 Sagnac Effect

A Sagnac effect is caused by the Earth's rotation during the transit of the satellite signal from a satellite to a receiver. Because of the rotation of the Earth, the receiver on the Earth surface moves with a velocity of up to 500 m/s (at the equator), which results in the Sagnac effect. This effect is very small and complicated to calculate. According to Parkinson and Ashby (1996), the Sagnac effect is proportional to the area swept out by the radius vector from the Earth's center to the light ray during the signal propagation from a satellite to a receiver, and can be written as:

$$\Delta t_s = + \frac{2\Omega_e \cdot A_e}{c^2} \quad (3.3.10)$$

where, Ω_e is the Earth angular rotation rate(WGS-84); A_e is the total area swept out by the radius vector from the center of the Earth to the light ray while the signal travels from a satellite to a receiver.

Chapter Four: Combined GPS and GLONASS PPP Models

4.1 Introduction

Current PPP models are implemented using only GPS observations. For such a GPS-based positioning system, the accuracy, availability and reliability of the positioning results are very dependent on the number of visible GPS satellites, which is often insufficient in the environments such as urban canyons and open-pit mines. Further, even in the open area where sufficient GPS satellites are available, the PPP accuracy and reliability could still be affected by poor satellite geometry. One possible strategy to increase the availability of satellites and improve the reliability and accuracy of positioning results is to integrate GPS and GLONASS.

In order to achieve high-accuracy positioning results in PPP, both GPS and GLONASS carrier phase observations are used in the combined data processing. Since the current GPS-based PPP models can't be used to process the combined GPS/GLONASS measurements, combined GPS/GLONASS PPP functional models and corresponding stochastic models are developed in this chapter. The functional models describe the mathematical relationship between the measurements and the unknown parameters, while the stochastic models describe the statistics of the measurements.

Firstly, a brief summary of the Kalman Filter method is provided. Secondly, the detailed GPS-based PPP mathematic models are described. Thirdly, the combined GPS and GLONASS PPP models including the combined GPS/GLONASS traditional and UofC models are presented. Finally, the corresponding stochastic models including observations' stochastic model and parameters' stochastic model are presented.

4.2 Kalman Filter Estimation

The Kalman filter is an optimal recursive data processing algorithm that combines all available measurement data and uses a priori knowledge about the system and measurements to produce an estimate of the desired variables with a statistically minimized error. The Kalman filter processes all available measurements regardless of their precision using any available information such as the initial conditions of the state variables and the statistical description of the system noises and measurement errors. The Kalman filter is recursive because it does not require all previous data to be saved and reprocessed when a new measurement is taken (Maybeck, 1979). The Kalman filter is optimal as it is designed to be a consistent and unbiased estimator with a minimum mean square error as given in the following equations (Mikhail and Ackermann, 1976):

$$\lim_{n \rightarrow \infty} P(|\hat{x} - x| < \varepsilon) = 1 \quad (4.2.1)$$

$$E(\hat{x}) = x \quad (4.2.2)$$

$$E\{(\hat{x} - E(\hat{x}))^T (\hat{x} - E(\hat{x}))\} = \min \quad (4.2.3)$$

where n is the sample size; x is the state vector; \hat{x} is the estimate of the state vector; ε is a very small value; $P()$ is the statistical probability; $E()$ is the statistical expectation.

In a discrete Kalman filter, the state equation and measurement equation may be written as:

$$x_k = \Phi_{k-1} x_{k-1} + w_{k-1} \quad (4.2.4)$$

$$z_k = H_k x_k + v_k \quad (4.2.5)$$

where x_k, x_{k-1} are the state vector at epoch k and $k-1$, respectively; Φ_{k-1} is the transition matrix relating the state at the previous time step $k-1$ to the state at the current step

k ; z_k is the measurement vector; H_k is the design matrix; w_k and v_k are random variables that represent the process and measurement noise, respectively. They are assumed to be independent and follow a normal probability distribution as given in the following equations (Welch and Bishop, 2001):

$$w_{k-1} \sim N(0, Q_{k-1}) \quad (4.2.6)$$

$$v_k \sim N(0, R_k) \quad (4.2.7)$$

where Q and R are the process noise covariance and measurement noise covariance matrix, respectively.

The discrete Kalman filter algorithm consists of two major steps: time update and measurement update. The time update equations are responsible for obtaining a priori estimate of the current state and error covariance for the next time step, while the measurement update equations are responsible for incorporating a new measurement into the priori estimate to obtain an improved estimate. The time update equations are also denoted as prediction equations, and the measurement update equations are often referred to as correction equations (Welch and Bishop, 2001). The specific equations for the time and measurement updates are given below:

Prediction:

$$\hat{x}_k^- = \Phi_{k-1} \hat{x}_{k-1} \quad (4.2.8)$$

$$P_k^- = \Phi_{k-1} P_{k-1} \Phi_{k-1}^T + Q_{k-1} \quad (4.2.9)$$

Correction:

$$K_k = P_k^- H_k^T (H_k P_k^- H_k^T + R_k)^{-1} \quad (4.2.10)$$

$$\hat{x}_k = \hat{x}_k^- + K_k (z_k - H_k \hat{x}_k^-) \quad (4.2.11)$$

$$P_k = (I - K_k H_k) P_k^- \quad (4.2.12)$$

where \hat{x}_k^- and \hat{x}_k are predicted and updated state vectors, respectively; P_k^- and P_k are predicted and updated state covariance matrix, respectively; K_k is a gain matrix. The Kalman filter operation process is illustrated in Figure 4-1.

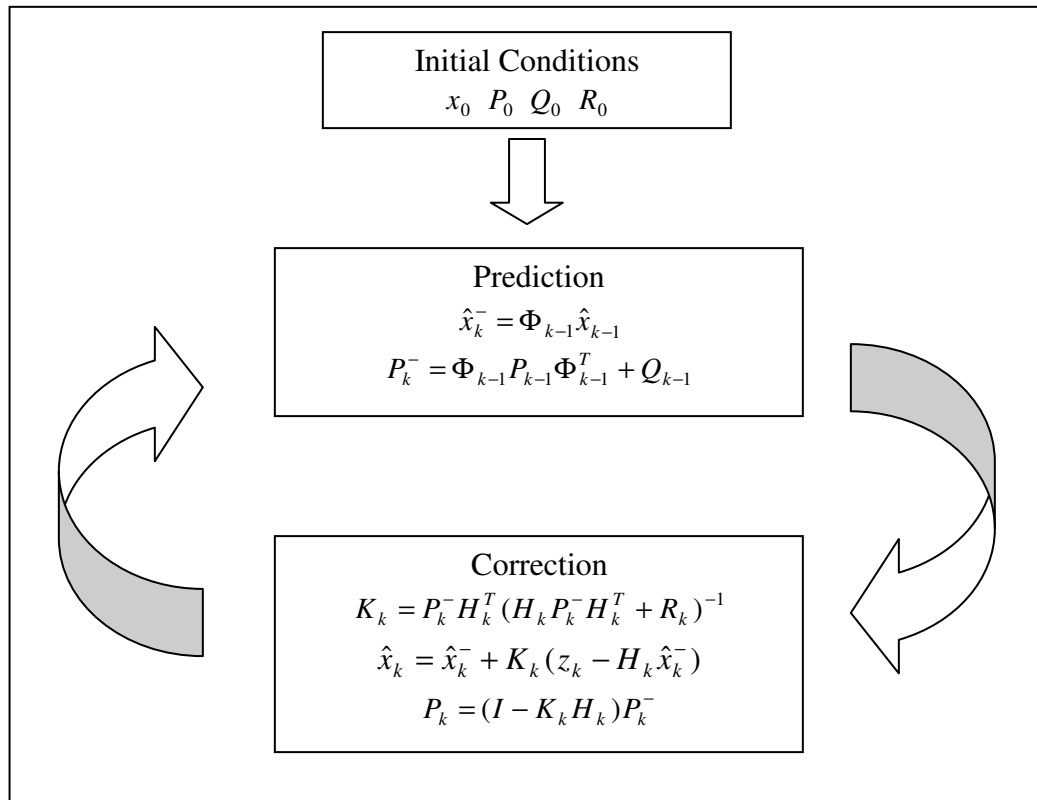


Figure 4-1 Kalman Filter Operation Illustration

4.3 GPS PPP Observation Model

The observation model, also called the functional model, describes a mathematical relationship between the GPS measurements and the unknown parameters. The existing PPP observation models, which are based on the ionosphere-free

observation combination, can be categorized into the traditional model and the UofC model.

4.3.1 Traditional Model

The traditional PPP model uses the ionosphere-free combinations between code observations from L1 and L2 data as well as between carrier phase observations on L1 and L2. This ionosphere-free code-code and phase-phase observation combinations are the most popular form used in PPP to alleviate the effect of the ionosphere error. The code pseudorange and carrier phase observations on L1 and L2 between a receiver and a satellite are described by the following equations:

$$P_i = \rho + cdt - cdT + d_{orb} + d_{trop} + d_{ion/P_i} + d_{mult/P_i} + \varepsilon_{P_i} \quad (4.3.1)$$

$$\Phi_i = \rho + cdt - cdT + d_{orb} + d_{trop} - d_{ion/\Phi_i} + \lambda_i N_i + d_{mult/\Phi_i} + \varepsilon_{\Phi_i} \quad (4.3.2)$$

where,

P_i is the measured pseudorange on L_i (m);

Φ_i is the measured carrier phase on L_i (m);

ρ is the true geometric range (m);

c is the speed of light (m/s);

dt is the receiver clock error (s);

dT is the satellite clock error (s);

d_{orb} is the satellite orbit error (m);

d_{trop} is the tropospheric delay (m);

d_{ion/L_i} is the ionospheric delay on L_i (m);

λ_i is the wavelength on L_i (m/cycle);

N_i is the integer phase ambiguity on L_i (cycle);

d_{mult/P_i} is the multipath effect in the measured pseudorange on L_i (m);

d_{mult/Φ_i} is the multipath effect in the measured carrier phase on L_i (m);

\mathcal{E} is the measurement noise (m);

The traditional PPP model has the form of the ionosphere-free code and phase observation combinations as expressed below in the unit of length (Shen, 2002):

$$\begin{aligned} P_{IF} &= \frac{f_1^2 \cdot P_1 - f_2^2 \cdot P_2}{f_1^2 - f_2^2} \\ &= \rho + c(dt - dT) + d_{orb} + d_{trop} + d_{mult/P_{IF}} + \mathcal{E}_{P_{IF}} \end{aligned} \quad (4.3.3)$$

$$\begin{aligned} \Phi_{IF} &= \frac{f_1^2 \cdot \Phi_1 - f_2^2 \cdot \Phi_2}{f_1^2 - f_2^2} \\ &= \rho + c(dt - dT) + d_{orb} + d_{trop} + \frac{cf_1 N_1 - cf_2 N_2}{f_1^2 - f_2^2} + d_{mult/\Phi_{IF}} + \mathcal{E}_{\Phi_{IF}} \end{aligned} \quad (4.3.4)$$

Before GPS observations are used for a position determination, the GPS precise orbit and clock data are first applied to alleviate satellite orbit and clock errors. The ionospheric refraction bias is eliminated by constructing combined ionosphere-free code pseudorange and phase observations from L1 and L2 data. After applying precise satellite orbit and clock corrections, the ionosphere-free code and phase observation combinations can be written as follows:

$$P'_{IF} = \rho + c \cdot dt + d_{trop} + \mathcal{E}'_{P_{IF}} \quad (4.3.5)$$

$$\Phi'_{IF} = \rho + c \cdot dt + d_{trop} + N'_{IF} + \epsilon'_{\Phi_{IF}} \quad (4.3.6)$$

where P'_{IF} is the corrected ionosphere-free code pseudorange observation in metres; Φ'_{IF} is the corrected ionosphere-free phase observation in metres; N'_{IF} is the combined ambiguity term in the unit of length; ϵ'_{IF} is the noise term including residual errors, multipath and noise.

The unknown parameters in the traditional model include three position coordinate components, one receiver clock offset, one zenith wet tropospheric delay component, and the combined ambiguity parameters associated with each observed satellites. The traditional observation model has some characteristics in terms of its mathematic expression (Shen, 2002). At first, its ionosphere-free combinations can't remove the high-order ionospheric effect which accounts for less than 0.1% of the total ionospheric effect. In addition, the combined ambiguity term can only be estimated as a single float value as its integer characteristic has disappeared after the ionosphere-free combination. Finally, the noise after the ionosphere-free combinations is three times larger than the original code and phase measurement noise.

4.3.2 UofC Model

Based on the fact that the code and phase measurements are subject to the same amount of ionospheric effect but with an opposite sign, the UofC observation model uses the ionosphere-free code-phase combination instead of the ionosphere-free code-code combination on L1 and L2 as used in the traditional model. The ionosphere-free phase-

phase combination has the same form for the traditional model and UofC model. The mathematic expression of the UofC model is given below (Shen, 2002):

$$\begin{aligned} P_{IF,L1} &= 0.5(P_1 + \Phi_1) \\ &= \rho + c(dt - dT) + d_{orb} + d_{trop} + 0.5\lambda_1 N_1 + 0.5d_{mult/P_{IF,L1}} + 0.5\epsilon_{P_{IF,L1}} \end{aligned} \quad (4.3.7)$$

$$\begin{aligned} P_{IF,L2} &= 0.5(P_2 + \Phi_2) \\ &= \rho + c(dt - dT) + d_{orb} + d_{trop} + 0.5\lambda_2 N_2 + 0.5d_{mult/P_{IF,L2}} + 0.5\epsilon_{P_{IF,L2}} \end{aligned} \quad (4.3.8)$$

$$\begin{aligned} \Phi_{IF} &= \frac{f_1^2 \cdot \Phi_1 - f_2^2 \cdot \Phi_2}{f_1^2 - f_2^2} \\ &= \rho + c(dt - dT) + d_{orb} + d_{trop} + \frac{cf_1}{f_1^2 - f_2^2} \cdot N_1 + \frac{cf_2}{f_1^2 - f_2^2} \cdot N_2 + d_{mult/\Phi_{IF}} + \epsilon_{\Phi_{IF}} \end{aligned} \quad (4.3.9)$$

After applying precise satellite orbit and clock corrections, the ionosphere-free code-phase and phase-phase observation combinations can be written as follows:

$$P'_{IF,L1} = \rho + c \cdot dt + d_{trop} + 0.5\lambda_1 N_1 + 0.5\epsilon'_{P_{IF,L1}} \quad (4.3.10)$$

$$P'_{IF,L2} = \rho + c \cdot dt + d_{trop} + 0.5\lambda_2 N_2 + 0.5\epsilon'_{P_{IF,L2}} \quad (4.3.11)$$

$$\Phi'_{IF} = \rho + c \cdot dt + d_{trop} + \frac{cf_1}{f_1^2 - f_2^2} \cdot N_1 + \frac{cf_2}{f_1^2 - f_2^2} \cdot N_2 + \epsilon'_{\Phi_{IF}} \quad (4.3.12)$$

where $P'_{IF,L1}$ and $P'_{IF,L2}$ are the corrected ionosphere-free code pseudorange observations in metres on L1 and L2, respectively; Φ'_{IF} is the corrected ionosphere-free phase observation in metres; ϵ'_{IF} is the noise term including residual errors, multipath and noise.

The unknown parameters in the UofC model include three position coordinate components, one receiver clock offset, one zenith wet tropospheric delay component, and the ambiguity parameters associated with each observed satellites on L1 and L2. In comparison with the traditional observation model, the UofC model has the lower

observation noise level after the ionosphere-free combination between code and phase observations. In addition, the integer characteristic of L1 and L2 ambiguities remains since they may be estimated separately, which provides a potential to develop an algorithm of fixed-ambiguity solutions.

4.4 Combined GPS and GLONASS PPP Models

Since the current GPS-based PPP models can't be applied to process the combined GPS/GLONASS measurement data, the combined GPS and GLONASS PPP models have been developed in this section, including the combined GPS/GLONASS traditional model and the combined GPS/GLONASS UofC model.

4.4.1 Combined GPS/GLONASS Traditional Model

For a GLONASS satellite r , the P code pseudorange and carrier phase observations on L1 and L2 between a receiver and a satellite can be expressed as:

$$P_i^r = \rho_r + cdt^r - cdT^r + d_{orb}^r + d_{trop}^r + d_{ion/L_i}^r + d_{mult/P_i}^r + b_{i/P}^r + \mathcal{E}_{P_i}^r \quad (4.4.1)$$

$$\Phi_i^r = \rho_r + cdt^r - cdT^r + d_{orb}^r + d_{trop}^r - d_{ion/L_i}^r + \lambda_i^r N_i^r + d_{mult/\Phi_i}^r + b_{i/\Phi}^r + \mathcal{E}_{\Phi_i}^r \quad (4.4.2)$$

where

P_i is the measured pseudorange on L_i (m);

Φ_i is the measured carrier phase on L_i (m);

ρ is the true geometric range (m);

c is the speed of light (m/s);

dt is the receiver clock error (s);

dT is the satellite clock error (s);

d_{orb} is the satellite orbit error (m);

d_{trop} is the tropospheric delay (m);

d_{ion/L_i} is the ionospheric delay on L_i (m);

λ_i is the wavelength on L_i (m/cycle);

N_i is the integer phase ambiguity on L_i (cycle);

d_{mult/P_i} is the multipath effect in the measured pseudorange on L_i (m);

d_{mult/Φ_i} is the multipath effect in the measured carrier phase on L_i (m);

b_i is the hardware delay bias on L_i (m);

\mathcal{E} is the measurement noise (m);

The hardware delay bias term in the above equations may be split into an average term and a satellite dependent bias term as given below:

$$b_i^r = b_{i,avg}^r + \delta b_i^r \quad (4.4.3)$$

Put Equation (4.4.3) into Equations (4.4.1) and (4.4.2) and consider that this average delay term $b_{i,avg}^r$ is not separable from the receiver clock offset term cdt^r , and the satellite dependent bias δb_i^r may be neglected in the code observation equation because its magnitude is in the order or below the noise level of the code measurements but could not be neglected in the phase observation equation since it is greater than the noise level of the carrier phase measurements (Roßbach, 2000), Equations (4.4.1) and (4.4.2) can therefore be rewritten as:

$$P_i^r = \rho_r + (cdt^r + b_{i,avg}^r) - cdT^r + d_{orb}^r + d_{trop}^r + d_{ion/L_i}^r + d_{mult/P_i}^r + \varepsilon_{P_i}^r \quad (4.4.4)$$

$$\Phi_i^r = \rho_r + (cdt^r + b_{i,avg}^r) - cdT^r + d_{orb}^r + d_{trop}^r - d_{ion/L_i}^r + \lambda_i^r N_i^r + d_{mult/\Phi_i}^r + \delta b_{i/\Phi}^r + \varepsilon_{\Phi_i}^r \quad (4.4.5)$$

In the same way, for a GPS satellite g , the P code pseudorange and carrier phase observations on L1 and L2 between a receiver and a satellite may be expressed as:

$$P_i^g = \rho_g + (cdt^g + b_{i,avg}^g) - cdT^g + d_{orb}^g + d_{trop}^g + d_{ion/L_i}^g + d_{mult/P_i}^g + \varepsilon_{P_i}^g \quad (4.4.6)$$

$$\Phi_i^g = \rho_g + (cdt^g + b_{i,avg}^g) - cdT^g + d_{orb}^g + d_{trop}^g - d_{ion/L_i}^g + \lambda_i^g N_i^g + d_{mult/\Phi_i}^g + \delta b_{i/\Phi}^g + \varepsilon_{\Phi_i}^g \quad (4.4.7)$$

The satellite orbit and clock errors are neglected after using the GPS and GLONASS precise satellite orbit and clock products. The ionospheric delay bias is removed by constructing the ionosphere-free code and phase observations from L1 and L2 data. After applying the precise satellite orbit and clock corrections, the ionosphere-free code-code and phase-phase observation combinations may be written as:

$$\begin{aligned} P_{IF}^g &= (f_{g1}^2 \cdot P_1^g - f_{g2}^2 \cdot P_2^g) / (f_{g1}^2 - f_{g2}^2) \\ &= \rho_g + (cdt^g + b_{IF,avg}^g) + d_{trop}^g + \varepsilon_{P_{IF}}^g \end{aligned} \quad (4.4.8)$$

$$\begin{aligned} \Phi_{IF}^g &= (f_{g1}^2 \cdot \Phi_1^g - f_{g2}^2 \cdot \Phi_2^g) / (f_{g1}^2 - f_{g2}^2) \\ &= \rho_g + (cdt^g + b_{IF,avg}^g) + d_{trop}^g \\ &\quad + (N_{IF}^g + \delta b_{IF/\Phi}^g) + \varepsilon_{\Phi_{IF}}^g \end{aligned} \quad (4.4.9)$$

$$\begin{aligned} P_{IF}^r &= (f_{r1}^2 \cdot P_1^r - f_{r2}^2 \cdot P_2^r) / (f_{r1}^2 - f_{r2}^2) \\ &= \rho_r + (cdt^r + b_{IF,avg}^r) + d_{trop}^r + \varepsilon_{P_{IF}}^r \end{aligned} \quad (4.4.10)$$

$$\begin{aligned} \Phi_{IF}^r &= (f_{r1}^2 \cdot \Phi_1^r - f_{r2}^2 \cdot \Phi_2^r) / (f_{r1}^2 - f_{r2}^2) \\ &= \rho_r + (cdt^r + b_{IF,avg}^r) + d_{trop}^r \\ &\quad + (N_{IF}^r + \delta b_{IF/\Phi}^r) + \varepsilon_{\Phi_{IF}}^r \end{aligned} \quad (4.4.11)$$

where

P'_{IF} is the corrected ionosphere-free code observation combination (m);

Φ'_{IF} is the corrected ionosphere-free phase observation combination (m);

f_i is the frequency of L_i (Hz);

N_{IF} is the combined ambiguity term (m);

$b_{IF,avg}$ is the combined average hardware delay bias term (m);

\mathcal{D}_{IF} is the combined satellite-dependent hardware delay bias term (m);

ε_{IF} contains measurement noise, multipath as well as other residual errors.

As can be seen from the above equations, the bias $\mathcal{D}_{IF/\Phi}$ is not separable from the combined ambiguity N_{IF} and therefore they will be estimated as a single sum parameter. In addition, this average delay bias $b_{IF,avg}$ will be absorbed into the receiver clock offset term in the practical processing. Equations (4.4.8) to (4.4.11) may be simply rewritten as:

$$P'_{IF}{}^g = \rho_g + cdt'^g + d_{trop}^g + \varepsilon_{P_{IF}}^g \quad (4.4.12)$$

$$\Phi'_{IF}{}^g = \rho_g + cdt'^g + d_{trop}^g + N'_{IF}{}^g + \varepsilon_{\Phi_{IF}}^g \quad (4.4.13)$$

$$P'_{IF}{}^r = \rho_r + cdt''^r + d_{trop}^r + \varepsilon_{P_{IF}}^r \quad (4.4.14)$$

$$\Phi'_{IF}{}^r = \rho_r + cdt''^r + d_{trop}^r + N'_{IF}{}^r + \varepsilon_{\Phi_{IF}}^r \quad (4.4.15)$$

where cdt'^g is the sum of the receiver clock offset and the combined average hardware delay bias in metres; N'_{IF} is the sum of the combined ambiguity and the combined satellite-dependent hardware delay bias.

Instead of estimating a GLONASS receiver clock offset parameter, a system time difference unknown parameter is often introduced in the mixed GPS/GLONASS processing (Habrich, 1999). A receiver clock error can be described as:

$$dt = t - t_{sys} \quad (4.4.16)$$

where t_{sys} in Equation (4.4.16) denotes the GPS system time t_{GPS} for GPS observations but for GLONASS observations it represents the GLONASS system time $t_{GLONASS}$. Since the receiver clock error is related to a system time, two receiver clock offset unknown parameters are involved in the combined GPS/GLONASS processing, one for the receiver clock offset with respect to the GPS time and one for the receiver clock offset with respect to the GLONASS time. We can also describe the GLONASS receiver clock offset as follows:

$$\begin{aligned} dt^r &= t - t_{GLONASS} \\ &= t - t_{GPS} + t_{GPS} - t_{GLONASS} \\ &= dt^g + dt_{sys} \end{aligned} \quad (4.4.17)$$

as can be seen from Equation (4.4.17), the GLONASS receiver clock offset may be expressed as the sum of the GPS receiver clock offset and the system time difference between GPS and GLONASS. Applying Equation (4.4.17), the following equation can be obtained:

$$\begin{aligned} cdt'^r &= cdt^r + b_{IF,avg}^r \\ &= cdt^g + cdt_{sys} + b_{IF,avg}^r \\ &= cdt^g + b_{IF,avg}^g + cdt_{sys} + b_{IF,avg}^r - b_{IF,avg}^g \\ &= cdt'^g + (cdt_{sys} + b_{IF,avg}^r - b_{IF,avg}^g) \\ &= cdt'^g + cdt'_{sys} \end{aligned} \quad (4.4.18)$$

where cdt'_{sys} is a single sum of the real GPS-GLONASS system time difference and a bias term ($b_{IF,avg}^r - b_{IF,avg}^g$). Applying Equation (4.4.18) into Equations (4.4.14) and (4.4.15) and rewriting Equations (4.4.12) and (4.4.13) results in the following code pseudorange and carrier phase observation equations:

$$P'_{IF}{}^g = \rho_g + cdt'{}^g + d_{trop}^g + \varepsilon_{P_{IF}}^g \quad (4.4.19)$$

$$\Phi'_{IF}{}^g = \rho_g + cdt'{}^g + d_{trop}^g + N'_{IF}{}^g + \varepsilon_{\Phi_{IF}}^g \quad (4.4.20)$$

$$P'_{IF}{}^r = \rho_r + cdt'{}^g + cdt'_{sys} + d_{trop}^r + \varepsilon_{P_{IF}}^r \quad (4.4.21)$$

$$\Phi'_{IF}{}^r = \rho_r + cdt'{}^g + cdt'_{sys} + d_{trop}^r + N'_{IF}{}^r + \varepsilon_{\Phi_{IF}}^r \quad (4.4.22)$$

The traditional GPS/GLONASS observation model consists of Equations (4.4.19) to (4.4.22). For the sake of convenience, $cdt'{}^g$ is simply regarded as the receiver clock offset and cd'_{sys} is simply regarded as the GPS-GLONASS system time difference.

The unknown parameters in the above observation model include three-dimension station coordinates, one receiver clock offset and one system time difference parameter, one zenith wet tropospheric delay, and ambiguity parameters equal to the number of observed GPS and GLONASS satellites. The dry tropospheric delay error is first corrected using Hopfield tropospheric model and the zenith wet tropospheric delay (ZWD) is then considered as an unknown. The Niell Mapping Functions are used as hydrostatic and wet mapping functions.

4.4.2 Combined GPS/GLONASS UofC Model

The P code pseudorange and carrier phase observations on L1 and L2 between a receiver and a satellite for GPS and GLONASS as expressed in Equations (4.4.4) to (4.4.7) are rewritten in the following:

$$P_i^r = \rho_r + (cdt^r + b_{i,avg}^r) - cdT^r + d_{orb}^r + d_{trop}^r + d_{ion/L_i}^r + d_{mult/P_i}^r + \varepsilon_{P_i}^r \quad (4.4.23)$$

$$\Phi_i^r = \rho_r + (cdt^r + b_{i,avg}^r) - cdT^r + d_{orb}^r + d_{trop}^r - d_{ion/L_i}^r + \lambda_i^r N_i^r + d_{mult/\Phi_i}^r + \delta_{i/\Phi}^r + \varepsilon_{\Phi_i}^r \quad (4.4.24)$$

$$P_i^g = \rho_g + (cdt^g + b_{i,avg}^g) - cdT^g + d_{orb}^g + d_{trop}^g + d_{ion/L_i}^g + d_{mult/P_i}^g + \varepsilon_{P_i}^g \quad (4.4.25)$$

$$\Phi_i^g = \rho_g + (cdt^g + b_{i,avg}^g) - cdT^g + d_{orb}^g + d_{trop}^g - d_{ion/L_i}^g + \lambda_i^g N_i^g + d_{mult/\Phi_i}^g + \delta_{i/\Phi}^g + \varepsilon_{\Phi_i}^g \quad (4.4.26)$$

The ionospheric delay bias is removed by constructing the ionosphere-free code-phase and phase-phase observation combinations from the L1 and L2 data. After applying the precise satellite orbit and clock corrections, the satellite orbit and clock errors are neglected and the ionosphere-free observation combinations for GPS and GLONASS may be expressed as:

$$\begin{aligned} P_{IF,L1}^g &= 0.5(P_1^g + \Phi_1^g) \\ &= \rho^g + (cdt^g + b_{avg}^g) + d_{trop}^g + 0.5(\lambda_1^g N_1^g + \delta_{L1}^g) + 0.5\varepsilon_{P_{IF,L1}}^g \end{aligned} \quad (4.4.27)$$

$$\begin{aligned} P_{IF,L2}^g &= 0.5(P_2^g + \Phi_2^g) \\ &= \rho^g + (cdt^g + b_{avg}^g) + d_{trop}^g + 0.5(\lambda_2^g N_2^g + \delta_{L2}^g) + 0.5\varepsilon_{P_{IF,L2}}^g \end{aligned} \quad (4.4.28)$$

$$\begin{aligned} \Phi_{IF}^g &= \frac{f_{1g}^2 \cdot \Phi_1^g - f_{2g}^2 \cdot \Phi_2^g}{f_{1g}^2 - f_{2g}^2} \\ &= \rho^g + (cdt^g + b_{avg}^g) + d_{trop}^g + \frac{f_{1g}^2}{f_{1g}^2 - f_{2g}^2} \cdot (\lambda_1^g N_1^g + \delta_{L1}^g) - \frac{f_{2g}^2}{f_{1g}^2 - f_{2g}^2} \cdot (\lambda_2^g N_2^g + \delta_{L2}^g) + \varepsilon_{\Phi_{IF}}^g \end{aligned} \quad (4.4.29)$$

$$\begin{aligned}
P'_{IF,L1} &= 0.5(P_1^r + \Phi_1^r) \\
&= \rho^r + (cdt^r + b_{avg}^r) + d_{trop}^r + 0.5(\lambda_1^r N_1^r + \delta b_{L1}^r) + 0.5\epsilon_{P_{IF,L1}}^r
\end{aligned} \tag{4.4.30}$$

$$\begin{aligned}
P'_{IF,L2} &= 0.5(P_2^r + \Phi_2^r) \\
&= \rho^r + (cdt^r + b_{avg}^r) + d_{trop}^r + 0.5(\lambda_2^r N_2^r + \delta b_{L2}^r) + 0.5\epsilon_{P_{IF,L2}}^r
\end{aligned} \tag{4.4.31}$$

$$\begin{aligned}
\Phi_{IF}^r &= \frac{f_{1r}^2 \cdot \Phi_1^r - f_{2r}^2 \cdot \Phi_2^r}{f_{1r}^2 - f_{2r}^2} \\
&= \rho^r + (cdt^r + b_{avg}^r) + d_{trop}^r + \frac{f_{1r}^2}{f_{1r}^2 - f_{2r}^2} \cdot (\lambda_1^r N_1^r + \delta b_{L1}^r) - \frac{f_{2r}^2}{f_{1r}^2 - f_{2r}^2} \cdot (\lambda_2^r N_2^r + \delta b_{L2}^r) + \epsilon_{\Phi_{IF}}^r
\end{aligned} \tag{4.4.32}$$

Similarly to the combined GPS/GLONASS traditional model, the bias δb_{L1} , δb_{L2} are not separable from the ambiguity N_1 and N_2 since the ambiguity parameters will be estimated as float values. In addition, this average delay bias b_{avg} will be absorbed into the receiver clock offset term in the practical processing. A GLONASS receiver clock offset can be expressed as a function of the GPS receiver clock offset and the GPS-GLONASS system time difference, as shown in Equation (4.4.18). Equations (4.4.27) to (4.4.32) may simply be rewritten as:

$$P'_{IF,L1}^g = \rho^g + c \cdot dt'^g + d_{trop}^g + 0.5N_1'^g + 0.5\epsilon_{P_{IF,L1}}^g \tag{4.4.33}$$

$$P'_{IF,L2}^g = \rho^g + c \cdot dt'^g + d_{trop}^g + 0.5N_2'^g + 0.5\epsilon_{P_{IF,L2}}^g \tag{4.4.34}$$

$$\Phi_{IF}^g = \rho^g + c \cdot dt'^g + d_{trop}^g + \frac{f_{1g}^2}{f_{1g}^2 - f_{2g}^2} \cdot N_1'^g - \frac{f_{2g}^2}{f_{1g}^2 - f_{2g}^2} \cdot N_2'^g + \epsilon_{\Phi_{IF}}^g \tag{4.4.35}$$

$$P'_{IF,L1}^r = \rho^r + cdt'^g + cdt'_{sys} + d_{trop}^r + 0.5N_1'^r + 0.5\epsilon_{P_{IF,L1}}^r \tag{4.4.36}$$

$$P'_{IF,L2}^r = \rho^r + cdt'^g + dt'_{sys} + d_{trop}^r + 0.5N_2'^r + 0.5\epsilon_{P_{IF,L2}}^r \tag{4.4.37}$$

$$\Phi_{IF}^{\prime r} = \rho^r + cdt^{\prime g} + cdt_{\text{sys}}^{\prime} + d_{\text{trop}}^r + \frac{f_{1r}^2}{f_{1r}^2 - f_{2r}^2} \cdot N_1^{\prime r} - \frac{f_{1r}^2}{f_{1r}^2 - f_{2r}^2} \cdot N_2^{\prime r} + \epsilon_{\Phi_{IF}}^{\prime r} \quad (4.4.38)$$

where

$cdt^{\prime g}$ is the sum of the receiver clock offset cdt^g and the average hardware delay bias

b_{avg}^g in metres;

$N_1^{\prime g}$ is the sum of the GPS ambiguity term $\lambda_1^g N_1^g$ and the satellite-dependent hardware delay bias δb_{L1}^g in metres on L1;

$N_2^{\prime g}$ is the sum of the GPS ambiguity term $\lambda_2^g N_2^g$ and the satellite-dependent hardware delay bias δb_{L2}^g in metres on L2;

$N_1^{\prime r}$ is the sum of the GLONASS ambiguity term $\lambda_1^r N_1^r$ and the satellite-dependent hardware delay bias δb_{L1}^r in metres on L1;

$N_2^{\prime r}$ is the sum of the GLONASS ambiguity term $\lambda_2^r N_2^r$ and the satellite-dependent hardware delay bias δb_{L2}^r in metres on L2;

$cdt_{\text{sys}}^{\prime}$ is a single sum of the real GPS-GLONASS system time difference in the unit of length and a bias term $(b_{\text{avg}}^r - b_{\text{avg}}^g)$.

The GPS/GLONASS UofC observation model consists of Equations (4.4.33) to (4.4.38). The unknown parameters in the above observation model include three station coordinate components, one receiver clock offset, one system time difference, one zenith wet tropospheric delay, and ambiguity parameters equal to twice the number of visible satellites. The dry tropospheric delay error is first corrected using Hopfield tropospheric

model and the zenith wet tropospheric delay (ZWD) is then considered as an unknown.

The Niell Mapping Functions are used as hydrostatic and wet mapping functions.

4.5 Stochastic Modeling

The stochastic model describes the statistical properties of the measurements, which are mainly defined by an appropriate covariance matrix (Satirapod, 2004). To employ the Kalman filter method, the stochastic models of both measurements and parameters need to be defined. Many researchers have emphasized the importance of proper stochastic models, especially for high-accuracy applications (Barnes et al., 1998; Han, 1997; Wang, 1999). The stochastic models in the combined GPS and GLONASS PPP have been developed and presented in this section. The stochastic model of measurements mainly describes the observations' covariance, while the stochastic model of parameters describes the kinematic behavior and the variation of the parameters with time.

4.5.1 Stochastic Model of Measurements

4.5.1.1 Traditional Model

The observations used in the traditional model consist of ionosphere-free code and phase observations. Their linear combination forms are given in the following:

$$P_{IF} = (f_1^2 \cdot P_1 - f_2^2 \cdot P_2) / (f_1^2 - f_2^2) \quad (4.5.1)$$

$$\Phi_{IF} = (f_1^2 \cdot \Phi_1 - f_2^2 \cdot \Phi_2) / (f_1^2 - f_2^2) \quad (4.5.2)$$

where P_1 and P_2 are the measured code pseudorange observations in metres on L1 and L2, respectively; Φ_1 and Φ_2 are the measured carrier phase observations in metres on L1 and L2, respectively; f_1 and f_2 are the frequency on L1 and L2.

Assume there is no correlation between the measurements on L1 and L2, the variance of the combined ionosphere-free observations can be obtained according to the rule of error propagation as follows:

GPS observations:

$$\sigma_{P_{IF}}^2 = \left(\frac{f_1^2}{f_1^2 - f_2^2} \right)^2 \sigma_{P_1}^2 + \left(\frac{f_2^2}{f_1^2 - f_2^2} \right)^2 \sigma_{P_2}^2 = 6.481\sigma_{P_1}^2 + 2.389\sigma_{P_2}^2 \quad (4.5.3)$$

$$\sigma_{\Phi_{IF}}^2 = \left(\frac{f_1^2}{f_1^2 - f_2^2} \right)^2 \sigma_{\Phi_1}^2 + \left(\frac{f_2^2}{f_1^2 - f_2^2} \right)^2 \sigma_{\Phi_2}^2 = 6.481\sigma_{\Phi_1}^2 + 2.389\sigma_{\Phi_2}^2 \quad (4.5.4)$$

GLONASS observations:

$$\sigma_{P_{IF}}^2 = \left(\frac{f_1^2}{f_1^2 - f_2^2} \right)^2 \sigma_{P_1}^2 + \left(\frac{f_2^2}{f_1^2 - f_2^2} \right)^2 \sigma_{P_2}^2 = 6.407\sigma_{P_1}^2 + 2.345\sigma_{P_2}^2 \quad (4.5.5)$$

$$\sigma_{\Phi_{IF}}^2 = \left(\frac{f_1^2}{f_1^2 - f_2^2} \right)^2 \sigma_{\Phi_1}^2 + \left(\frac{f_2^2}{f_1^2 - f_2^2} \right)^2 \sigma_{\Phi_2}^2 = 6.407\sigma_{\Phi_1}^2 + 2.345\sigma_{\Phi_2}^2 \quad (4.5.6)$$

where $\sigma_{P_1}^2$, $\sigma_{P_2}^2$ are the variance of P code observations on L1 and L2, respectively;

$\sigma_{\Phi_1}^2$, $\sigma_{\Phi_2}^2$ are the variance of carrier phase observations on L1 and L2, respectively. The

covariance matrix in traditional model is diagonal.

4.5.1.2 UofC Model

The observations used in the UofC model consist of the combined ionosphere-free code-phase observation for each frequency channel, and phase-phase observations from L1 and L2 data. Their observation combinations are given in the following:

$$P_{IF,L1} = 0.5(P_1 + \Phi_1) \quad (4.5.7)$$

$$P_{IF,L2} = 0.5(P_2 + \Phi_2) \quad (4.5.8)$$

$$\Phi_{IF} = \frac{f_1^2 \cdot \Phi_1 - f_2^2 \cdot \Phi_2}{f_1^2 - f_2^2} \quad (4.5.9)$$

The variance of the combined ionosphere-free observations can be obtained according to the rule of error propagation as follows:

GPS observations:

$$\sigma_{P_{IF1}}^2 = 0.25\sigma_{P_1}^2 + 0.25\sigma_{\Phi_1}^2 \quad (4.5.10)$$

$$\sigma_{P_{IF2}}^2 = 0.25\sigma_{P_2}^2 + 0.25\sigma_{\Phi_2}^2 \quad (4.5.11)$$

$$\sigma_{\Phi_{IF}}^2 = \left(\frac{f_1^2}{f_1^2 - f_2^2} \right)^2 \sigma_{\Phi_1}^2 + \left(\frac{f_2^2}{f_1^2 - f_2^2} \right)^2 \sigma_{\Phi_2}^2 = 6.481\sigma_{\Phi_1}^2 + 2.389\sigma_{\Phi_2}^2 \quad (4.5.12)$$

$$\sigma_{P_{IF1}P_{IF2}} = \sigma_{P_{IF2}P_{IF1}} = 0 \quad (4.5.13)$$

$$\begin{aligned} \sigma_{P_{IF1}\Phi_{IF}} &= [0.5 \quad 0] \begin{bmatrix} \sigma_{\Phi_1}^2 & 0 \\ 0 & \sigma_{\Phi_2}^2 \end{bmatrix} \begin{bmatrix} \frac{f_1^2}{f_1^2 - f_2^2} & \frac{-f_2^2}{f_1^2 - f_2^2} \end{bmatrix}^T \\ &= 0.5 \frac{f_1^2}{f_1^2 - f_2^2} \sigma_{\Phi_1}^2 \\ &= 1.273 \sigma_{\Phi_1}^2 \end{aligned} \quad (4.5.14)$$

$$\sigma_{\Phi_{IF}P_{IF1}} = \sigma_{P_{IF1}\Phi_{IF}} = 1.273\sigma_{\Phi_1}^2 \quad (4.5.15)$$

$$\begin{aligned}
\sigma_{P_{IF2}\Phi_{IF}} &= [0 \quad 0.5] \begin{bmatrix} \sigma_{\Phi_1}^2 & 0 \\ 0 & \sigma_{\Phi_2}^2 \end{bmatrix} \begin{bmatrix} \frac{f_1^2}{f_1^2 - f_2^2} & \frac{-f_2^2}{f_1^2 - f_2^2} \end{bmatrix}^T \\
&= -0.5 \frac{f_2^2}{f_1^2 - f_2^2} \sigma_{\Phi_2}^2 \\
&= -0.773 \sigma_{\Phi_2}^2
\end{aligned} \tag{4.5.16}$$

$$\sigma_{\Phi_{IF}P_{IF2}} = \sigma_{P_{IF2}\Phi_{IF}} = -0.773 \sigma_{\Phi_2}^2 \tag{4.5.17}$$

GLONASS observations:

$$\sigma_{P_{IF1}}^2 = 0.25 \sigma_{P_1}^2 + 0.25 \sigma_{\Phi_1}^2 \tag{4.5.18}$$

$$\sigma_{P_{IF2}}^2 = 0.25 \sigma_{P_2}^2 + 0.25 \sigma_{\Phi_2}^2 \tag{4.5.19}$$

$$\sigma_{\Phi_{IF}}^2 = 6.407 \sigma_{\Phi_1}^2 + 2.345 \sigma_{\Phi_2}^2 \tag{4.5.20}$$

$$\sigma_{P_{IF1}P_{IF2}} = \sigma_{P_{IF2}P_{IF1}} = 0 \tag{4.5.21}$$

$$\sigma_{P_{IF1}\Phi_{IF}} = \sigma_{\Phi_{IF}P_{IF1}} = 1.266 \sigma_{\Phi_1}^2 \tag{4.5.22}$$

$$\sigma_{P_{IF2}\Phi_{IF}} = \sigma_{\Phi_{IF}P_{IF2}} = -0.766 \sigma_{\Phi_2}^2 \tag{4.5.23}$$

where $\sigma_{P_1}^2, \sigma_{P_2}^2$ are the variance of P code observations on L1 and L2, respectively;

$\sigma_{\Phi_1}^2, \sigma_{\Phi_2}^2$ are the variance of carrier phase observations on L1 and L2, respectively. The

covariance matrix for each satellite's observations in the UofC model can be expressed as:

$$Q = \begin{bmatrix} \sigma_{P_{IF1}}^2 & \sigma_{P_{IF1}P_{IF2}} & \sigma_{P_{IF1}\Phi_{IF}} \\ \sigma_{P_{IF2}P_{IF1}} & \sigma_{P_{IF2}}^2 & \sigma_{P_{IF2}\Phi_{IF}} \\ \sigma_{\Phi_{IF}P_{IF1}} & \sigma_{\Phi_{IF}P_{IF2}} & \sigma_{\Phi_{IF}}^2 \end{bmatrix} \tag{4.5.24}$$

4.5.2 Stochastic Model of Parameters

The combined GPS and GLONASS PPP can be implemented using the Kalman filter parameter estimation method. The unknown parameters in the combined GPS/GLONASS traditional model and UofC model include three position coordinates, one receiver clock offset, one GPS-GLONASS system time difference, one zenith wet tropospheric delay, and ambiguity parameters. The coordinate components, receiver clock offset, system time difference and zenith wet tropospheric delay may be simply modeled as Random Walk, while the ambiguity parameters are treated as constants. The transition and noise matrices are given in this section.

Using the Kalman filter estimation method, the differential equation of the system dynamic for Random Walk is given as follows (Gao, 2005):

$$\dot{x}(t) = w(t), q(t) \quad (4.5.25)$$

$$Q = \int_0^{\Delta t} \Phi(t) q(t) \Phi^T(t) dt \quad (4.5.26)$$

where

$x(t)$ is the state vector;

$w(t)$ is the white noise;

$q(t)$ is the spectral density;

Q is the process noise matrix;

$\Phi(t)$ is the transition matrix.

The state vectors for the traditional and UofC models when with combined GPS/GLONASS data are provided in the following:

$$x_{traditional} = \left\{ \delta\phi, \delta\lambda, \delta h, \delta dt, \delta dt_{sys}, \delta d_{trop}, \delta N_1^g, \dots, \delta N_n^g, \delta N_1^r, \dots, \delta N_m^r \right\}^T \quad (4.5.27)$$

$$x_{UofC} = \left\{ \delta\phi, \delta\lambda, \delta h, \delta dt, \delta dt_{sys}, \delta d_{trop}, \delta N_1^g, \dots, \delta N_{2n}^g, \delta N_1^r, \dots, \delta N_{2m}^r \right\}^T \quad (4.5.28)$$

where $\delta\phi, \delta\lambda, \delta h$ are positions in latitude, longitude and height components; δdt is the receiver clock offset; δdt_{sys} is the system time difference; δd_{trop} is the zenith wet tropospheric delay component; δN represents the ambiguity; n and m are the number of GPS and GLONASS satellites, respectively. Comparing Equation (4.5.27) and (4.5.28), it is noted that more ambiguities need to be estimated in the combined GPS/GLONASS UofC model than the combined GPS/GLONASS traditional model.

The position parameters may be modeled as a Random Walk process. The transition matrix for position coordinates is an identity matrix. The process noise matrix is given as follows (Abdel-salam, 2005):

$$Q_{position} = \begin{bmatrix} \frac{q_\phi \Delta t}{(R_m + h)^2} & 0 & 0 \\ 0 & \frac{q_\lambda \Delta t}{(R_n + h)^2 \cos^2 \phi} & 0 \\ 0 & 0 & q_h \Delta t \end{bmatrix} \quad (4.5.29)$$

where

q_ϕ, q_λ, q_h are spectral density of positions in latitude, longitude and height components;

R_m, R_n are the Earth radius in meridian and prime meridian directions;

h is the station height above the ellipsoid;

Δt is the time increment;

ϕ is the latitude of a station.

Similarly, the receiver clock offset, zenith wet tropospheric delay and system time difference parameters may be modeled as a Random Walk process. The transition matrix of these parameters is still an identity matrix and the process noise matrices for these parameters are given as follows, respectively:

$$Q_{clock} = [q_{dt} \Delta t] \quad (4.5.30)$$

$$Q_{trop} = [q_{trop} \Delta t] \quad (4.5.31)$$

$$Q_{Tsys} = [q_{Tsys} \Delta t] \quad (4.5.32)$$

where q_{dt} is the spectral density of the receiver clock; q_{trop} is the spectral density of the zenith wet tropospheric delay; q_{Tsys} is the spectral density of the system time difference.

Chapter Five: Results and Analysis

To assess the performance of the combined GPS and GLONASS PPP models in both static and kinematic processing modes, numerical computations were conducted and their results are presented in this chapter. This chapter starts with an introduction to the development of the combined GPS and GLONASS PPP software package. Then the static and kinematic processing results are presented using the combined GPS/GLONASS traditional PPP model.

5.1 Software Development

P^3 is a software package that implements the PPP technology, providing users centimetre to decimetre accuracies with a single GPS receiver. It was developed in the Department of Geomatics Engineering at the University of Calgary. Since the current version of the P^3 software package does not include a function of the combined GPS and GLONASS PPP, a new version of the P^3 software package has been developed to enable the processing of the combined GPS/GLONASS data. The software package starts with a single main screen where some information is displayed during the data processing, such as the parameter estimation results, observation residuals, satellite elevation and azimuth angle, converging process of the static or kinematic solutions, and acceptance or rejection status of the satellite observations. The main screen of the P^3 software package is shown in Figure 5-1.

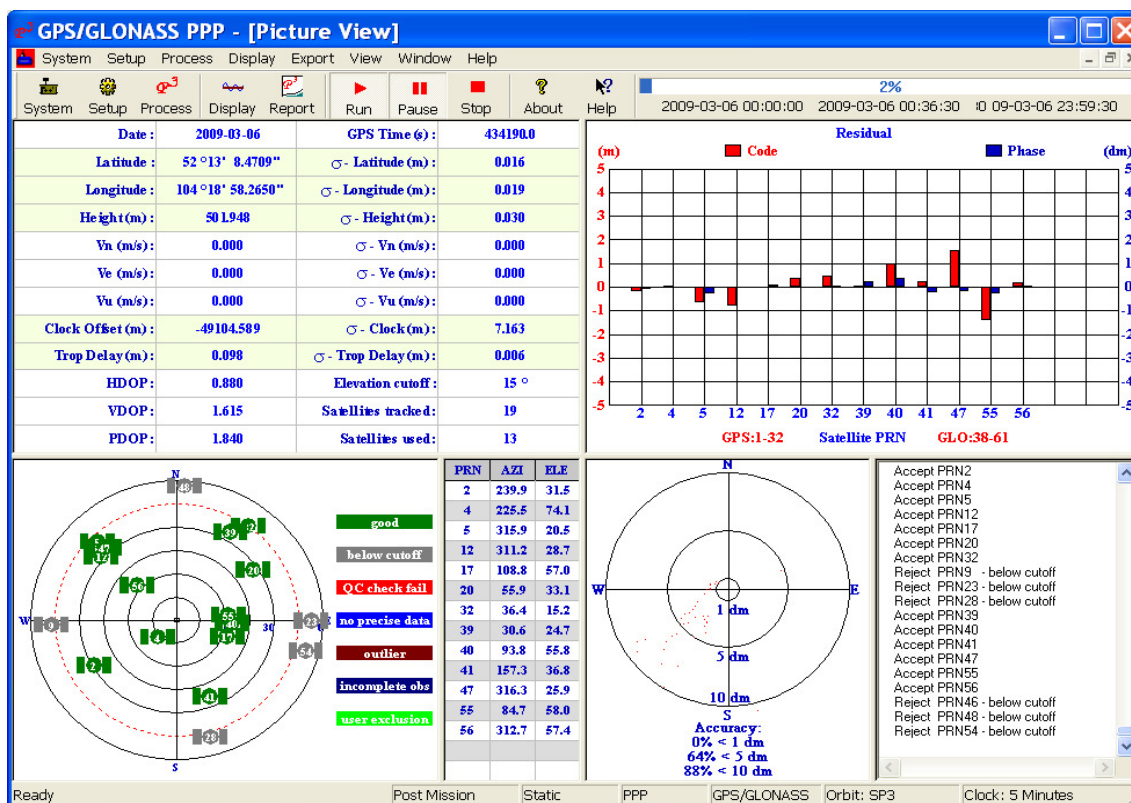


Figure 5-1 Main Screen of P³ Software Package

Various processing result graphs can be activated after the processing is completed, including: (a) position errors with respect to initial coordinates in a static mode; (b) trajectory in a kinematic mode; (c) number of GPS or GLONASS satellites used in data processing; (d) various dilutions of precision; (e) receiver clock offset; (f) GPS-GLONASS system time difference estimates; (g) zenith tropospheric delay. Figure 5-2 displays some results of the parameter estimation in the combined GPS and GLONASS PPP.

This new version of P³ is also compatible with the processing of only GPS observations. Further development will make the P³ software package be able to process GLONASS-only observations when sufficient GLONASS observations become available.

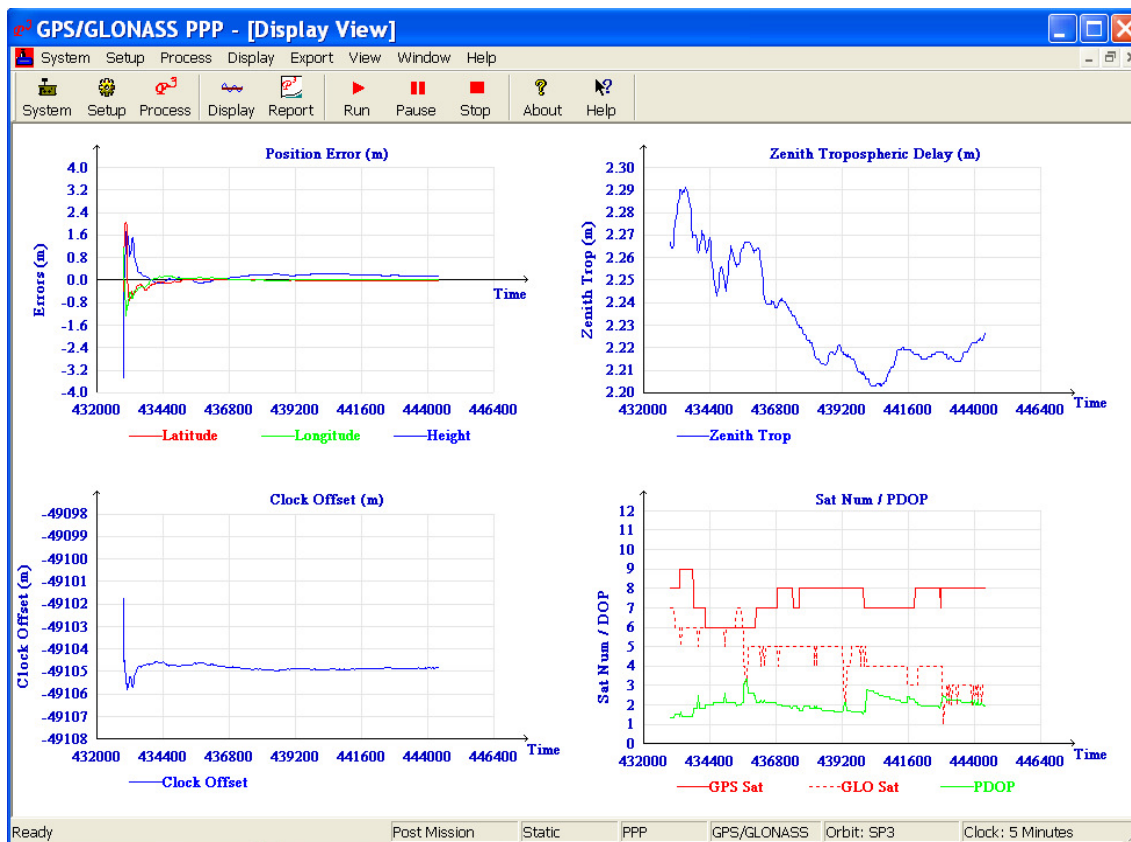


Figure 5-2 Processing Result Graphs

The basic procedure of the combined GPS and GLONASS PPP processing is illustrated in Figure 5-3. First of all, the combined GPS/GLONASS measurement data and precise satellite orbit and clock corrections are needed before the data processing. The entire processing starts with the data pre-processing, such as the cycle slip detection of carrier phase observations, initial station coordinate computation, and initial ambiguity determination. Afterwards, various error corrections are made including corrections to some conventional errors and some others specific to PPP. The Kalman filter method is used to estimate the unknown parameters. The functional and stochastic models of the combined GPS and GLONASS PPP have been implemented in this module with outputs

including the station coordinates, receiver clock offset, zenith tropospheric delay, and GPS-GLONASS system time difference estimates.

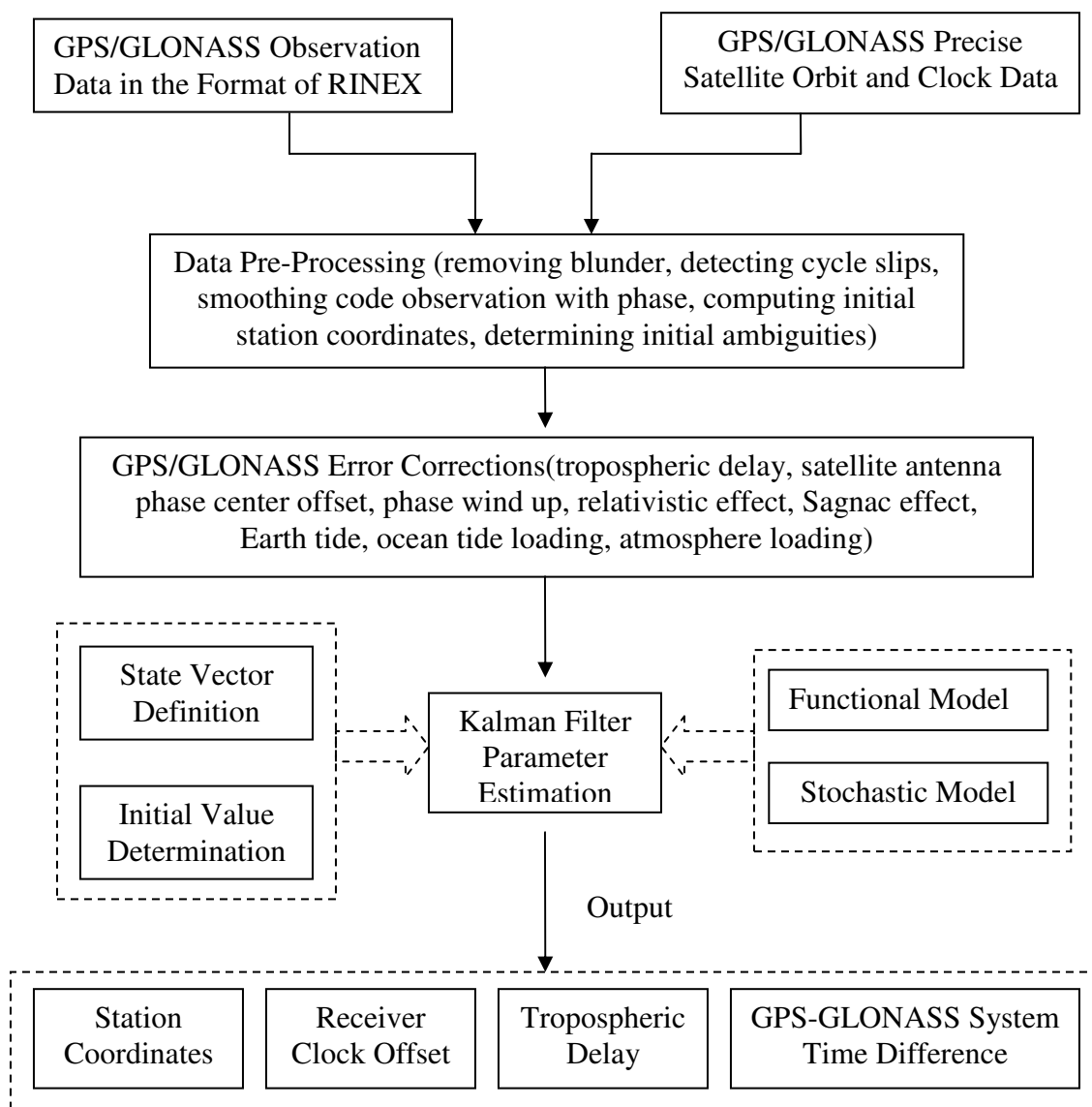


Figure 5-3 Basic Procedure of Combined GPS/GLONASS PPP Processing

5.2 Data Description

GPS/GLONASS observation datasets collected on March 6, 2009 from seven IGS permanent stations, including IRKJ, CONZ, RCMN, UNBJ, ANKR, LHAZ and NTUS were used for the numerical computation. These stations are equipped with dual-frequency GPS/GLONASS receivers and are distributed globally as seen in Figure 5-4. Table 5-1 shows a list of these stations as well as the receiver and antenna types.

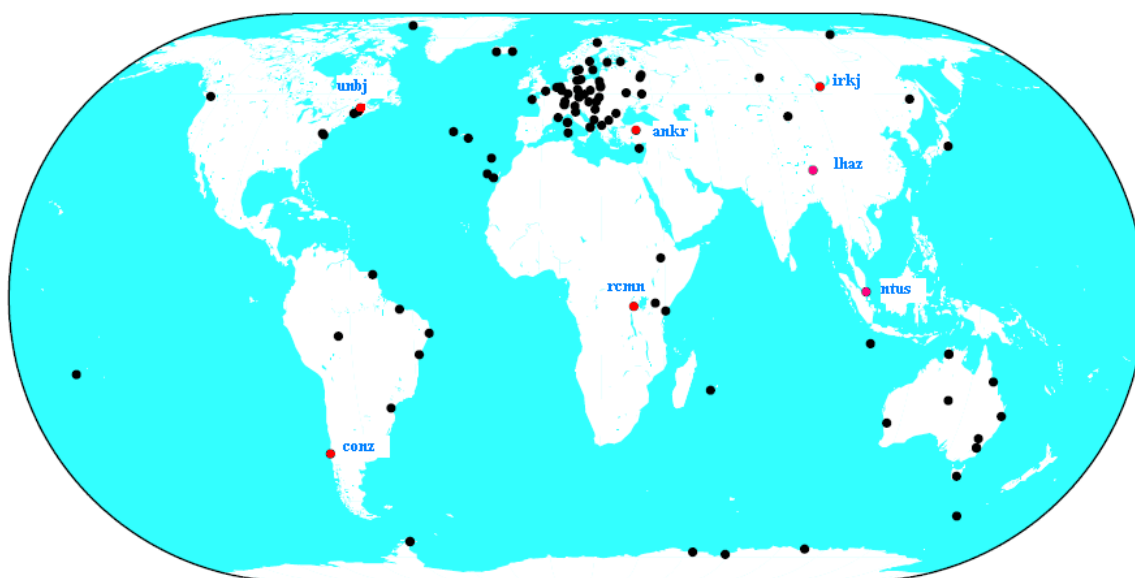


Figure 5-4 GPS/GLONASS Stations in the IGS Tracking Network

Table 5-1 GPS/GLONASS Stations

Station	Receiver type	Antenna type
IRKJ	JPS LEGACY	JPSREGANT_SD_E NONE
CONZ	TPS E_GGD	TPSCR3_GGD CONE
RCMN	LEICA GRX1200GGPRO	LEIAT504GG
UNBJ	TPS LEGACY	JPSREGANT_DD_E
ANKR	TPS E_GGD	TPSCR3_GGD CONE
LHAZ	TPS E_GGD	ASH701941.B SNOW
NTUS	LEICA GRX1200GGPRO	LEIAT504GG NONE

The mixed GPS/GLONASS precise satellite orbit data at an interval of 15 minutes and 5-minute clock data generated by IAC (Information-analytical center) were downloaded from the IAC website and used to remove the orbit and clock errors. The data sampling rate was 30s and the elevation mask was set to 15 degrees. In the Kalman filter estimation, the coordinate components, zenith wet tropospheric delay, receiver clock offset, and GPS-GLONASS system time difference parameters are modeled as Random Walk processes while a constant process is used for all the ambiguities. In the static processing, the spectral density of $0 \text{ m}^2 / \text{sec}$ was used for the horizontal and vertical coordinate components. The spectral density of the zenith wet tropospheric delay is set to $10^{-9} \text{ m}^2 / \text{sec}$ while the spectral density values of $10^5 \text{ m}^2 / \text{sec}$ and $10^{-7} \text{ m}^2 / \text{sec}$ are used for the receiver clock and system time difference parameters, respectively (PMIS, 2005).

5.3 Parameter Estimation Results and Analysis

To analyze the results of the combined GPS and GLONASS PPP, a two-hour dataset collected at IRKJ on March 6, 2009 is chosen randomly to estimate the station position. The detailed information such as the satellite number, PDOP, observation residuals and parameter estimation results during the data processing is provided to demonstrate how this combined GPS and GLONASS PPP model works in this section. The GPS only and mixed GPS/GLONASS observations were processed, respectively. The site coordinates from CODE Analysis Centers were used as true coordinates to assess the accuracy of PPP. The three-dimension station coordinate estimates have been converted to position discrepancies in north, east, and up components with respect to the true coordinates.

Figure 5-5 shows the precise point positioning errors at IRKJ station using the GPS observations and combined GPS/GLONASS observations. It can be clearly observed that the position errors for the GPS only and mixed GPS/GLONASS processing are at a quite similar level in the east, north, and up directions. After half an hour, the positioning errors in both east and north directions converge to a centimetre level while longer time is needed for the vertical component. The convergence time of the east and north coordinate components in the combined GPS/GLONASS processing is shorter than that of the GPS-only processing. However, no improvement of the convergence time is found in the vertical coordinate component. Table 5-2 shows the mean, RMS, and standard deviation (one-sigma) of the converged position errors based on the statistical results from 1:30 to 2:00. The RMS differences in all three coordinate components are less than 1 cm for the GPS and combined GPS/GLONASS processing. In order to help analyze the results, more processing details are provided in the following.

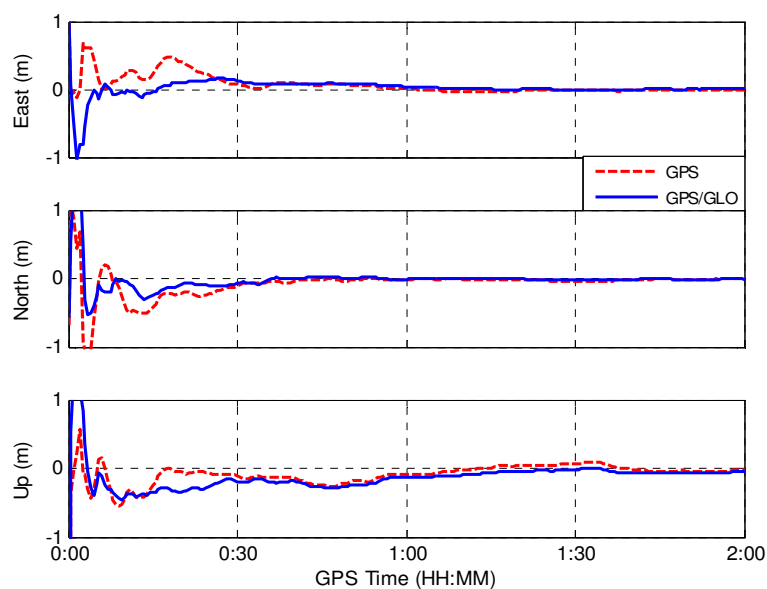


Figure 5-5 GPS Only vs. GPS/GLONASS Positioning Errors

Table 5-2 Statistics of Position Results (m)

		GPS Only	GPS/GLONASS
Mean	East	-0.011	-0.003
	North	-0.023	-0.016
	Up	-0.005	-0.051
STD	East	0.005	0.006
	North	0.015	0.008
	Up	0.046	0.022
RMS	East	0.012	0.006
	North	0.027	0.018
	Up	0.046	0.055

Shown in Figure 5-6 is the number of satellites used in the data processing and the corresponding HDOP and VDOP values. The number of satellites at each epoch and the satellite geometry as illustrated by the DOP can provide valuable information for the analysis, especially when problems occur. The computation of the DOP in the combined GPS/GLONASS processing is based on the design matrix with respect to three position components, one receiver clock offset and one system time difference, which has one more column when compared with the design matrix for the DOP computation in the GPS-only processing. During the entire test period, the number of satellites used ranges between six and nine in the GPS-only processing and changes between nine and fifteen in the combined GPS/GLONASS processing. The observations from approximately seven GPS satellites and five GLONASS satellites on average are processed.

As can be seen from Figures 5-5 and 5-6, the improvement of the HDOP and VDOP during the first fourteen minutes after adding GLONASS satellites is not considerable. As a result, the improvement of the positioning results during this period of time is not significant. However, the large drop of the HDOP brings a significant improvement on positioning errors in the both east and north directions from 0:14 to

0:30. However, the decrease of the VDOP does not bring an improvement of the positioning errors in the up direction. This is because the residual GLONASS ranging errors have a greater effect in the vertical component after GLONASS observations are introduced. Longer time needed to reach a convergence value for the vertical component even after adding GLONASS observations is due to relatively poorer satellite geometry in the up direction as seen in Figure 5-6.

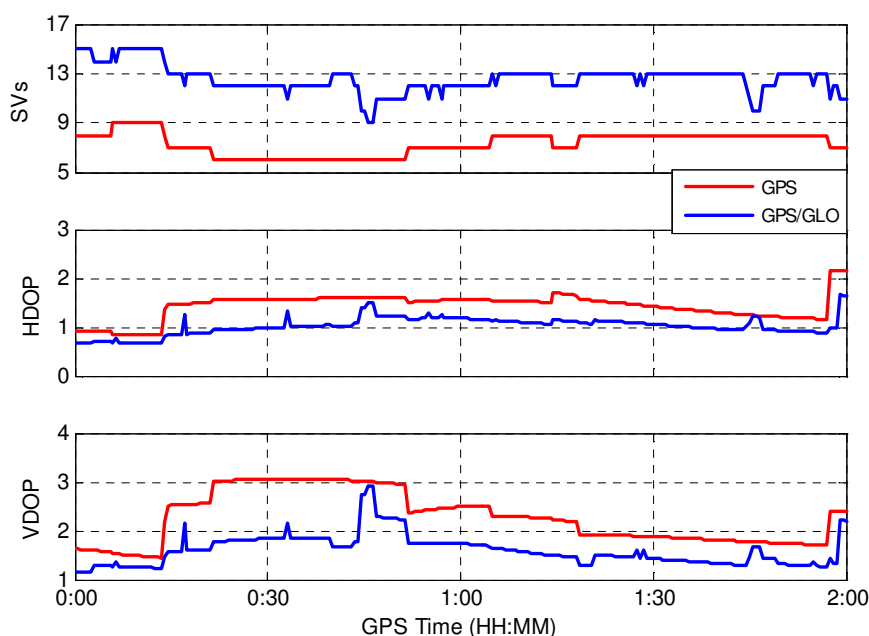


Figure 5-6 Satellite Number Used and DOP

Figure 5-7 displays the residuals of the ionosphere-free code and carrier phase observations at a certain epoch. The elevation angles of the satellites observed in Figure 5-7 can be found in Figure 5-8. The residuals of the code observations are in the unit of metres, while the residuals of the carrier phase observations are expressed in the unit of decimetres. The GPS satellites are numbered from 1 to 32, while GLONASS satellites

have the number from 38 to 61. At this epoch, observations from seven GPS satellites and five GLONASS satellites are processed. It is clear that the maximum code observation residual comes from the GPS satellite of PRN 32. This is because of the lower elevation of this satellite, as can be seen from Figure 5-8. Normally, the observations from low elevation satellites have comparatively larger residuals due to greater effect of remaining observation errors like the atmospheric delay, multipath, and measurement noise. It is observed that GLONASS phase observations have larger residuals than the GPS phase observations at this epoch, which is due to the relatively lower accuracy of the GLONASS precise orbit and clock products.

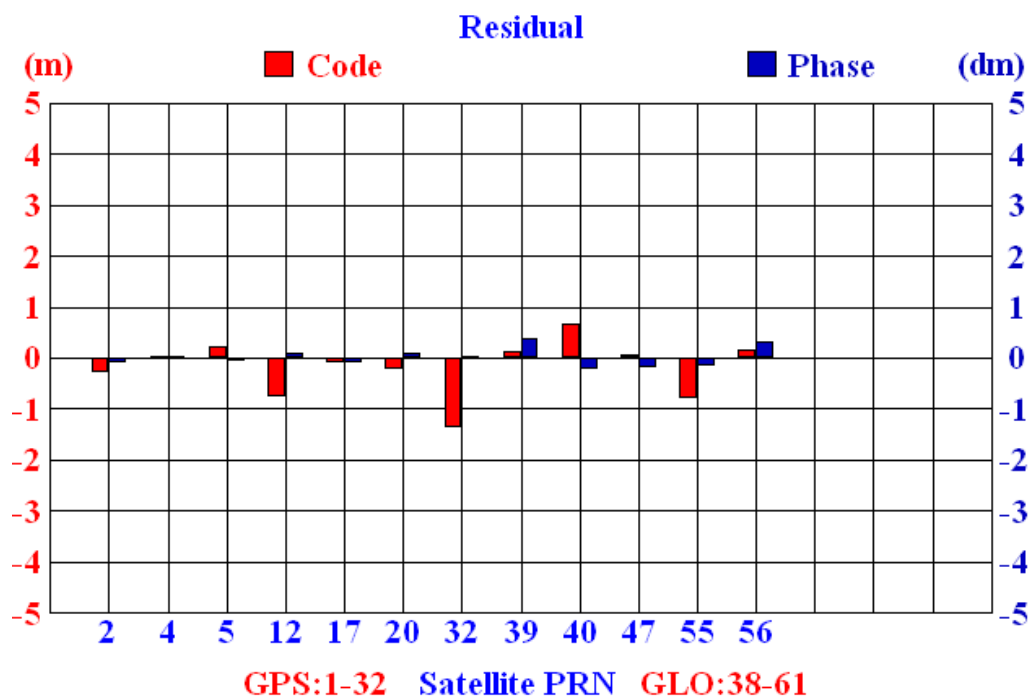


Figure 5-7 Observation Residuals at a Certain Epoch

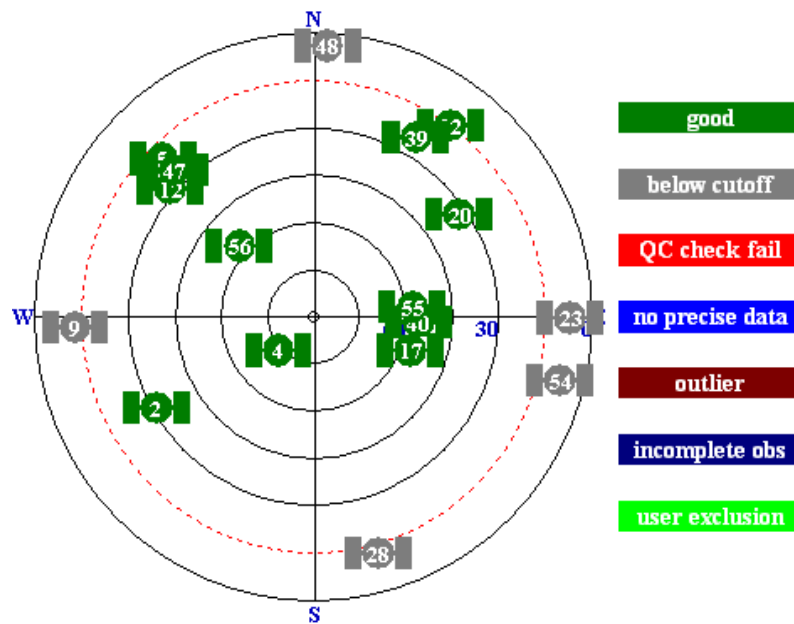


Figure 5-8 Satellite Sky Plot at a Certain Epoch

Figures 5-9 and 5-10 show the residuals of ionosphere-free code and phase observations for all satellites in the combined GPS/GLONASS processing during the entire test period, respectively. As mentioned above, the satellites with the lower elevations usually have the larger residuals and therefore an elevation dependent weight strategy has been utilized in the implementation of the Kalman filter. Consequently the larger residuals caused by observations with lower elevation angles will not cause a big impact on the positioning results. However this is not always true that observations with larger residuals come from the low elevation satellites since the large residuals may be caused by other error sources such as the residual satellite orbit and clock errors. Therefore analyzing the residuals to assess the quality of ranging measurements should be conducted after some error corrections have been applied.

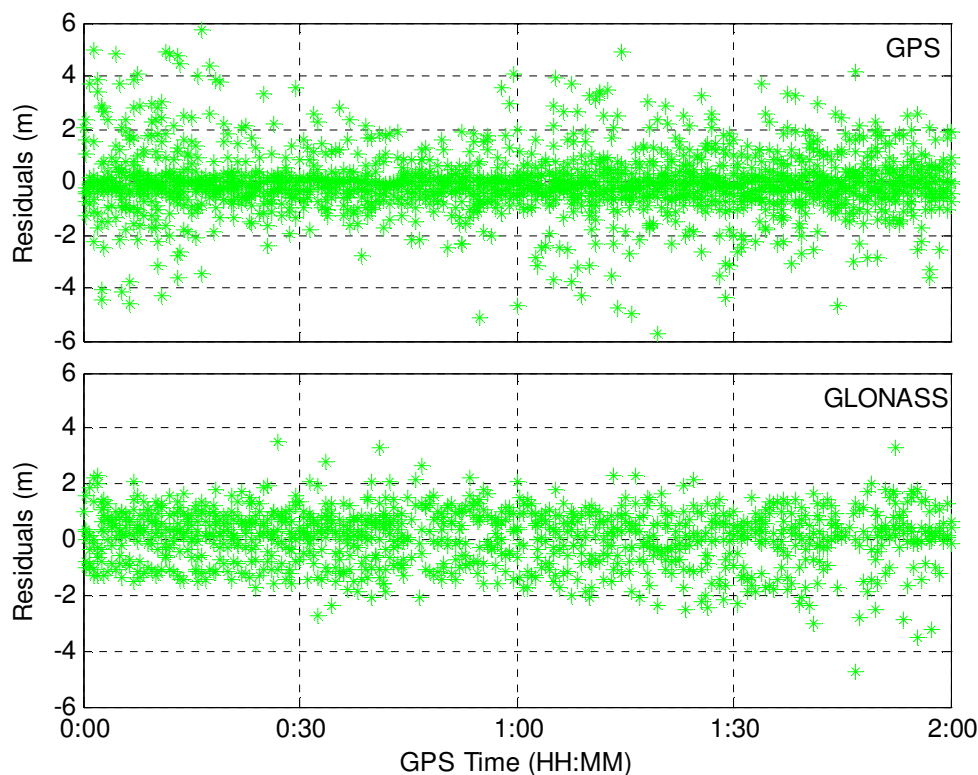


Figure 5-9 Code Observation Residuals in GPS/GLONASS Processing

In Figures 5-9 and 5-10, the observations from an average of seven GPS satellites and five GLONASS satellites are used in the combined GPS/GLONASS processing. The GPS code observation residuals range from -6 to 6 m while the GLONASS code observation residuals have a variation range from -5 to 4 m. Similarly to the code observation residuals, the GLONASS phase observation residuals have a smaller varying range than the GPS phase observation residuals. Despite this, we could not conclude that GLONASS observations have smaller residual errors since the residuals are dependent on the satellite elevation angles. To further analyze the observation residuals, we examine the relationship of the observation residuals and the satellite elevation. The code

observation residuals in Figure 5-9 and the phase observation residuals in Figure 5-10 are re-plotted against the satellite elevation in Figure 5-11 and 5-12, respectively. The elevation angles of GPS and GLONASS satellites involved in the processing are shown in Figure 5-13.

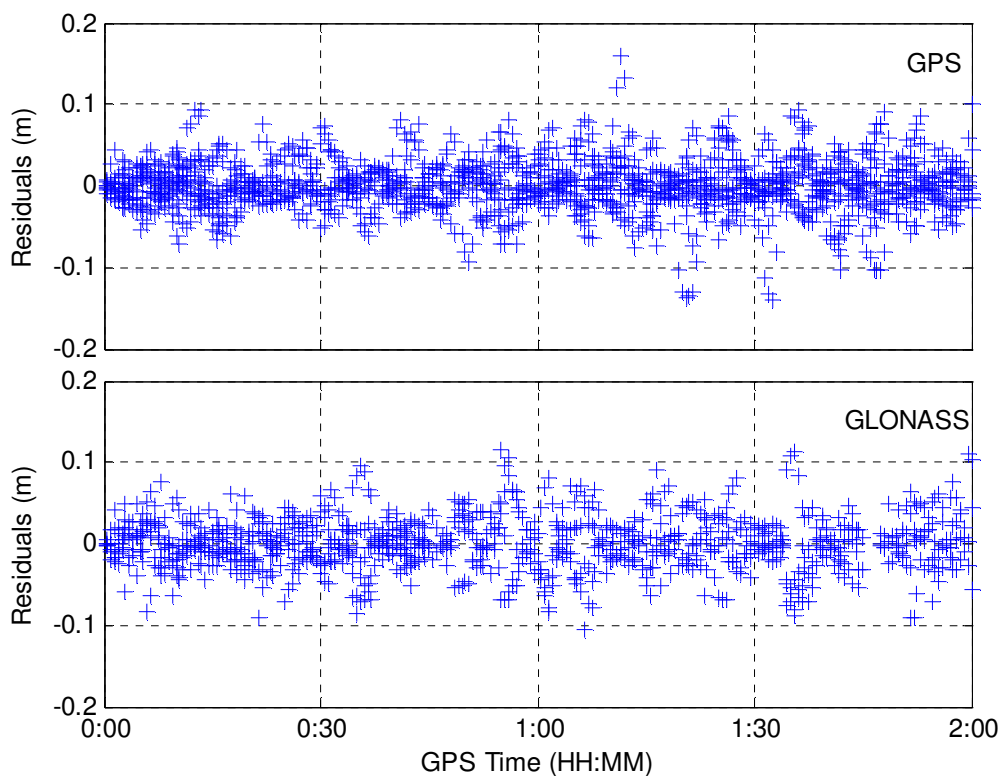


Figure 5-10 Phase Observation Residuals in GPS/GLONASS Processing

As expected, GPS residuals decrease with increasing elevation angles but the elevation dependence of the GLONASS residuals is not significant, which confirms that the residual elevation-independent errors such as satellite orbit and clock errors are dominant in all GLONASS residual errors.

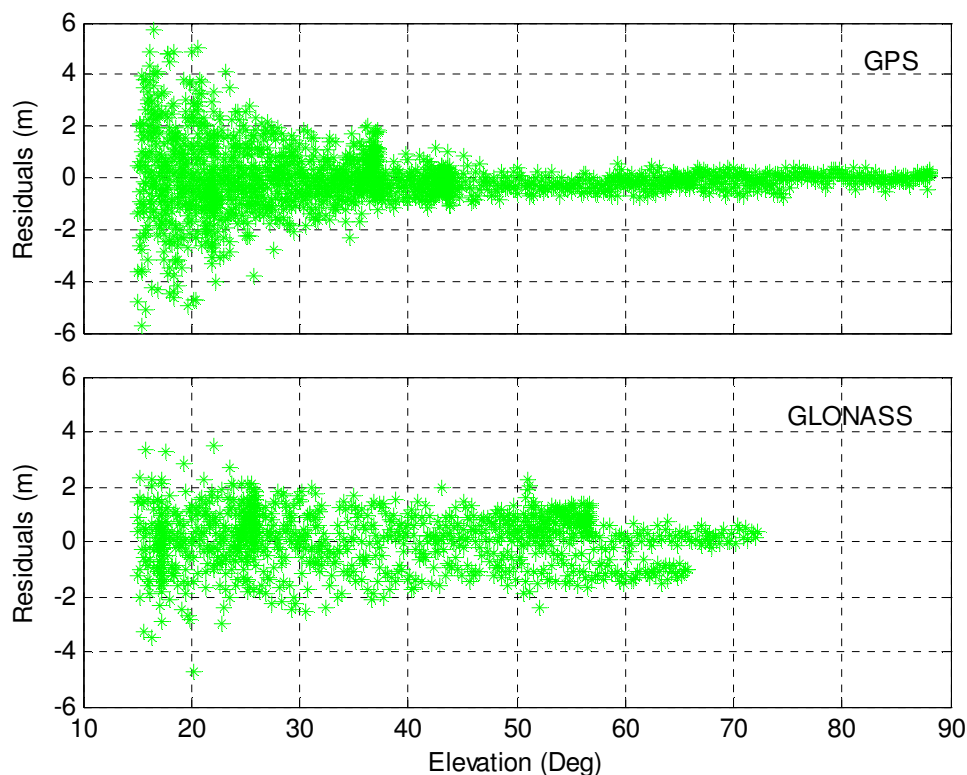


Figure 5-11 Elevation Dependence of Code Observation Residuals

The code residual plot (see Figure 5-11) indicates that the GLONASS code observations have larger residuals than the GPS code observations. This is caused by the lower accuracy of the GLONASS code measurements as well as the satellite orbit and clock corrections. To reduce their effect on the positioning results, the GLONASS code observations are assigned a smaller weight in the data processing. The phase residual plot (see Figure 5-12) also indicates that GLONASS phase observations have slightly larger residuals than GPS phase observations, which is especially obvious when the elevation angles are located between 50 and 60 degrees. RMS values of code and phase observation residuals in each elevation bin are calculated and the results are presented in

Table 5-3. It is noticed that GLONASS code observation residuals are approximately 1.8 times larger than GPS code observations residuals when satellite elevations are over 30 degrees in terms of an average of RMS value. The slightly larger GLONASS phase observation residuals can also be found in this table. This demonstrates that the accuracy of the GLONASS precise satellite orbit and clock corrections really has a large influence on the GLONASS observation residuals. In comparison with the influence on the code observations, the influence of the residual satellite orbit and clock errors on the phase observations is smaller, because the systematic part of these errors is completely absorbed by the carrier-phase ambiguity parameters.

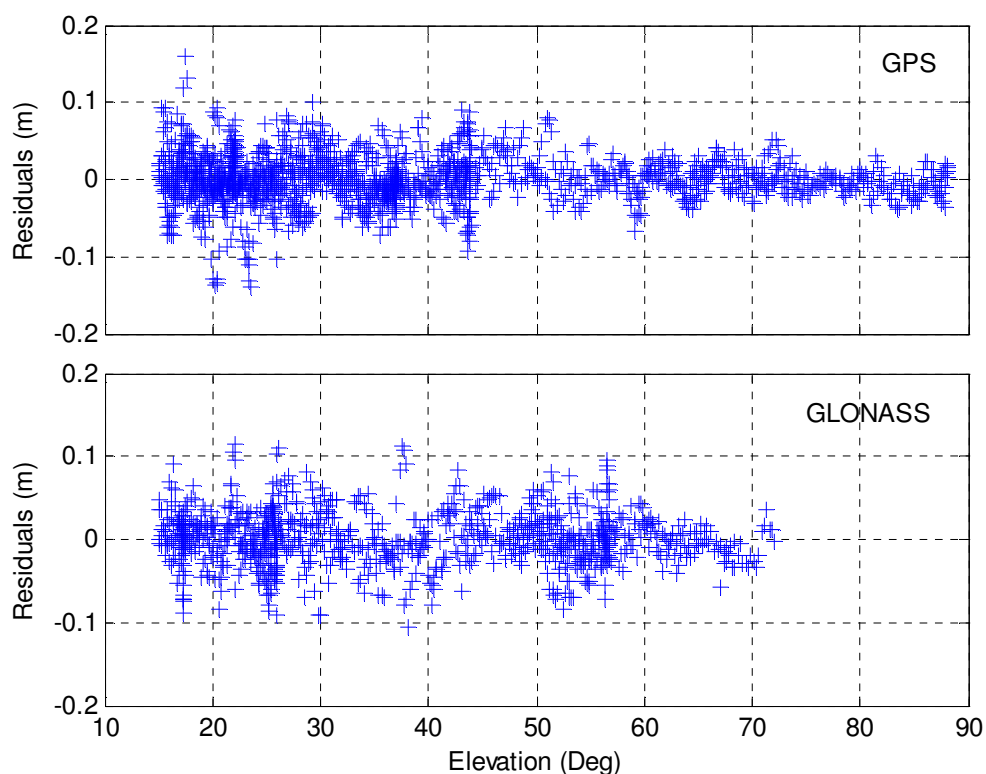
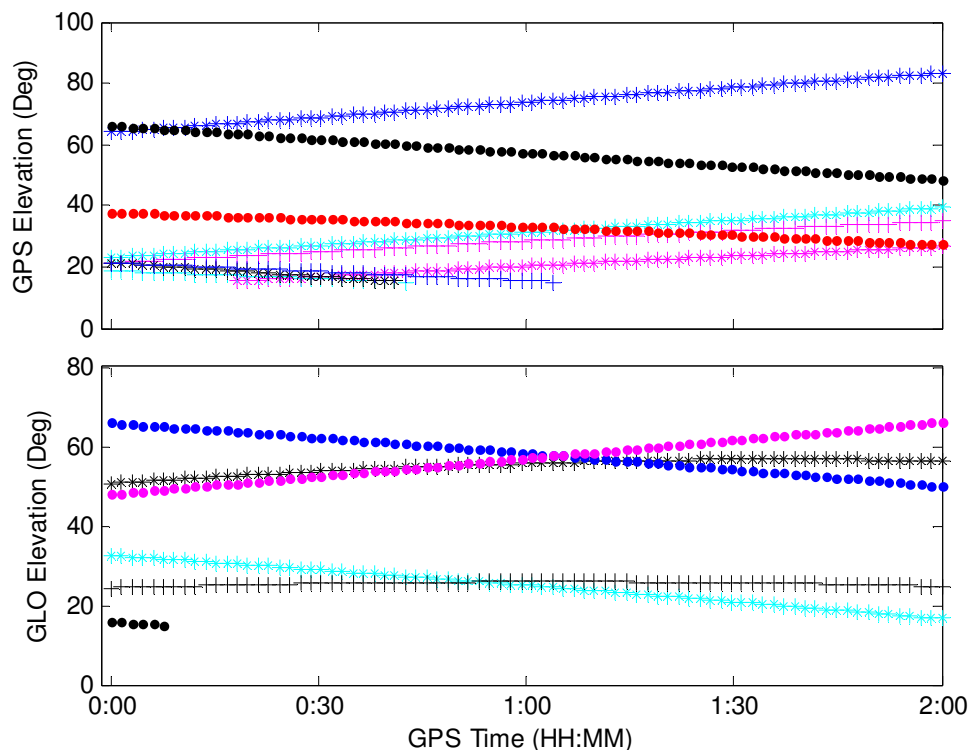


Figure 5-12 Elevation Dependence of Phase Observation Residuals

Table 5-3 RMS Statistics of Observation Residuals in Each Elevation Bin (m)

	10°-20°	20°-30°	30°-40°	40°-50°	50°-60°	60°-70°	70°-80°	80°-90°
GPS Code	2.178	1.404	0.746	0.463	0.355	0.283	0.266	0.170
GLO Code	1.280	1.109	1.002	0.837	0.908	0.720	0.344	---
GPS Phase	0.036	0.037	0.026	0.034	0.027	0.018	0.016	0.018
GLO Phase	0.029	0.036	0.035	0.031	0.032	0.018	0.023	---

**Figure 5-13 Satellite Elevation Angles in GPS/GLONASS Processing**

The larger remaining errors in the GLONASS code and phase observations will cause a side effect for the combined use of GPS and GLONASS in the precise point positioning if the stochastic information of observations could not be given properly. On

the other hand, adding the GLONASS observations can improve the satellite geometry (see Figure 5-6), which will contribute to enhancing the positioning accuracy as well as reducing the convergence time in PPP.

Shown in Figure 5-14 is the ambiguity estimates for both GPS and GLONASS satellites during the entire combined GPS/GLONASS processing. Different colors and symbols represent the ambiguity estimates from different satellites. Since the ambiguities have lost their natural integer characteristics after constructing ionosphere-free observation combinations, they are estimated as float values. Comparing Figure 5-5 and 5-14, it is clearly observed that the ambiguities take a slightly shorter time to reach stable values than the position parameters.

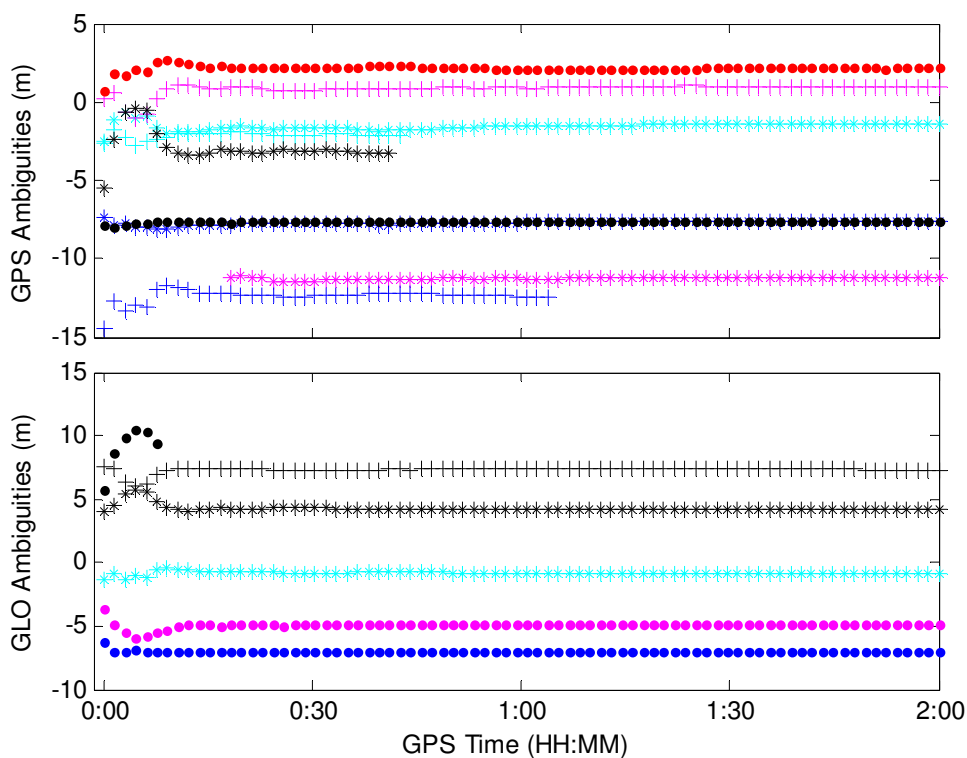


Figure 5-14 Ambiguity Estimates in GPS/GLONASS Processing

In addition to the position determination, PPP can also output receiver clock offset solutions which have the potential to support precise timing applications. The estimated receiver clock offsets in the combined GPS/GLONASS processing are presented in Figure 5-15. The receiver clock offset estimates are very stable with small variations during the two-hour processing, depending on the stability of the receiver clock.

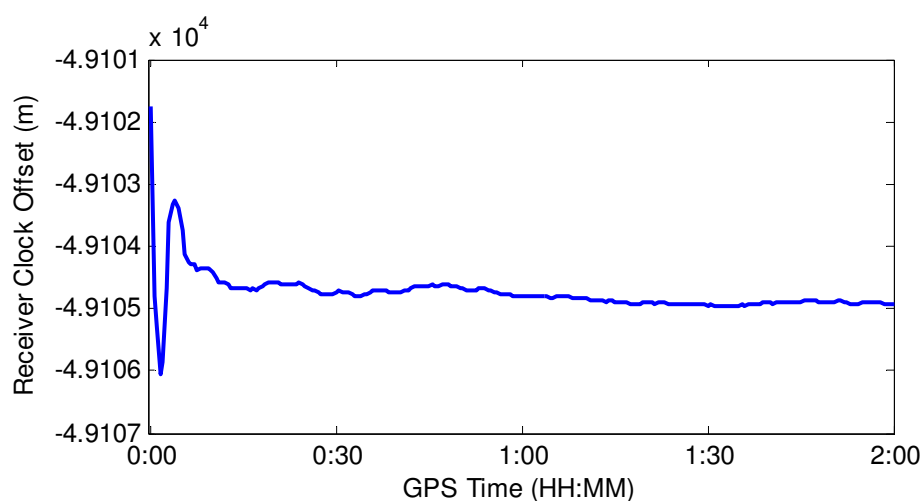


Figure 5-15 Receiver Clock Offset Estimates

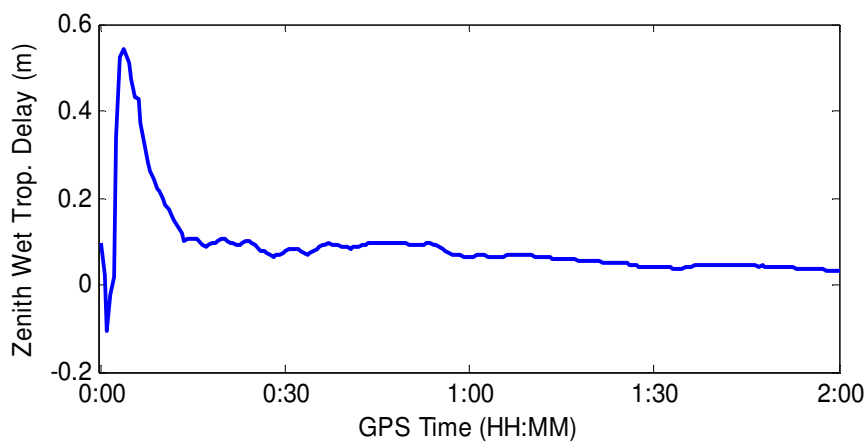


Figure 5-16 Zenith Wet Tropospheric Delay Estimates

Presented in Figure 5-16 is the estimated zenith wet tropospheric delay (ZWD). As the wet tropospheric delay changes with time and space, it is estimated as an unknown parameter in the PPP model. The ZWD varies from 10 cm to 4 cm during the period of two hours. This PPP method that is capable of estimating the ZWD may be applied to the numerical weather prediction.

The estimated system time difference between GPS and GLONASS is presented in Figure 5-17. The system time difference varies in a range of about 1.5 ns over the two hours, which partially reflects the accuracy of the GLONASS system time scale. The larger variation in the beginning is due to the position convergence process. The obtained system time difference from the PPP model includes not only the real time difference between GPS and GLONASS system times but also the receiver inter-system hardware delay. Since they can't be separated from each other, the obtained estimate is therefore a sum of the real system time difference and the receiver inter-system hardware delay. Therefore, the estimated system time difference, which is quite dependent on the receiver used, is only an approximation value to the real system time difference. The further investigation to the system time difference is carried out in the next chapter.

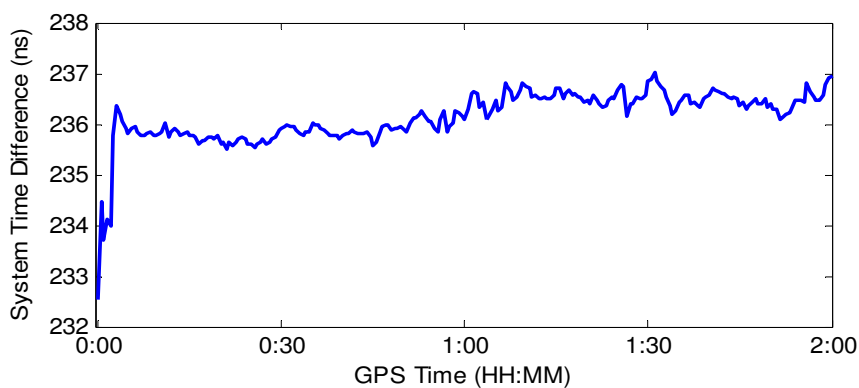


Figure 5-17 Estimated GPS-GLONASS System Time Difference

5.4 Performance Comparison between GPS-only and GPS/GLONASS PPP

The PPP performance is usually assessed through the converged positioning accuracy and the corresponding convergence time. The positioning accuracy may be measured by the mean, standard deviation (STD) and root-mean-square (RMS) of the position errors, which reflect how different the position estimate is from its true coordinate. The convergence time shows how long it takes a position filter to reach a stable condition.

To compare the performance between the GPS-only PPP and the combined GPS/GLONASS PPP, a total of 36 two-hour datasets from six stations were processed. For each station, a total 12-hour dataset is processed separately in six sessions. To analyze the positioning accuracy, the positioning errors are obtained by comparing the positioning results of PPP and the true station coordinate components in east, north and up directions. Afterwards the RMS value, which is a statistic result of the positioning errors, is then calculated in each session using the samples of the last one hour. To define the convergence time, different users may adopt a different criterion, which depends on what accuracy is required. In this section, the convergence time is defined when the coordinate error is smaller than 10 cm, and is described in the unit of epochs with an epoch interval of 30 seconds.

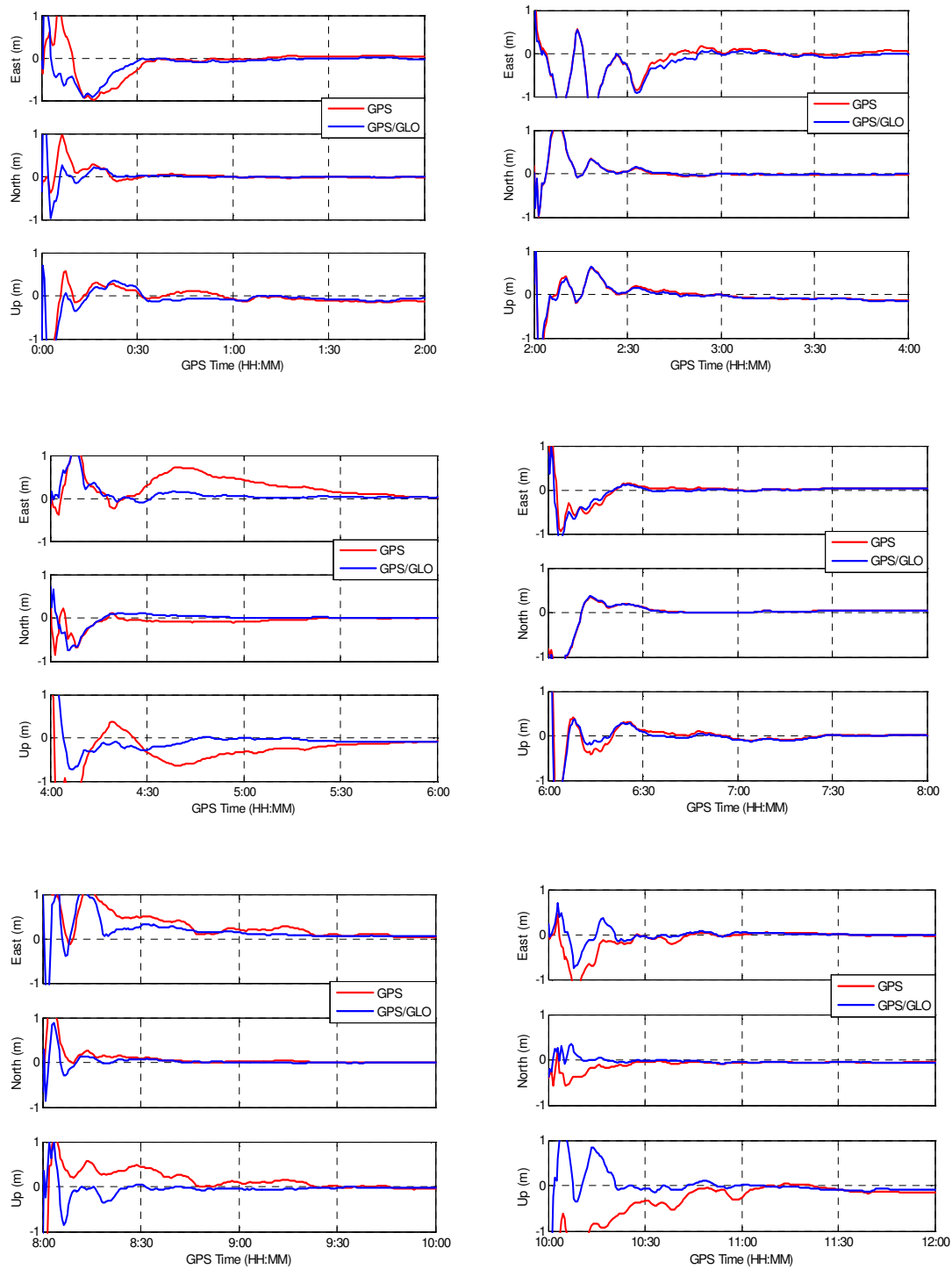


Figure 5-18 Processing Results at CONZ

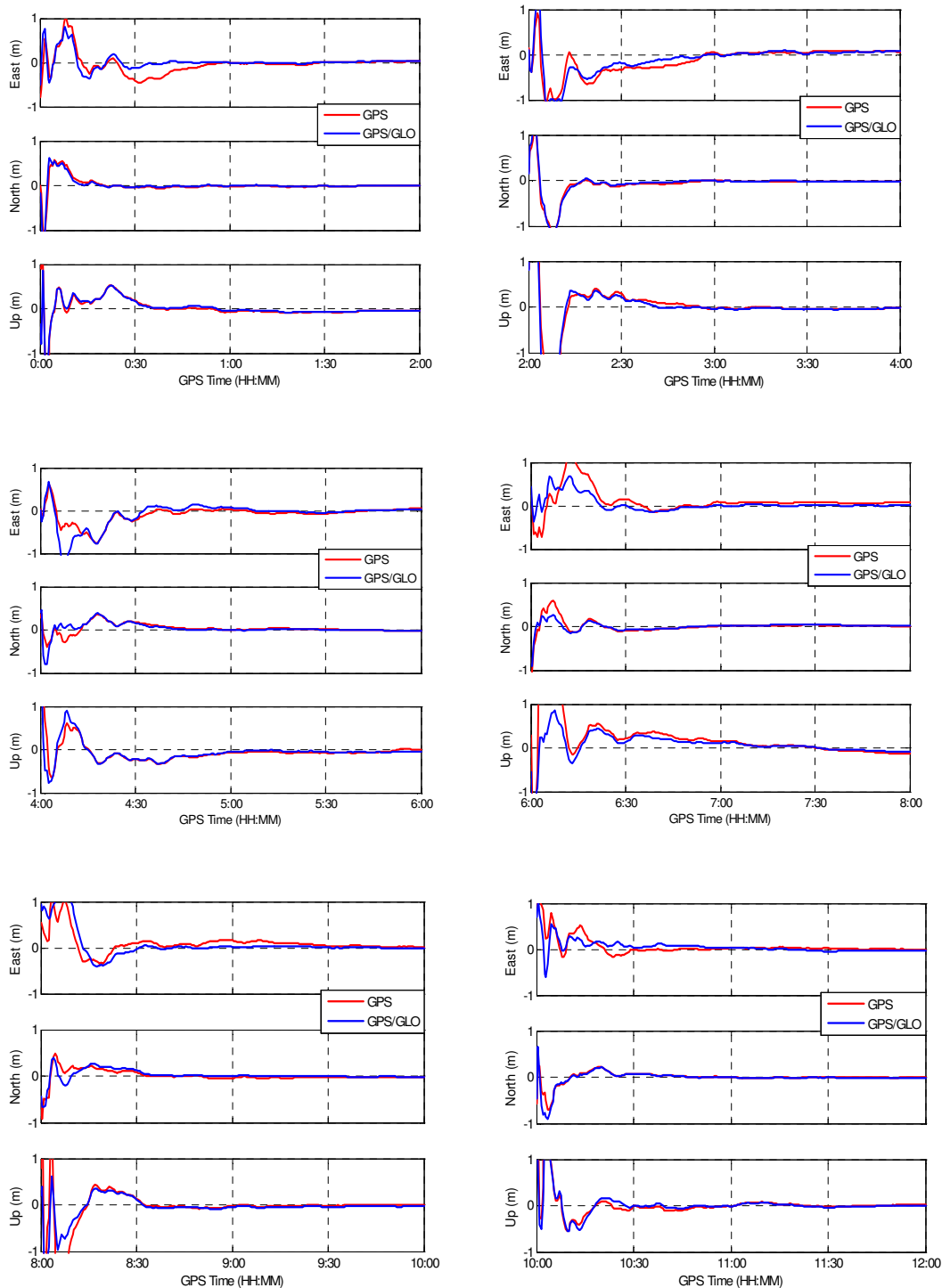


Figure 5-19 Processing Results at RCMN

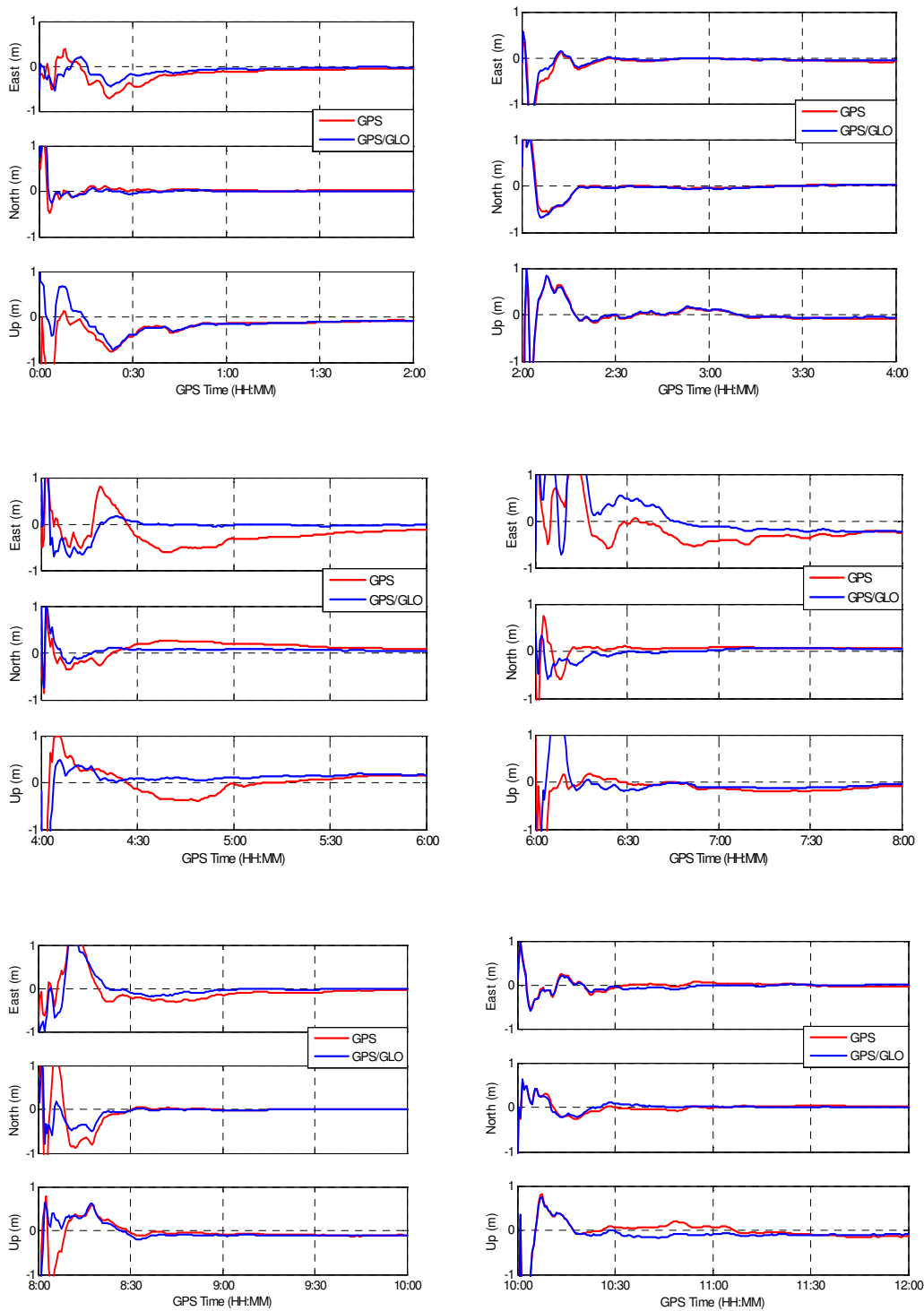


Figure 5-20 Processing Results at UNBJ

Figures 5-18 to 5-20 show the processing results of three stations in six sessions, including the positioning errors in east, north and up directions with respect to the true station coordinates obtained from the CODE analysis center. The processing results of the other three stations are given in Appendix A. The red curves represent the results of the GPS-only processing, while the blue curves represent the GPS/GLONASS processing results. As can be seen from these plots, half an hour or longer time is needed for the position filter to reach a stable value. This is especially true for the GPS-only processing. After adding GLONASS observations, a significant improvement on the convergence time can be clearly observed in some plots, such as the third subplot at CONZ, the first subplot at RCMN, and the third subplot at UNBJ. A further analysis on the positioning results is carried out in the following.

Figures 5-21 to 5-23 display the RMS of the positioning errors in east, north and up directions of all the 36 samples. The absolute positioning errors in the last one hour of each session are used to calculate the RMS. As can be seen from the three figures, the combined GPS and GLONASS PPP can achieve a better converged positioning accuracy in east, north and up directions than the GPS-only PPP in most cases. The improvement of positioning accuracy in the horizontal coordinate components is more significant than that in the vertical component. An average RMS of 36 samples is calculated and the results are given in Table 5-4. The improvement ratios of the converged positioning accuracy are 40%, 28%, and 24% for the east, north, and up coordinate components, respectively.

A few exceptions such as the east RMS in the 27th and 31st samples, the north RMS in the 10th and 28th samples, and the up RMS in the 15th and 23rd samples are the

positioning results with a degraded accuracy caused by the introduction of GLONASS data. This degradation of the positioning accuracy reaches up to 4.7 cm in the east component and 7.0 cm in the up component. The residuals inspection of these stations shows that the degradation of the RMS is caused by the relatively larger GLONASS phase observation residuals. The main reason causing the larger GLONASS observation residuals is because of the lower short-term stability of some older GLONASS-M cesium clocks. With more operational new GLONASS satellites, the old GLONASS satellites will be decommissioned gradually. The combined use of GPS and GLONASS will be able to achieve better performance.

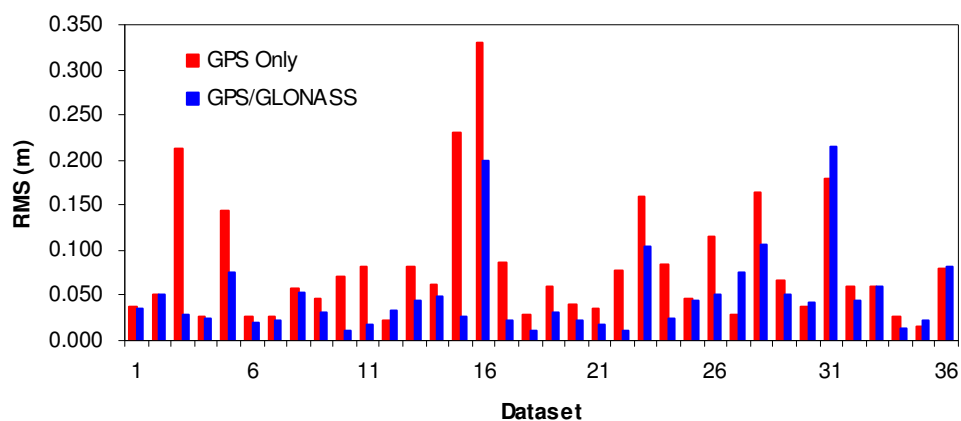


Figure 5-21 RMS Statistics of East Position Errors of 36 Samples

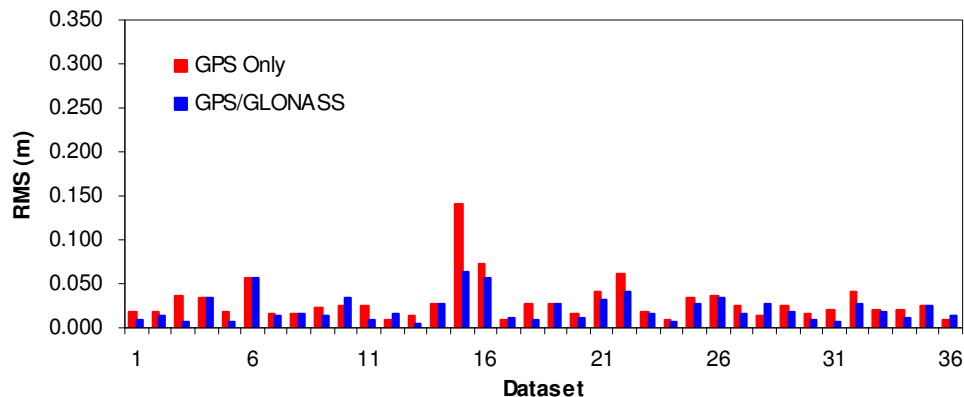


Figure 5-22 RMS Statistics of North Position Errors of 36 Samples

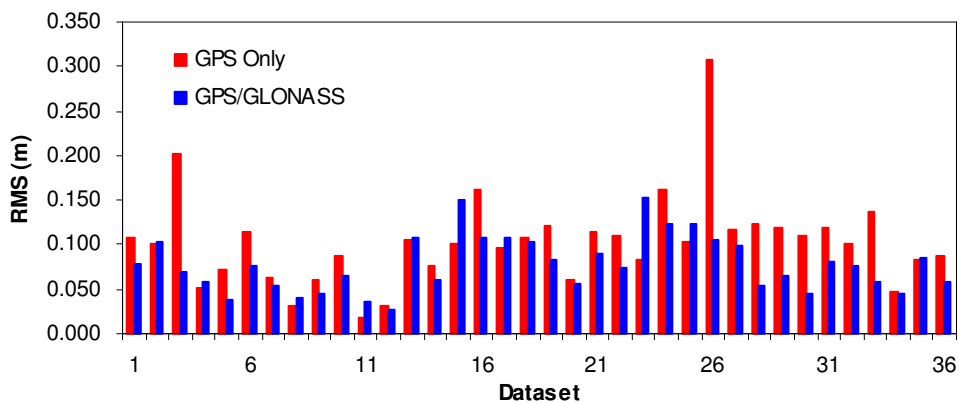


Figure 5-23 RMS Statistics of Height Errors of 36 Samples

Table 5-4 Average RMS of 36 Samples (m)

	GPS Only	GPS/GLONASS	Improvement Ratio
East	0.082	0.049	40 %
North	0.029	0.021	28 %
Up	0.102	0.078	24 %

Figures 5-24 to 5-26 show the convergence time for all the 36 samples in east, north, and up directions. The convergence time is expressed in the unit of epochs and defined when the position filter reaches a stable condition with a 10 cm position error.

The improvement of the convergence time is significant in most cases in east, north, and up directions for GPS/GLONASS PPP. An average convergence time of 36 samples is calculated and the results are provided in Table 5-5. The improvement ratios on the convergence time are 21%, 24%, and 19% for the east, north, and up coordinate components, respectively. Similarly to the position accuracy, a few exceptions with slightly longer convergence time can be found after adding GLONASS data. However, the decrease of the convergence time is obvious in most samples, although the GLONASS constellation is still incomplete. A further reduction of the convergence time may be expected when more GLONASS satellites are operational.

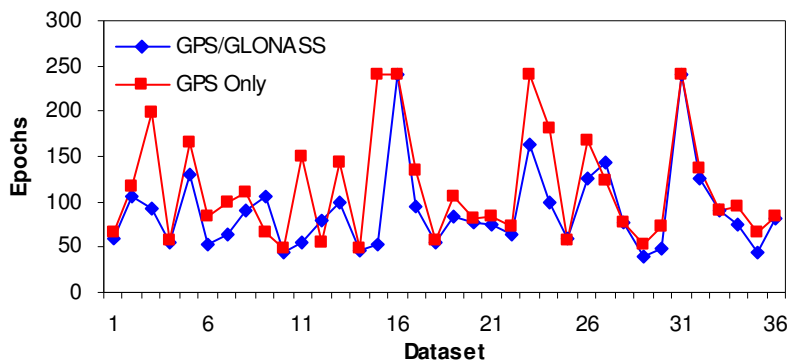


Figure 5-24 Convergence Time in East Component of 36 Samples

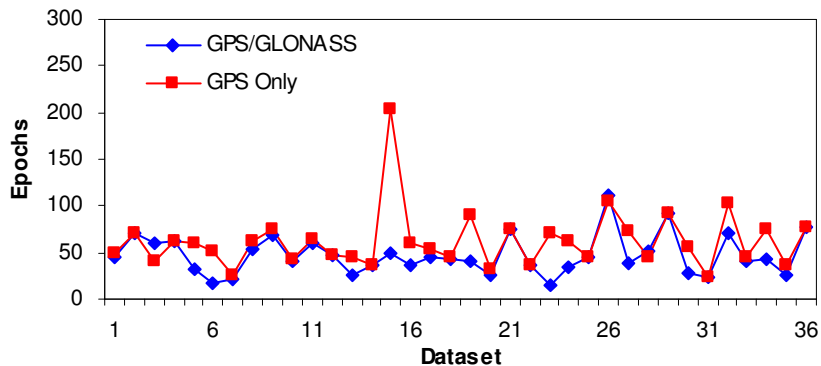


Figure 5-25 Convergence Time in North Component of 36 Samples

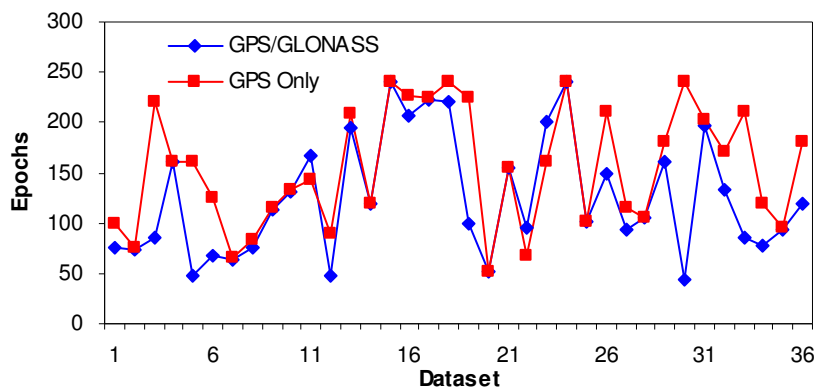


Figure 5-26 Convergence Time in Height Component of 36 Samples

Table 5-5 Average Convergence Time of 36 Samples (Epochs)

	GPS Only	GPS/GLONASS	Improvement Ratio
East	114	90	21 %
North	62	47	24 %
Up	155	125	19 %

5.5 Kinematic Positioning Results and Analysis

To assess the performance of the precise point positioning in the kinematic mode, a kinematic experiment was carried out and the kinematic positioning results and their analysis are presented in this section.

5.5.1 Data Description

A land vehicle equipped with the NovAtel's ProPak-V3 dual-frequency GPS/GLONASS receiver was operated as a roving station for about 42 minutes in an open sky area near the University of Calgary on May 6, 2009. The installation of the experimental equipment can be seen in Figure 5-27.



Figure 5-27 Equipments in the Kinematic GPS/GLONASS Experiment

The experimental data has a sampling rate of 1 second and cut off angle of 5 degrees. An initial 30 minutes static observation was made in the entire kinematic test. A base station with known coordinates was installed on the roof of the Engineering Building of The University of Calgary and the software package GrafNavTM capable of computing the differential position coordinates was used to obtain the reference coordinates of the roving station.

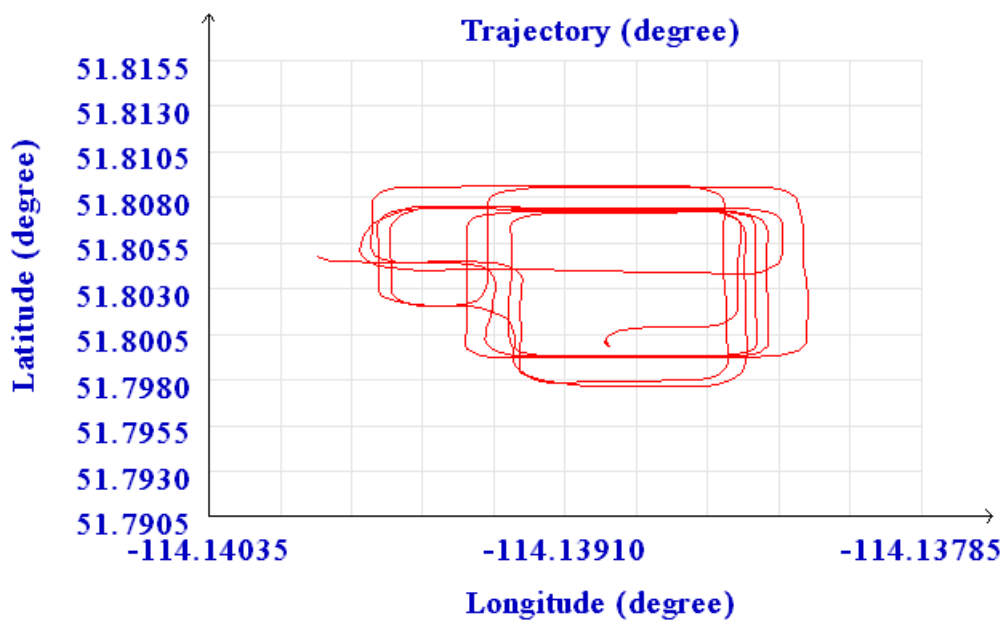


Figure 5-28 Trajectory Plotted with P³ Software Package

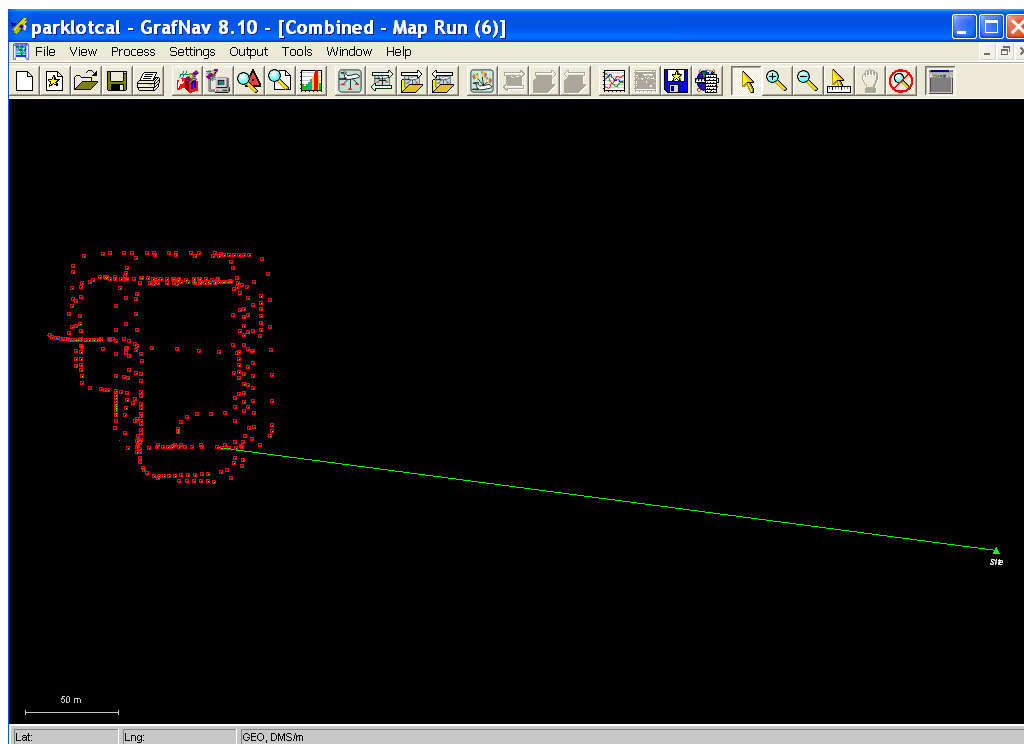


Figure 5-29 Trajectory Produced by GrafNavTM Software Package

In the PPP processing, the Random Walk (RW) process was used to model the dynamics of the vehicle and the spectral density of $10^2 \text{ m}^2 / \text{sec}$ was used for the horizontal and vertical coordinate parameters of the rover station. The spectral density of the zenith wet tropospheric delay is set to $10^{-9} \text{ m}^2 / \text{sec}$ while the spectral density values of $10^5 \text{ m}^2 / \text{sec}$ and $10^{-7} \text{ m}^2 / \text{sec}$ are used for the receiver clock and system time difference parameters, respectively (PMIS, 2005). The mask elevation angle was set to 15 degrees in the processing. Figures 5-28 and 5-29 produced from the P³ software package and GrafNavTM software package, respectively, show the trajectory of the kinematic test.

5.5.2 Positioning Results and Discussion

The final IAC precise GPS/GLONASS satellite orbit data was used in this test with sampling intervals of 15 minutes. Since the 30-second precise GPS/GLONASS clock product is unavailable, the final IAC precise clock product with 5-minute intervals was used to estimate the position of the rover station. As some float solutions occurred in the differential processing with the GrafNavTM software package, the differential positioning results with fixed integer Double Difference (DD) ambiguities and the positioning precision better than 10 cm were chosen as the benchmark of the PPP solutions.

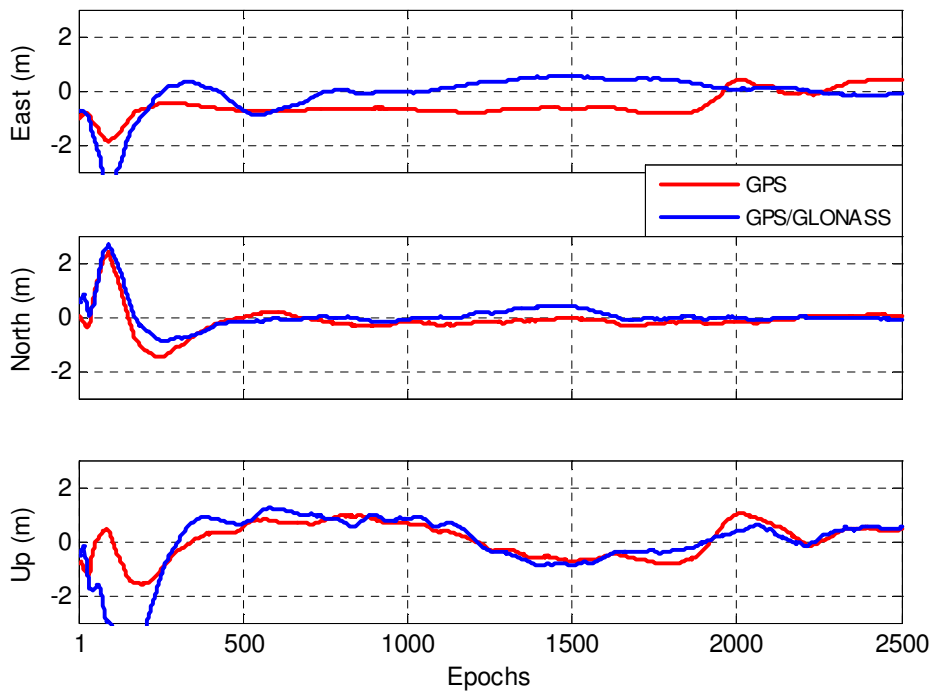


Figure 5-30 PPP Positioning Errors with Respect to Differential Solutions

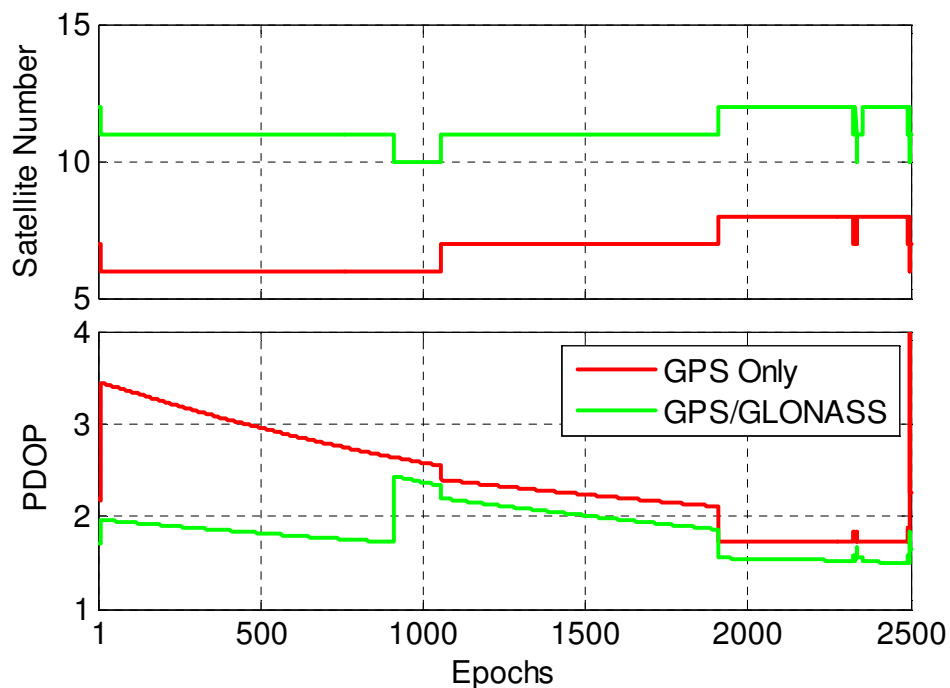


Figure 5-31 Satellite Number Used and PDOP in the Kinematic Test

Figure 5-30 shows the difference between the PPP solutions and DD solutions in the east, north and up directions, including the static initialization process of the first 1800 epochs. Figure 5-31 indicates the number of the satellites used in the entire PPP processing and PDOP values. Observations from an average of 4.3 GLONASS satellites and 6.8 GPS satellites are used in the combined GPS/GLONASS processing. Compared with the GPS PPP solutions, the positioning results of the combined GPS/GLONASS PPP are closer to the DD solutions in the east direction. For the vertical component, a fluctuation of the positioning errors is observed for both GPS and GPS/GLONASS cases. Longer time is needed for the position filter in the up direction to reach a stable value.

In order to look at the positioning errors in more detail under the kinematic mode, the kinematic processing results shown in Figure 5-30 are given in Figures 5-32 with a larger scale. It can be clearly observed that the combined GPS/GLONASS positioning errors remain more stable and closer to the central line in the horizontal components. This reflects a faster convergence as well as higher positioning accuracy achieved by the GPS/GLONASS kinematic precise point positioning.

Given in Table 5-6 are the RMS statistical results of the PPP positioning errors from 1800 to 2500 epochs, which represents the kinematic positioning accuracy of PPP. The position results of the combined GPS and GLONASS PPP have RMS values of 0.161, 0.056, and 0.357 m in the east, north, and up directions, respectively. The improvement of the positioning accuracy reaches approximate 60% in the horizontal components and 36% in the vertical component after adding GLONASS observations in terms of the RMS statistics.

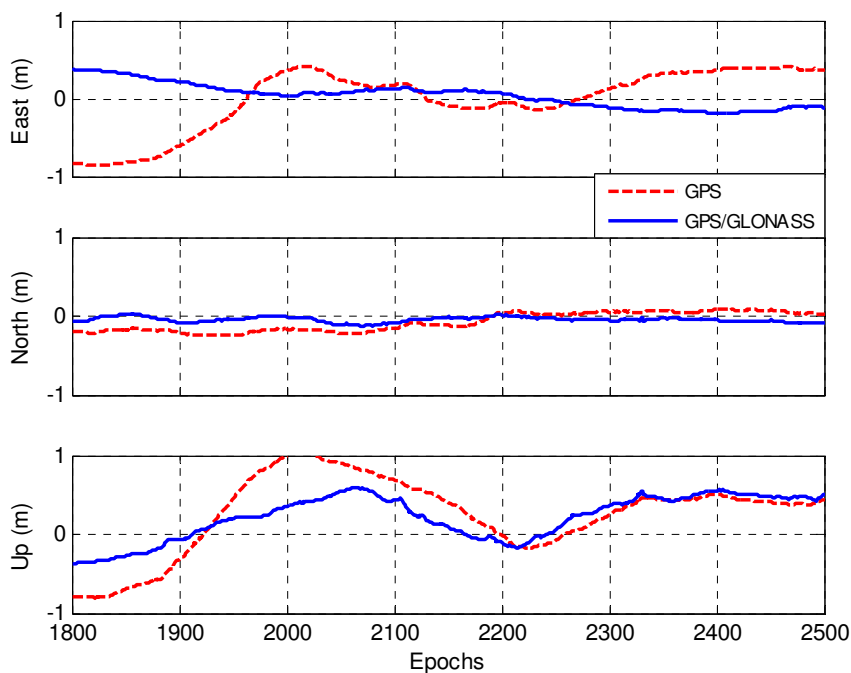


Figure 5-32 Kinematic PPP Positioning Errors

Table 5-6 RMS Statistics of Kinematic PPP Positioning Errors (m)

		GPS Only	GPS / GLONASS	Improvement Ratio
MEAN	East	-0.010	0.038	--
	North	-0.076	-0.046	39%
	Up	0.261	0.219	16%
STD	East	0.395	0.156	61%
	North	0.118	0.033	72%
	Up	0.492	0.281	43%
RMS	East	0.396	0.161	59%
	North	0.140	0.056	60%
	Up	0.557	0.357	36%

Although the positioning accuracy is improved after adding GLONASS observations, the position filters have not reached stable values during the period of about 42 minutes, especially for the vertical component. This is because the 5-minute satellite clock data is used in the computation because the combined GPS/GLONASS clock

products with shorter sampling interval are currently not available. It is well known that the quality of the precise satellite orbit and clock products has a large impact on the position results. To examine the influence of the satellite orbit and clock products, different GPS precise orbit and clock products with different sampling intervals are chosen to estimate the position of the rover station.

The precise GPS satellite orbit and 5-minute clock products from IAC and IGS are used to compare the positioning results. The processing results are presented in Figure 5-33 where the positioning errors are obtained through comparing the PPP solutions with DD solutions. No significant difference is found using the satellite orbit and clock data from IAC and IGS. To investigate the effect of the precise satellite clock data with different sampling intervals, 30-second clock corrections from IGS and 5-second clock corrections from CODE are used to compare the positioning results with 5-minute clock data. The comparison results are given in Figure 5-34 and the RMS statistics of the positioning errors in the last 100 epochs are shown in Table 5-7.

The positioning results using 30-second clock data and 5-second clock data are very close, while they are quite different from the processing results using the clock corrections with the sampling intervals of 5 minutes in terms of the changing trend of the position errors. According to the RMS statistical results given in Table 5-7, the position filters can converge to a centimetre level and remain a stable value if 30-second or 5-second satellite clock products are used, which reflects that the positioning accuracy that PPP can achieve is quite dependent on the satellite clock products. This is because a mathematical interpolation algorithm is used to obtain the clock corrections at the observation time. As the interpolation algorithm could not account for the random

behaviour of the satellite clocks, the longer interval clock products will result in larger observation residuals and positioning errors. According to the investigating results, we may expect that higher accuracy positioning results can be achieved by the combined GPS and GLONASS PPP when higher-rate GPS/GLONASS satellite clock products become available.

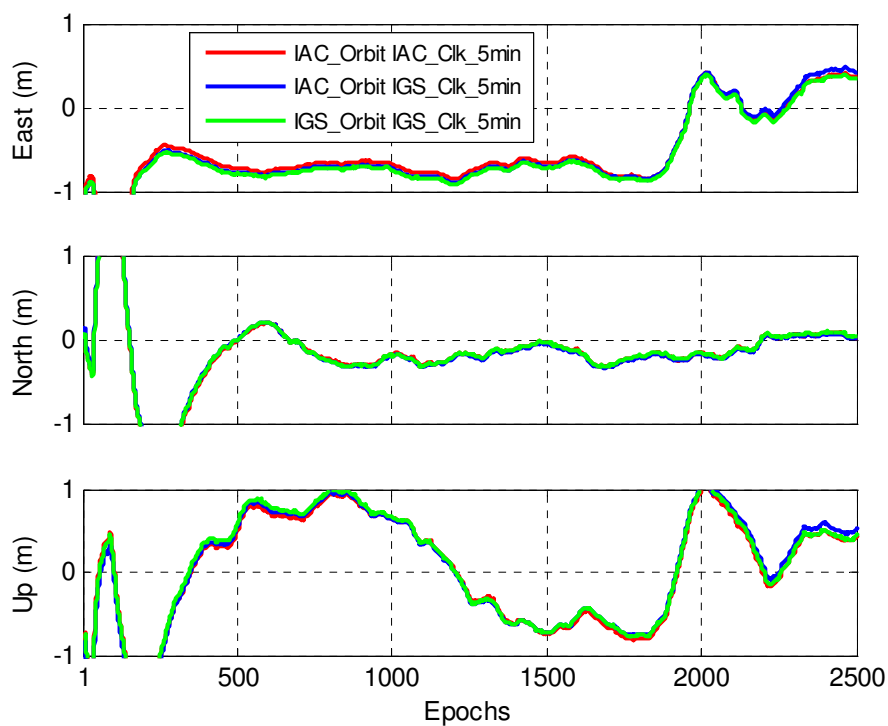


Figure 5-33 GPS Positioning Errors with Different Orbit and Clock Products

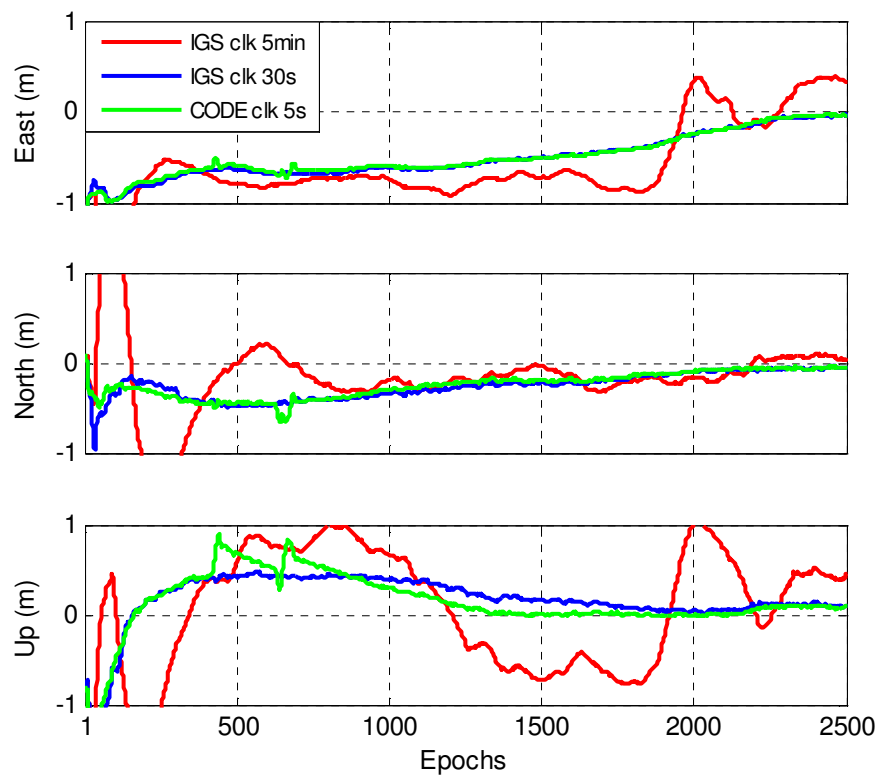


Figure 5-34 GPS Positioning Errors with Different Sampling Clock Products

Table 5-7 RMS Statistics of Positioning Errors with Different Clock Products (m)

		IGS clock 5min	IGS clock 30s	CODE clock 5s
MEAN	East	0.363	-0.043	-0.034
	North	0.070	-0.053	-0.053
	Up	0.432	0.108	0.087
STD	East	0.012	0.007	0.004
	North	0.022	0.010	0.009
	Up	0.038	0.011	0.013
RMS	East	0.364	0.044	0.035
	North	0.074	0.054	0.054
	Up	0.434	0.108	0.088

Chapter Six: Stability Analysis of GPS-GLONASS System Time Difference

6.1 Introduction

The combination of GPS and GLONASS is able to effectively increase the number of visible satellites and therefore improve the availability of positioning solutions as well as the positioning accuracy. But for combined GPS/GLONASS processing, two receiver clock offsets must be estimated, one with respect to GPS time and the other with respect to GLONASS time. This is because an offset exists between GPS and GLONASS system times and thus causes a bias between GPS and GLONASS measurements (Moudrak, 2005). This system time difference may be obtained by comparing GLONASS and GPS receiver clock offsets. Alternatively, the system time difference could be estimated directly along with position coordinates.

System time difference is an important parameter in stand-alone positioning with a GPS/GLONASS receiver. Its estimation based on single point positioning (SPP) has been reported but only with an accuracy of several tens of nanoseconds (Habrich, 1999; Zinoviev, 2005). To obtain a better understanding of this system time difference, the PPP method capable of offering a centimetre-level positioning accuracy is applied to estimate this system time difference using data from different types of receivers.

6.2 Estimation of System Time Difference

GLONASS time is generated on a base of GLONASS Central Synchronizer (CS) time by means of a set of hydrogen clocks and synchronized to the Russian National Etalon time scale UTC (SU) (GLONASS ICD, 2002). In addition to a fractional part less

than one millisecond, a constant offset of three hours exists between the UTC (SU) and GLONASS time. GPS time is established by the GPS Master Control Station and referenced to a UTC (USNO) being maintained by the U.S. Naval Observatory. The GPS time differs from the UTC (USNO) because the former is a continuous time scale while the latter is corrected periodically with an integer number of leap seconds (GPS ICD, 2000). Therefore, there is a difference of leap seconds between the GPS and GLONASS times. The GLONASS time could be transformed into the GPS time by the following equation (Kang et al., 2002):

$$t_{GPS} = t_{GLONASS} + \tau_c + \tau_u + \tau_g \quad (6.2.1)$$

where, τ_c is the time difference between the GLONASS time and the UTC(SU); τ_u is the time difference between the UTC(SU) and the UTC; τ_g is the time difference between the UTC and the GPS time. The system time difference is the sum of τ_c , τ_u and τ_g after the number of leap seconds is taken into consideration.

The GPS-GLONASS system time difference may be interpreted as the offset between the GPS receiver clock and the GLONASS receiver clock and estimated as an unknown parameter along with three coordinate components (Habrich, 1999). Alternatively, two receiver clock offsets with respect to the GPS and GLONASS system times could be estimated independently whereas the system time difference becomes the difference between the two clock offsets. Since the system time difference may be expressed as the difference between the GPS and GLONASS receiver clock offsets, its

estimate therefore is a function of the estimated GPS and GLONASS receiver clock offsets as follows (Cai and Gao, 2008):

$$\begin{aligned}
 \hat{dt}_{sys} &= \hat{dt}^r - \hat{dt}^g \\
 &= 1/c \cdot ((cdt^r + b_{IF,avg}^r) - (cdt^g + b_{IF,avg}^g)) \\
 &= dt_{sys} + 1/c \cdot (b_{IF,avg}^r - b_{IF,avg}^g)
 \end{aligned} \tag{6.2.2}$$

where, r, g represent GLONASS and GPS, respectively; c is the speed of light; dt is the receiver clock offset; dt_{sys} is the system time difference; $b_{IF,avg}$ is the average hardware delay bias after an ionosphere-free combination. The last term $(b_{IF,avg}^r - b_{IF,avg}^g)$ in Equation (6.2.2) is called the inter-system hardware delay. Since it can't be separated from the real system time difference, the estimated system time difference is only an approximation value to the real system time difference.

6.3 Stability of GPS-GLONASS System Time Difference

An important consideration in the handling of system time difference is its stability over time. To obtain a better understanding of its temporal variation, the short-term stability of the system time difference has been investigated by processing the combined GPS/GLONASS data from 30 stations, globally distributed and randomly chosen from the IGS tracking network. All stations are equipped with dual-frequency GPS/GLONASS receivers. The results included in this section have been presented in Cai and Gao (2008).

Table 6-1 GPS/GLONASS Stations

Station	Receiver type	Antenna type
ntus	LEICA GRX1200GGPRO	LEIAT504GG NONE
lama		LEIAT504GG LEIS
wtzr		AOAD/M_T NONE
penc		LEIAT504GG LEIS
wroc		LEIAT504GG LEIS
orid		AOAD/M_T NONE
rcmn		LEIAT504GG LEIS
khaj	TPS E_GGD	JPSREGANT_SD_E NONE
sofi		AOAD/M_T NONE
ankr		TPSCR3_GGD CONE
reyk		TPSCR.G3 TPSH
ohi3		ASH701941.B SNOW
lhaz		ASH701941.B SNOW
conz		TPSCR3_GGD CONE
hofn		TPSCR3_GGD CONE
irkj	JPS LEGACY	JPSREGANT_SD_E NONE
hueg		TPSCR3_GGD CONE
dlft		JPSREGANT_DD_E
kour		ASH701945C_M
ffmj		TPSCR3_GGD CONE
leij		TRM29659.00 NONE
sass		TPSCR3_GGD CONE
titz		TPSCR3_GGD CONE
zimj		JPSREGANT_SD_E NONE
onsa	JPS E_GGD	AOAD/M_B OSOD
mar6		AOAD/M_T
park		ASH701945C_M NONE
ohi2		AOAD/M_T DOME
unbj	TPS LEGACY	JPSREGANT_DD_E NONE
glsv	NOV OEMV3	NOV702GG NONE

The observation data, collected on June 11, 2008 from the 30 GPS/GLONASS stations, are used in the data analysis. The data sampling rate was 30s and the elevation mask was set to 10 degrees. The mixed GPS/GLONASS precise satellite orbit and 5-minute clock data generated by IAC were downloaded from the IAC website. Table 6-1

shows the list of stations as well as the receiver and antenna types. There are six receiver types among the 30 stations but our analysis mainly focuses on four of them.

Figure 6-1 shows the estimates of the system time difference for 30 GPS/GLONASS stations. Different colors represent different types of receivers. As can be seen, the estimates from identical receiver types are very close. However, discrepancies of up to 170 ns occur between different receiver types. In addition, all system time difference estimates remain stable within one day.

In order to look at the system time difference estimates of different types of receivers in more detail, the estimates obtained using different receiver types are given separately in Figures 6-2 to 6-5. The temporal variations of the system time difference estimates from all LEICA GRX1200GGPRO receivers can be seen in Figure 6-2. The estimates for different receiver stations agree with each other within 10 ns except for the station ORID. A jump at stations WROC and LAMA occurred due to the change of GLONASS satellite number. The system time difference estimates from TPS E_GGD receivers are given in Figure 6-3. The estimates vary from receiver to receiver in the range of 5 ns to 30 ns. Shown in Figure 6-4 is the estimated system time difference using JPS LEGACY receivers. The estimated system time difference has values between 896 to 944 ns with variations between receivers in the range of 2 to 40 ns. Some small spikes are due to the fact that some residual errors still remain during the processing. It is interesting to observe that there is a clear grouping associated with each two of four receivers in Figure 6-5. The largest discrepancy reaches 40 ns between receivers, which confirms the existence of an inter-system hardware delay.

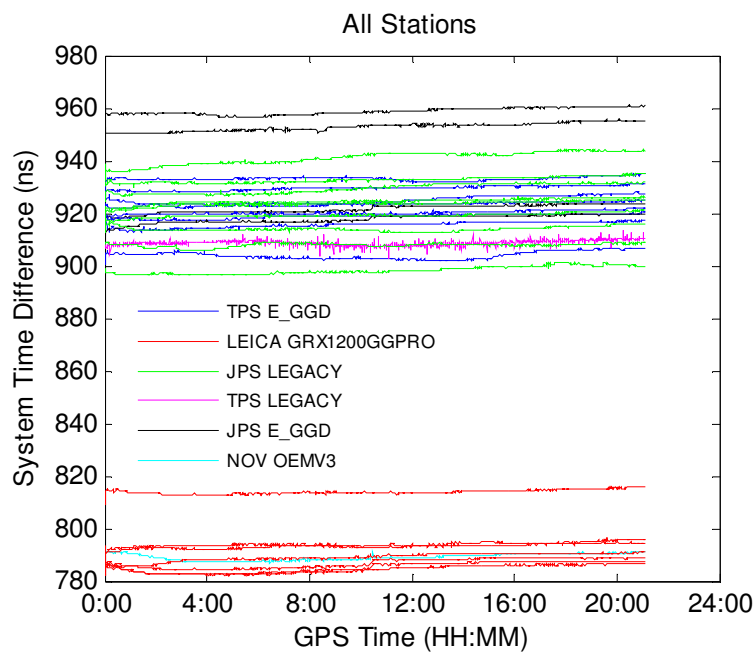


Figure 6-1 Estimated System Time Difference for 30 IGS Stations

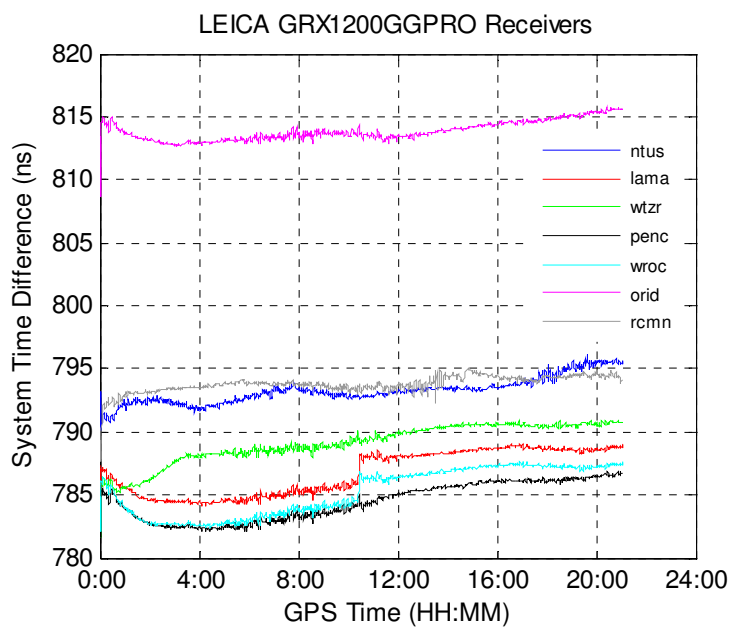


Figure 6-2 Estimated System Time Difference of LEICA GRX1200GGPRO Receivers

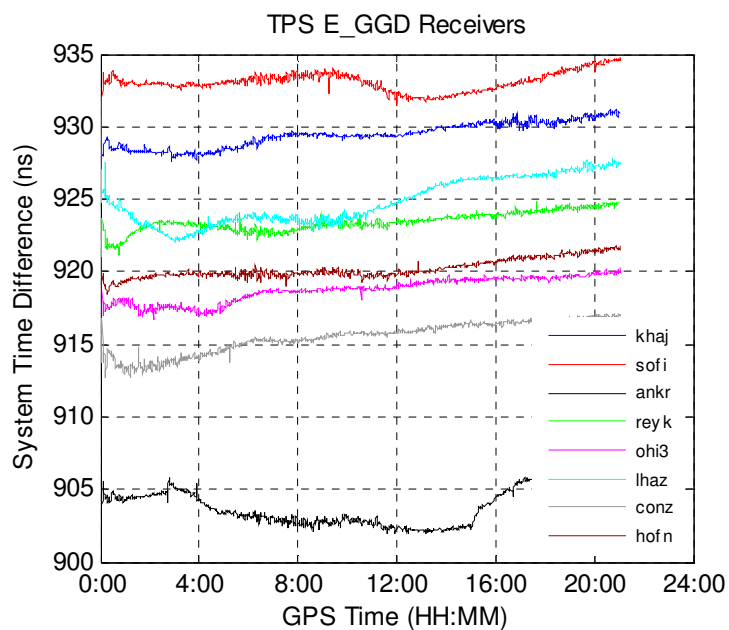


Figure 6-3 Estimated System Time Difference of TPS E_GGD Receivers

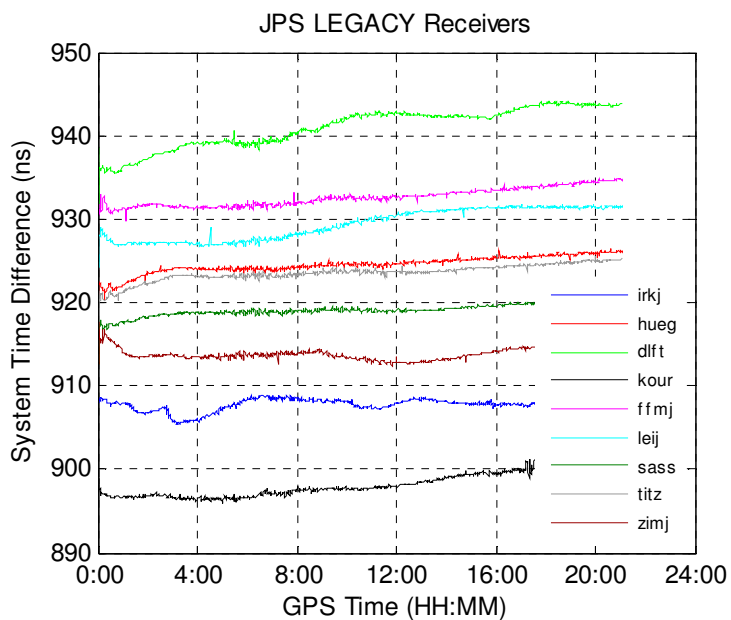


Figure 6-4 Estimated System Time Difference of JPS LEGACY Receivers

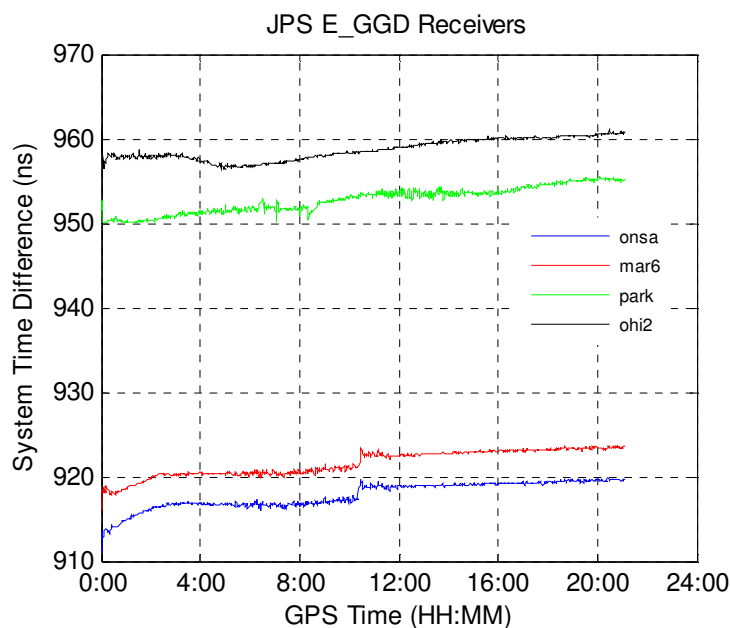


Figure 6-5 Estimated System Time Difference of JPS E_GGD Receivers

Table 6-2 demonstrates the statistic value of the system time difference estimates for each station. As can be noticed in this table, the maximum mean difference between the same types of receivers is around 43 ns, while the maximum mean difference reaches 174 ns between different types of receivers. This reflects that the inter-system bias difference between different types of receivers is larger than that between the same types of receivers. The system time difference remains stable in terms of its standard deviation and the difference between the maximum and minimum values at each station. A slight linear drift however may be seen for almost all stations.

The estimation results in this section show that the system time difference is very stable within one day with a standard deviation of less than 2.5 ns. The system time difference estimates are quite dependent on a specific receiver due to the existence of an inter-system bias which is caused by hardware delay. This bias makes the maximum

estimate discrepancy reach 40 ns between the same types of receivers and 170 ns between different types of receivers.

Table 6-2 Statistics of Estimated System Time Difference (ns)

Station	Mean	STD	Max	Min
ntus	793.30	1.00	796.18	790.84
lama	786.78	1.79	789.06	784.13
wtzr	789.17	1.48	790.93	785.11
penc	784.46	1.51	786.85	782.15
wroc	785.24	1.90	787.66	782.35
orid	813.86	0.77	815.81	812.62
rcmn	793.84	0.52	795.00	792.04
khaj	929.44	0.84	931.15	927.59
sofi	933.08	0.66	934.78	931.40
ankr	903.90	1.38	906.48	901.92
reyk	923.46	0.64	924.83	921.10
ohi3	918.78	0.83	920.26	916.69
lhaz	924.82	1.59	927.79	922.11
conz	915.53	1.07	917.14	912.67
hofn	920.21	0.63	921.76	918.91
irkj	907.80	0.74	908.99	905.42
hueg	924.59	0.93	926.50	921.45
dlft	941.10	2.31	944.10	935.44
kour	898.22	1.44	901.40	896.00
ffmj	932.63	1.05	934.96	929.81
leij	929.40	1.85	931.89	926.65
sass	919.19	0.74	920.89	916.93
titz	923.62	0.90	925.48	920.13
zimj	913.91	0.79	916.06	912.45
onsa	917.87	1.42	919.78	913.75
mar6	921.63	1.48	923.60	917.80
park	952.79	1.52	955.52	950.00
ohi2	958.69	1.25	960.94	956.36
unbj	908.71	0.93	913.25	903.02
glsv	789.09	1.24	791.43	786.90

Chapter Seven: Conclusions and Recommendations

The main goal of this research was to investigate the precise point positioning (PPP) using both GPS and GLONASS un-differenced code and carrier phase observations in addition to their precise satellite orbit and clock data. To meet this goal, two combined GPS and GLONASS PPP models, namely combined GPS/GLONASS traditional model and combined GPS/GLONASS UofC model, were developed and their algorithms were implemented. The combined GPS and GLONASS PPP models include not only the functional models but also the stochastic models. The performance of the combined GPS and GLONASS PPP has been assessed through a comparison with that of the GPS-only PPP in terms of the positioning accuracy and convergence time using static data collected from a few IGS stations and kinematic data collected from an experiment. Several conclusions from this investigation and recommendations for future research have been made and are provided in the following.

7.1 Conclusions

- 1) GLONASS is a counterpart to the GPS in terms of its constellation characteristics and positioning principle. However, GLONASS adopts a different time system and a different coordinate reference. In addition, each satellite transmits signals on a different frequency using originally a 25-channel frequency division multiple access (FDMA) technique. These will bring difficulties to a combined use of GPS and GLONASS. As the same coordinate frame is used in the combined GPS/GLONASS precise satellite orbit products, the difference

between GPS and GLONASS coordinate systems does not need to be considered in PPP but the difference of the time reference and signal frequency must be taken into account.

- 2) GLONASS is on the way to revitalization and modernization. So far there have been 20 GLONASS satellites in orbit and a full constellation of 24 satellites will be reached by 2010. In addition, the precise GLONASS satellite orbit and clock products have been available from IAC. The availability of sufficient visible GLONASS satellites and precise orbit and clock data provides a basis for developing the combined GPS and GLONASS PPP technique.
- 3) In PPP, the error mitigation methods play a vital role to provide decimetre to centimetre position accuracies. Although GLONASS may adopt the same error correction models and mitigating methods as GPS for almost all error sources, some errors need to be specially treated for GLONASS such as the satellite antenna phase center offset and frequency dependent error sources.
- 4) Since the existing GPS precise point positioning models can't be directly used to process the combined GPS/GLONASS observation data, the combined GPS and GLONASS PPP models have been developed in this research. Similarly to the GPS PPP models, the combined GPS and GLONASS PPP models include the combined GPS/GLONASS traditional and UofC models, which are established on the ionosphere-free observation combinations. Due to a different system time

adopted by GLONASS, an additional unknown parameter referred to as the system time difference has to be introduced in the combined GPS and GLONASS PPP models.

- 5) In addition to the functional models, the corresponding stochastic models have also been developed for the combined GPS and GLONASS PPP, which include the stochastic models of measurements and parameters. The stochastic model of measurements can be obtained through applying the rule of error propagation. For unknown parameters, the position coordinates, zenith wet tropospheric delay, receiver clock and system time difference are modeled as Random Walk processes, while the ambiguity parameters are treated as constants.

- 6) Numerical computation was carried out with the combined GPS/GLONASS traditional model using data collected at IGS stations. The specific processing detail was provided to help analyze the positioning results. The investigation results show that the GLONASS ionosphere-free code observation residuals are about 1.8 times larger than GPS ionosphere-free code observation residuals when satellite elevation angles are over 30 degrees, while the GLONASS phase observations have slightly larger residuals than the GPS phase observations. This is mainly caused by the lower accuracy of GLONASS precise orbit and clock corrections.

- 7) To assess the performance of the combined GPS and GLONASS PPP model, the static data collected at six globally distributed IGS stations was used to carry out the numerical computation. Numerical results indicate that the combined GPS and GLONASS PPP system has a significant improvement on the position accuracy as well as convergence time when compared with GPS-only PPP according to the statistic results from 36 samples. The improvement ratios of the positioning accuracy are 40%, 28%, and 24% and the improvement ratios of the corresponding convergence time are 21%, 24%, and 19% for the east, north, and up coordinate components, respectively.

- 8) A kinematic experiment was carried out to assess the performance of the combined GPS and GLONASS PPP in a kinematic mode. The differential positioning technique was used to produce reference coordinates. The experiment results show that the positioning accuracy has more than 50% improvement for the horizontal components and over 30% improvement for the vertical component after adding GLONASS data, although the GLONASS constellation is incomplete.

- 9) With more visible GLONASS satellites and the improved GLONASS precise satellite orbit and clock products in the future, the combined GPS and GLONASS PPP will be expected to achieve better performance in terms of the converged positioning accuracy and convergence time of position filters.

10) System time difference is an important parameter for stand-alone positioning with a GPS/GLONASS receiver. It has to be taken into account in the combined GPS and GLONASS PPP due to the difference between GPS and GLONASS system times. To obtain a better understanding of this system time offset, the GPS-GLONASS system time difference was investigated using the data from various types of receivers. The investigation results show that the system time difference remains very stable within one day and its estimates are quite dependent on a specific receiver due to the existence of an inter-system bias caused by hardware delay.

7.2 Recommendations for Future Work

For further research in the future, the following recommendations can be made.

- 1) With the emergence of GPS real-time precise orbit and clock products from several organizations, real-time PPP using GPS-only observations has been developed. Similarly to GPS, the GLONASS real-time orbit and clock data will be expected to be available in the future. The combined GPS and GLONASS PPP should be further developed to support real-time applications.
- 2) Currently four organizations can provide GLONASS precise satellite orbit products and two data analysis centers can provide GLONASS precise satellite clock data. The accuracy of these products should be assessed and their impact on the combined GPS and GLONASS PPP should be analyzed.

- 3) With more and more available GLONASS satellites, the precise point positioning using only GLONASS observations may be implemented in the near future. Its performance should be assessed and analyzed with a comparison to the GPS-only PPP and the combined GPS/GLONASS PPP.
- 4) With the availability of Galileo signals in the future, the integration between GPS and Galileo, and the integration among GPS, GLONASS and Galileo will be possible to be applied for precise point positioning. The model and algorithm of the combined satellite systems for PPP applications may be studied in advance using the simulated data.
- 5) The performance of the combined GPS and GLONASS PPP needs to be further assessed when more visible GLONASS satellites can be observed and the quality of GLONASS precise satellite orbit and clock products is improved in the future.

Appendix A Processing Results of PPP at IGS Stations

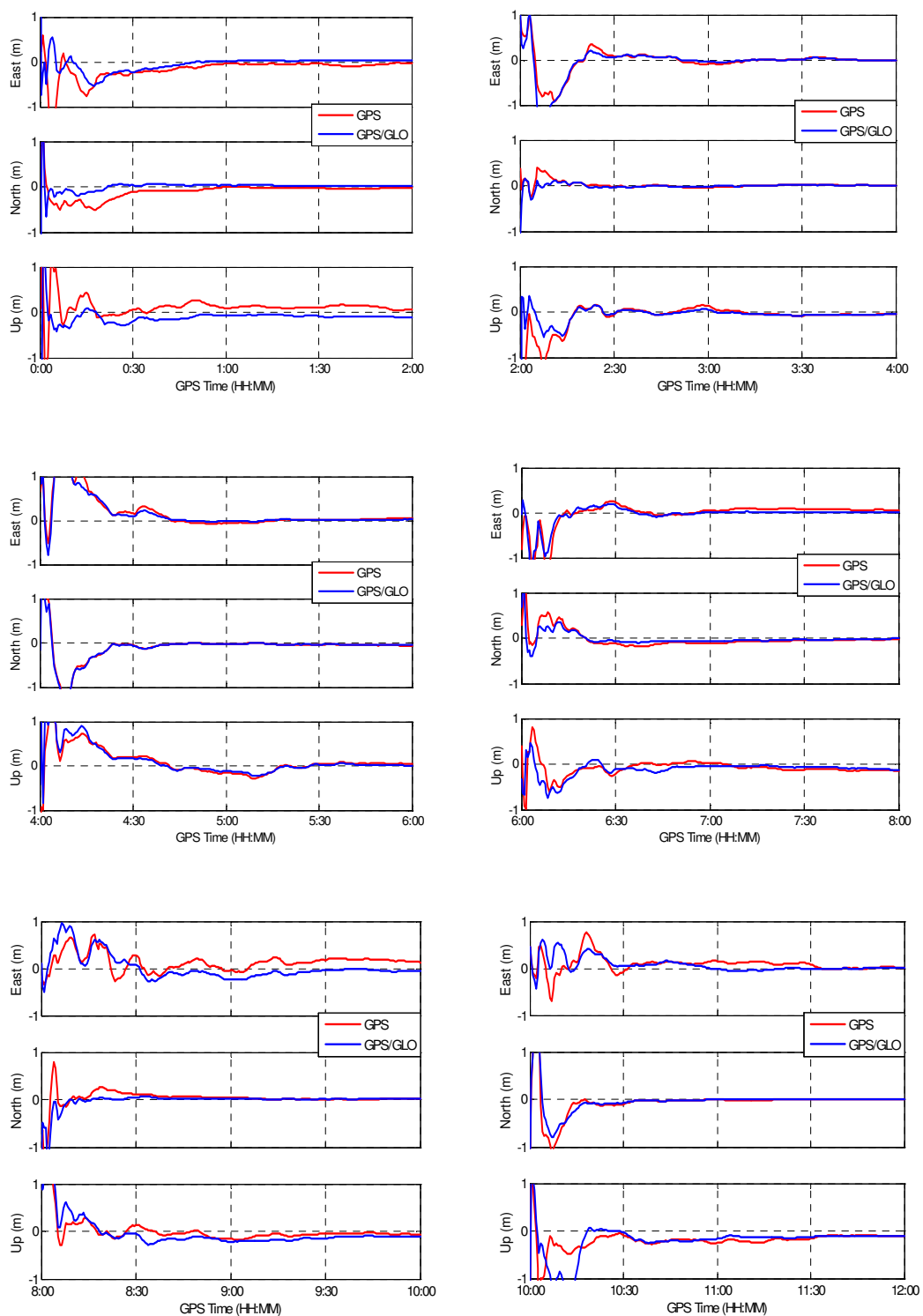


Figure A-1 Processing Results at ANKR

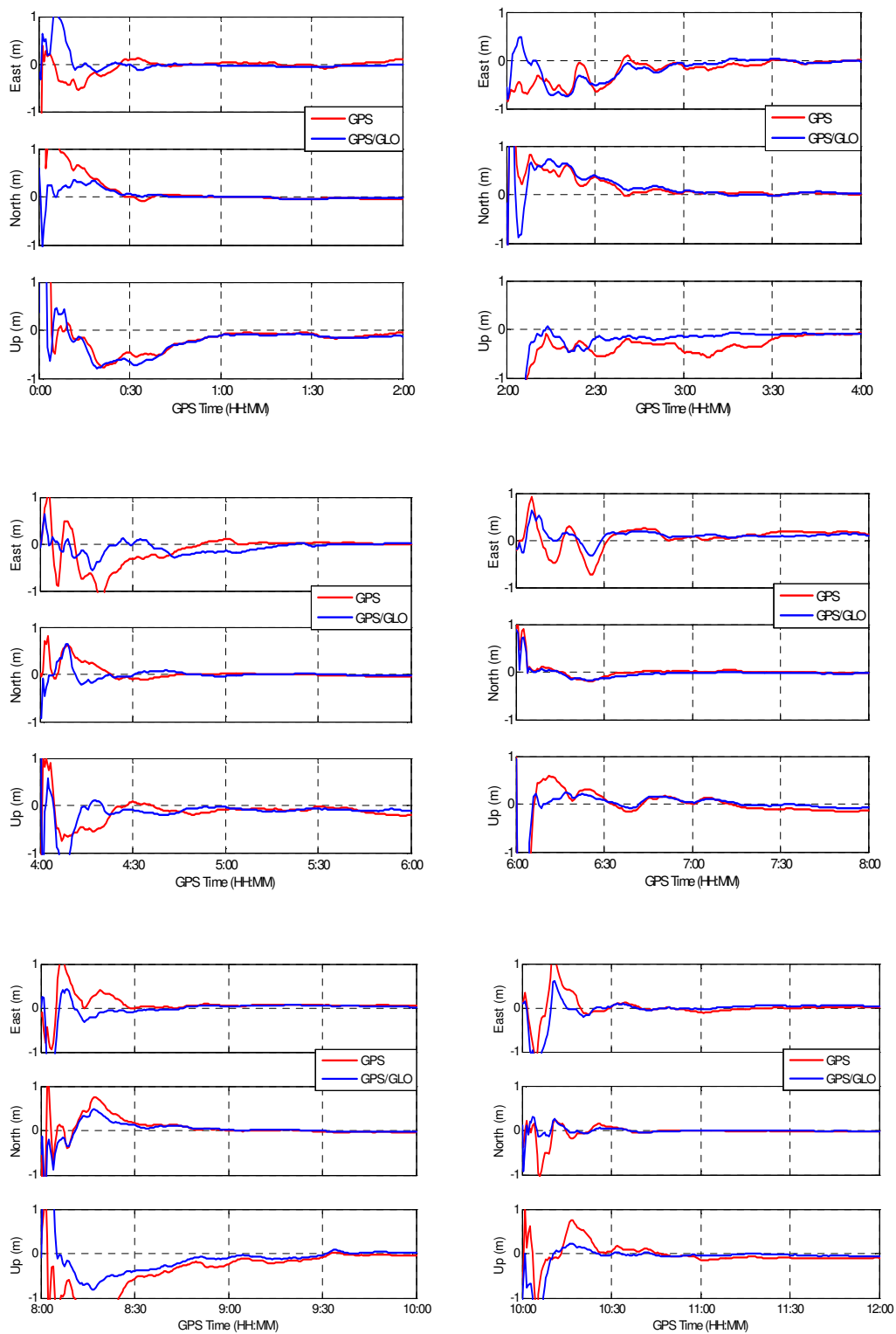


Figure A-2 Processing Results at LHAZ

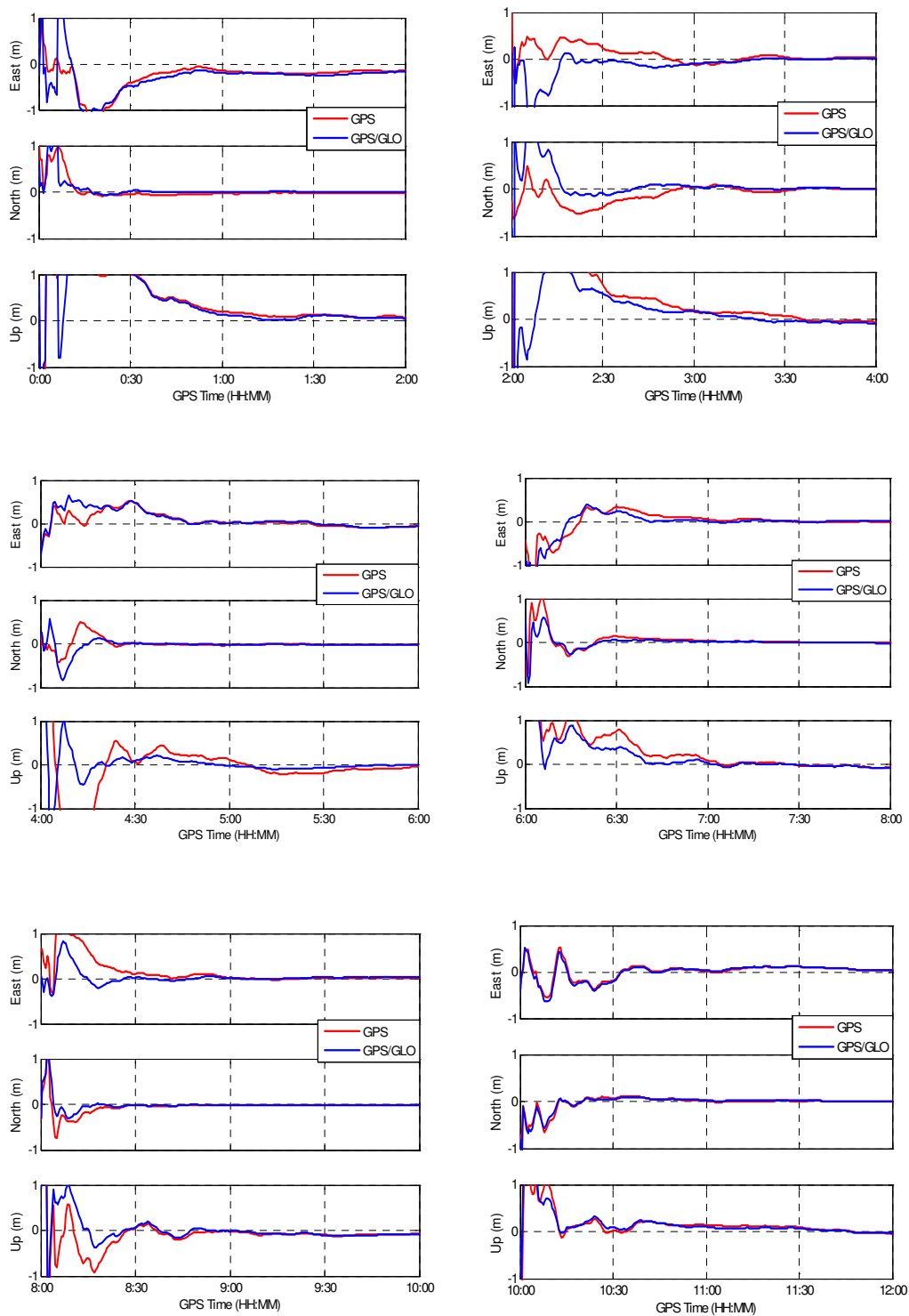


Figure A-3 Processing Results at NTUS

Appendix B Tropospheric Mapping Functions

The mapping functions can be used to transform or map the zenith tropospheric delay to the delay at an arbitrary elevation angle. Many mapping functions have been developed in the past forty years. Table B-1 is a list of some tropospheric mapping functions, which have been tested by Mendes and Langley to determine their effects at low elevation angles. The functions BL, BE, HM, ST, and YI are based on the Hopfield model and the functions CH, DA, HE, IF, MM, and NI are based on the Marini continued fraction form (Bisnath et al., 1997).

**Table B-1 Tropospheric Mapping Functions
(Mendes and Langley, 1994)**

Mapping Function	Year developed	ID
Baby et al.	1988	BB
Black	1978	BL
Black and Eisner	1984	BE
Chao	1972	CH
Davis et al.	1985	DA
Goad and Goodman	1974	GG
Herring	1992	HE
Moffett	1973	HM
Ifadis	1986	IF
Lanyi	1984	LA
Marini and Murray	1973	MM
Niell	1993, 1994	NI
Saastamoinen	1973	SA
Santerre	1987	ST
Yionoulis	1970	YI

Marini & Murray Mapping Function

The Marini & Murray mapping function maps total tropospheric delay, which is based on the Saastamoinen model (Marini and Murray, 1973):

$$m(E) = \frac{1 + \zeta}{\sin E + \frac{\zeta}{\sin E + 0.015}} \quad (\text{B.1})$$

where

$$\zeta = \frac{G}{T_k^Z}$$

$$G = \frac{0.002644}{g'} e^{-0.14372h_0}$$

$$T_k^Z = \frac{0.002277}{g'} \left[P_0 + \left(\frac{1255}{T} + 0.05 \right) e_0 \right]$$

$$g' = 1 - 0.0026 \cos 2\varphi - 0.00028 h_0$$

φ and h_0 are station latitude and orthometric height (km); P_0 is the pressure at the observed station in millibars; T is temperature at the tracking station; e_0 is the water vapor pressure. The Marini & Murray mapping function is considered to be valid when an elevation angle is greater than 10° .

Herring Mapping Function

The Herring Mapping Function was first applied in 1992. Its equation is given in the following (Herring, 1992):

$$m(E) = \frac{1 + \frac{a}{1 + \frac{b}{1 + c}}}{\sin E + \frac{a}{\sin E + \frac{b}{\sin E + c}}} \quad (\text{B.2})$$

where $a, b,$ and c may be estimated through the least-squares of $m(E)$ to ray traces of idealized temperature and humidity profiles. Their values are linearly dependent on the surface temperature, the cosine of the station latitude and the station height.

Chao Mapping Function

Chao (1974) proposed a tropospheric mapping function which was applied for radio tracking corrections of the Mariner Mars spacecraft. Wet and dry component mapping functions are obtained by empirical fitting to an average refractivity profile acquired from two-year radiosonde data. The mapping functions of the dry and wet components are given below:

$$m_h(E) = \frac{1}{\sin E + \frac{a_h}{\tan E + b_h}} \quad (\text{B.3})$$

$$m_w(E) = \frac{1}{\sin E + \frac{a_w}{\tan E + b_w}} \quad (\text{B.4})$$

where $a_h = 0.00143$, $b_h = 0.0445$, $a_w = 0.00035$,and $b_w = 0.0170$. Chao's dry mapping function has an accuracy of 1% down to 1° with respect to the ray trace of the annual average refractivity profiles while the wet mapping function was accurate enough for space geodetic measurements (Niell, 1996).

Davis Mapping Function

Davis et al (1985) modified the Chao's mapping function by adding a fraction of the sine term in order to improve the accuracy at low elevation angles. The Davis mapping function is written as:

$$m_h(\varepsilon) = \frac{1}{\sin \varepsilon + \frac{a}{\tan \varepsilon + \frac{b}{\sin \varepsilon + c}}} \quad (\text{B.5})$$

where

$$a = 0.001185 [1 + 6.071 \cdot 10^{-5} (P_0 - 1000) - 1.471 \cdot 10^{-4} e_0 + 3.072 \cdot 10^{-3} (T_0 - 20) + 0.01965 (\alpha + 6.5) - 0.005645 (H_t - 11.231)]$$

$$b = 0.001144 [1 + 1.164 \cdot 10^{-5} (P_0 - 1000) - 2.795 \cdot 10^{-4} e_0 + 3.109 \cdot 10^{-3} (T_0 - 20) + 0.03038 (\alpha + 6.5) - 0.001217 (H_t - 11.231)]$$

$$c = -0.0090$$

In the above equations, H_t is the height of the tropopause (km); α is the tropospheric temperature lapse rate value; P_0 is the pressure at the observed station in millibars; T_0 is temperature at the tracking station; e_0 is the water vapor pressure.

References

- Abdel-salam, M.A. (2005). Precise Point Positioning Using Un-Differenced Code and Carrier Phase Observations. Calgary: University of Calgary, PhD Thesis, 2005.
- Averin, S.V. (2006). GLONASS System: Present Day and Prospective Status and Performance. Report of European Navigation Conference GNSS-2006, Manchester, UK, May 7-10, 2006.
- Barnes, B.J., N. Ackroyd and P.A. Cross (1998). Stochastic Modeling for Very High Precision Real-time Kinematic GPS in an Engineering Environment. FIG XXI International Conference, Brighton, U.K., July 21-25, Commission 6, pp. 61-76.
- Bartenev, V.A., V.E. Kosenko and V.E. Chebotarev (2006). Russian GLONASS at the Stage of Active Implementation. InsideGNSS, April 2006, pp.40-43, Available at <http://www.insidegnss.com/node/884>, Last accessed on January 29, 2009.
- Beran, T., D. Kim and R.B. Langley (2003). High Precision Single-Frequency GPS Point Positioning. Proceedings of ION GPS 2003, Portland, Oregon, September 9-12.
- BIPM (1995). Annual Report of the BIPM Time Section. Technical Report, Vol. 8, BIPM, Pavillon de Breteuil.
- Bisnath, S. and Y. Gao (2008). Current State of Precise Point Positioning and Future Prospects and Limitations. International Association of Geodesy Symposia, Vol.133, No.4, 2008, pp.615-623.
- Bisnath, S.B., V.B. Mendes and R.B. Langley (1997). Effects of Tropospheric Mapping Functions on Space Geodetic Data, Presented at the 1997 IGS Analysis Center Workshop, Pasadena, CA, March 12-14, 1997.
- Bruyninx, C. (2007). Comparing GPS-only with GPS+GLONASS Positioning in a Regional Permanent GNSS Network. GPS Solution, 11:97-106, 2007.
- Cai, C. and Y. Gao (2008). Estimation of GPS/GLONASS System Time Difference with Application to PPP. ION GNSS 2008, September 16-19, 2008, Savannah, Georgia, USA.
- CDGPS (2009). Overview, Available at <http://www.cdgps.com/e/desc.htm>, Last accessed on February 6, 2009.
- Chamberlain, S.M. (1991). Combined GPS/GLONASS Navigation. Proceedings of Telesystems Conference, Vol.1, Atlanta, GA, USA, pp. 205-210.

- Chao, C. C . (1974). The Tropospheric Calibration Model for Mariner Mars 1971. JPL Technical Report, pp.61-76.
- Chen, K. (2004). Real-Time Precise Point Positioning and Its Potential Applications. Proceedings of ION GNSS-2004, Sep.21-24,2004,Long Beach, California, pp.1844-1854.
- Chen, K. and Y. Gao (2005). Real-Time Precise Point Positioning Using Single Frequency Data. Proceedings of ION GNSS-2005, September 2005, Long Beach,CA,pp.1514-1523.
- Chen, K. and Y. Gao (2008). Ionospheric Effect Mitigation for Real-Time Single-Frequency Precise Point Positioning. Journal of the Institute of Navigation, Vol.55, No.3, Fall 2008, pp.205-213.
- Czopek, F. and G. Mader (2002). Calibrating Antenna Phase Centers. GPS World, May 1, 2002, Available at <http://www.gpsworld.com/>, Last accessed on February 16, 2009.
- Davis, J. L., T. A. Herring, I. I.Shapiro, A. E. E. Rogers and G.Elgered (1985). Geodesy by Radio Interferometry: Effects of Atmospheric Modeling Errors on Estimates of Baseline Length. Radio Sci., 20(6), November-December, pp.1593-1607.
- Gakstatter, E. (2006). GPS Modernization-What's in It for the Surveyor? GPS World, May 30, 2006, Available at <http://www.gpsworld.com/>, Last accessed on July 12, 2009.
- Gao,Y. (2005). Advanced Estimation Methods and Analysis. University of Calgary, Lecture Notes, 2005.
- Gao, Y., K. Chen and X. Shen (2003). Real-Time Kinematic Positioning Based on Undifferenced Carrier Phase Data Processing. Proceedings of ION NTM-2003,Jan.22 - 24, 2003, Anaheim, California, pp.362-368.
- Gao, Y.and K. Chen (2004). Performance Analysis of Precise Point Positioning Using Real-Time Orbit and Clock Products. Journal of Global Positioning Systems,Vol.3,No 1-2,pp.95-100.
- Gao, Y. and X. Shen (2002). A New Method for Carrier Phase Based Precise Point Positioning. Journal of the Institute of Navigation, Vol. 49, No.2, 2002, pp.109-116.
- Gao, Y. and X. Shen (2001). Improving Ambiguity Convergence in Carrier Phase-Based Precise Point Positioning. Proceedings of ION GPS-2001, Salt Lake City, Utah, USA, September 11-14, 2001.

- Gao, Y., Y. Zhang and K. Chen (2006). Development of a Real-Time Single-Frequency Precise Point Positioning System and Test Results. Proceedings of ION GNSS-2006, September 26-27, 2006, Fort Worth, TX, pp.2297-2303.
- Gibbons, G. (2006). GLONASS: The Once and Future GNSS. InsideGNSS, January-February 2006, pp.28-30, Available at <http://www.insidegnss.com/node/503>, Last accessed on January 29, 2009.
- Gibbons, G. (2008). Russia Approves CDMA Signals for GLONASS, Discussing Common Signal Design. InsideGNSS, April 28,2008, Available at <http://www.insidegnss.com/node/648>, Last accessed on January 29, 2009.
- Gibbons, G. (2008). GLONASS–A New Look for the 21st Century. InsideGNSS, May/June 2008, Available at <http://www.insidegnss.com/node/694>, Last accessed on January 29, 2009.
- GLONASS ICD (2002). Global Navigation Satellite System GLONASS Interface Control Document, Version 5.0, Moscow, 2002.
- GPS ICD (2000). Interface Control Document – Navstar GPS Space Segment / Navigation User Interfaces, ICD-GPS-200C, 2000.
- Habrich, H. (1999). Geodetic Applications of the Global Navigation Satellite System (GLONASS) and GLONASS/GPS Combinations. PhD Thesis, University of Berne.
- Habrich, H., P. Neumaier and K. Fisch (2004). GLONASS Data Analysis for IGS. Proceedings of IGS Workshop and Symposium, University of Berne, 2004.
- Han, S. (1997). Quality Control Issues Relating to Instantaneous Ambiguity Resolution for Real-time GPS Kinematic Positioning. Journal of Geodesy, 71, pp. 351-361.
- Heflin, M.B. (2000). Near Real Time Products from JPL, [IGSMail-3082].
- Herring, T. A. (1992). Modeling Atmospheric Delays in the Analysis of Space Geodetic Data. Proc. the Symposium: Refraction of the Transatmospheric Signals in Geodesy, the Hague, the Netherlands.
- Hesselbarth, A. and L. Wanninger (2008). Short-term Stability of GNSS Satellite Clocks and its Effects on Precise Point Positioning. Proceedings of ION GNSS 2008,September 16-19,2008,Savannah,GA,USA, pp.1855-1863.
- Hofmann-Wellenhof, B., H. Lichtenegger and J. Collins (2001). GPS Theory and Practice Fifth Revised Edition, Springer-Verlag Wien New York, ISBN 3-211-83534-2.

- IAC (2009). GLONASS Constellation Status. Information-Analytical Centre, Available at <http://www.glonass-ianc.rsa.ru.>, Last accessed on January 29, 2009.
- IERS (1989). IERS Standards, IERS Technical Note 3, (ed. D.D. McCarthy), 1989.
- IERS (1996). IERS Conventions, IERS Technical Note 21, (ed. D.D. McCarthy), 1996.
- IGS (2008). IGS Products. Available at <http://www.igs.org/components/prods.html>, Last accessed on February 4, 2009.
- IGS (2009a). IGS Organization Information. Available at <http://www.igs.org/organization/figure1.html>, Last accessed on February 6, 2009.
- IGS (2009b). Tracking Network. Available at <http://www.igs.org/network/iglos.html>, Last accessed on February 6, 2009.
- IGS (2009). Satellite Antenna Corrections, Available at <ftp://igscb.jpl.nasa.gov/pub/station/general/igs05.atx>, Last accessed on February 14, 2009.
- Inside GNSS (2008a). Putin Backs \$2.62-Billion Addition to GLONASS Budget, Available at <http://www.insidegnss.com/node/790>, Last accessed on January 23, 2009.
- Inside GNSS (2008b). Russia Approves CDMA Signals for GLONASS, Discussing Common Signal Design, Available at <http://www.insidegnss.com/node/648>, Last accessed on January 23, 2009.
- Kang, J., Y. Lee, J. Park and E. Lee (2002). Application of GPS/GLONASS Combination to the Revision of Digital Map. Proceedings of FIG XXII International Congress, Washington, D.C. USA, April 19-26, 2002.
- Kaplan, E.D. and C.J. Hegarty (2006). Understanding GPS: Principles and Applications. 2nd Edition. Artech House.
- Klobuchar, J.A. (1996). Ionospheric Effects on GPS. In Parkinson & Spilker, Jr. (Eds.), Global Positioning Systems: Theory and Applications. Progress in Astronautics and Aeronautics, Volume 163, American Institute of Aeronautics and Astronautics, Inc.
- Kouba, J. and P. Héroux (2001). GPS Precise Point Positioning Using IGS Orbit Products. GPS Solutions, Vol.5, No.2, pp.12-28.
- Le, A.Q. and C. Tiberius (2007). Single-frequency Precise Point Positioning with Optimal Filtering. GPS Solut (2007) 11:61-69.
- Leick, A. (2004). GPS Satellite Surveying. 3rd Edition. Wiley, 2004, ISBN: 0471059307.

- Lewandowski, W., J. Danaher and W.J. Klepczynski (1996). Experiment Using GPS/GLONASS Common View Time Transfer Between Europe and North America. In Proceedings of ION Satellite Division GPS-96 International Technical Meeting, pp. 271–277, Kansas City, Missouri, Institute of Navigation.
- Liao, X. (2000). Carrier Phase Based Ionosphere Recovery Over A Regional Area GPS Network. MSc Thesis, Calgary: University of Calgary, 2000.
- Marini, J.W. and C.W. Murray (1973). Correction of Satellite Tracking Data for Atmospheric Refraction at Elevations above 10 Degrees. NASA Report X-591-73-351, Goddard Space Flight Center.
- Maybeck, P.S. (1979). Stochastic Models, Estimation, and Control, Vol.1, Copyright 1979 by Academic Press.
- Mekik, C. (1997). Tropospheric Delay Models in GPS. Presented at the International Symp. on GIS/GPS, Istanbul/Turkey, September 15-18, 1997, pp. 156-170.
- Mendes, V.B. and R.B. Langley (1994). A Comprehensive Analysis of Mapping Functions Used in Modeling Tropospheric Propagation Delay in Space Geodetic Data, Proceedings of KIS94, International Symposium on Kinematic Systems in Geodesy, Geomatics and Navigation, Banff, Alberta, Canada, August 30- September 2, 1994, pp. 87-98.
- Mikhail, E.M. and F. Ackermann (1976). Observation and Least Square, IEP-A Dun-Donnelley Publisher, New York.
- Misra, P.N., R. I. Abbot and E.M. Gaposchkin (1996). Transformation Between WGS-84 and PZ-90, Proceedings of the 9th International Technical Meeting of the Satellite Division of the Institute of Navigation, ION GPS-96, Kansas City, Missouri.
- Misra, P. and P. Enge (2001). Global Positioning System: Signals, Measurements and Performance, Ganga-Jumuna Press.
- Moudrak, A., A. Konovaltsev, J. Furthner, J. Hammesfahr, A. Bauch, P. Defraigne, S. Bedrich and A. Schroth (2005). Interoperability on Time GPS-Galileo Offset Will Bias Position. GPS World, March, pp. 24-32, 2005, Available at <http://www.gpsworld.com>, Last accessed on April 27, 2009.
- Muellerschoen, R.J., W.I. Bertiger and M.F. Lough (2000). Results of an Internet-Based Dual-Frequency Global Differential GPS System. Proceedings of IAIN World Congress, San Diego, CA, June 2000.
- Niell, A.E. (1996). Global Mapping Functions for the Atmosphere Delay at Radio Wavelengths. Journal of Geophysical Research, Vol. 101, pp 3227-3246, Feb. 10, 1996.

- Oleynik, E.G., V.V. Mitrikas, S.G. Revniviykh, A.I. Serdukov, E.N. Dutov and V.F. Shiriaev (2006). High-Accurate GLONASS Orbit and Clock Determination for the Assessment of System Performance. Proceedings of ION GNSS 2006, Fort Worth, TX, September 26-29, 2006.
- Parkinson, B.W. and N. Ashby (1996). Introduction to Relativistic Effects on the Global Positioning System, in Global Positioning System: Theory and Applications Volume I, Volume 163, Progress in Astronautics and Aeronautics, The American Institute of Aeronautics and Astronautics, Washington, 1996, pp.679-682.
- Petrov, L. and J.P. Boy (2004). Study of the Atmospheric Pressure Loading Signal in VLBI Observations. Journal of Geophysical Research, Vol. 109, No. B03405, 2004.
- PMIS (2005). P³ User Manual, Version 1.0, Department of Geomatics Engineering at the University of Calgary.
- Rabbel, W. and H. Schuh (1986). The Influence of Atmospheric Loading on VLBI-experiments. J. Geophys., 59, pp.164-170, 1986.
- Rizos, C. (1999). Satellite Ephemeris Bias. Principles and Practice of GPS Surveying. The University of New South Wales, Sydney, Australia.
- Romero, I., J.M. Dow, R. Zandbergen, J. Feltens, C. Garcia, H. Boomkamp and J. Perez (2004). The ESA/ESOC IGS Analysis Center Report 2002, IGS 2001-2002 Technical Report, 53-58, IGS Central Bureau, JPL-Publication, 2004.
- Rosbach U., H. Habrich and N. Zarraoa (1996). Transformation Parameters between PZ-90 and WGS-84. Proceedings of the 9th International Technical Meeting of the Satellite Division of the Institute of Navigation, ION GPS-96, Kansas City, Missouri.
- Roßbach, U. (2000). Positioning and Navigation Using the Russian Satellite System GLONASS. PhD Thesis, University of the Federal Armed Forces Munich, Germany (Universität der Bundeswehr München), June, 2000.
- Rothacher, M. and G. Beutler (2002). Advanced Aspects of Satellite Positioning, Lecture Notes for ENGO 609.90, The University of Calgary, AB, Canada.
- Royal Observatory of Belgium (2004). Present Status and Modernization Plans, Available at http://www.gps.oma.be/gb/modern_gb_ok_css.htm, Last accessed on January 26, 2009.
- Satirapod, C. (2004). A Review of Stochastic Models Used in Static GPS Positioning Technique. Proceedings of ACRS 2004. Available at http://www.gisdevelopment.net/aars/acrs/2004/gps_ns/acrs2004_f001.shtml, Last accessed on January 26, 2009.

- Schaer, S., W. Gurtner and J. Feltens (1998). IONEX: The Ionosphere Map Exchange Format Version 1, February 25, 1998. Proceedings of the 1998 IGS Analysis Centers Workshop, ESOC, Darmstadt, Germany, February 9-11, 1998.
- Schaer, S.T., U. Hugentobler, R. Dach, M. Meindl, H. Bock, C. Urschl and G. Beutler (2004). GNSS Analysis at CODE. Proceedings of IGS Workshop and Symposium, University of Berne.
- Seeber, G. (1993). Satellite Geodesy: Foundations, Methods & Applications. Walter de Gruyter, Berlin New York.
- Shen, X. (2002). Improving Ambiguity Convergence in Carrier Phase-based Precise Point Positioning. MSc Thesis, Calgary: University of Calgary, 2002.
- Shrestha, S.M. (2003). Investigations into the Estimation of Tropospheric Delay and Wet Refractivity Using GPS Measurements. MSc Thesis, Calgary: University of Calgary, 2003.
- Space-based PNT (2009). The Global Positioning System, Available at <http://pnt.gov/public/images/>, Last accessed on January 26, 2009.
- Stansell, T. (2006). GPS Civil Signal Modernization, Report of Rocky Mountain Section of the ION, February 16, 2006. Available at <http://www.rms-ion.org/Presentations/GPS%20Signal%20Modernization.pdf>, Last accessed on January 26, 2009.
- Tao, W. (2008). Near Real-time GPS PPP-inferred Water Vapor System Development and Evaluation. MSc Thesis, University of Calgary, Calgary, Canada.
- Tripod (2007). Introduction to the Russian Global Navigation Satellite System GLONASS, Available at <http://members.tripod.com/ibank/lecture/GPS90.HTM>, Last accessed on January 26, 2009.
- Tsujii, T., M. Harigae, T. Inagaki and T. Kanai (2000). Flight Tests of GPS/GLONASS Precise Positioning versus Dual Frequency KGPS Profile. Earth Planets Space, Vol.52, No.10, pp.825-829.
- UNAVCO (2009). Science & Technology-GNSS Modernization, Available at http://facility.unavco.org/science_tech/gnss_modernization.html, Last accessed on January 26, 2009.
- USNO (2008). GPS System Description, Available at <ftp://tycho.usno.navy.mil/pub/gps/gpssy.txt>, Last accessed on January 26, 2009.

- Wang, J. (1999). Modelling and Quality Control for Precise GPS and GLONASS Satellite Positioning. PhD Thesis, School of Spatial Sciences, Curtin University of Technology, Perth, Australia.
- Weber, R. and E. Fragner (2002). The Quality of Precise GLONASS Ephemerides. *Adv. Space Res.*, 30(2), 271-279, 2002.
- Weber, R., J.A. Slater, E. Fragner, V. Glotov, H. Habrich, I. Romero and S. Schaer (2005). Precise GLONASS Orbit Determination within the IGS/IGLOS Pilot Project. *Advances in Space Research*, 36: 369-375.
- Weill, L. R. (2003). Multipath Mitigation. *GPS World*, June 1, 2003, Available at <http://www.gpsworld.com/>, Last accessed on February 13, 2009.
- Welch, G. and G. Bishop (2001). An Introduction to the Kalman Filter, Copyright 2001 by ACM, Inc. Available at <http://info.acm.org/pubs/toc/CRnotice.html>, Last accessed on February 13, 2009.
- Welch, G. and G. Bishop (2006). An Introduction to the Kalman Filter, July 24, 2006. Available at http://www.cs.unc.edu/%7Ewelch/media/pdf/kalman_intro.pdf, Last accessed on April 8, 2009.
- Witchayangkoon, B. (2000). Elements of GPS Precise Point Positioning. PhD Thesis, University of Maine, 2000.
- Wu, J. T., S. C. Wu, G. A. Hajj, W. I. Bertiger and S. M. Lichten (1993). Effects of Antenna Orientation on GPS Carrier Phase, *Manuscripta Geodaetica*, Vol. 18, No. 2, 1993, pp. 91-98.
- Yang, Y., R. R. Hatch and R.T. Sharpe (2004). GPS Multipath Mitigation in Measurement Domain and its Applications for High Accuracy Navigation. *Proceedings of ION GNSS 2004*, Long Beach, California, 2004.
- Zheng, Y. (2009). Introduction to Satellite Navigation and Positioning Systems, Available at <http://www.ee.tsinghua.edu.cn/~zhengyouquan/positioning.htm>, Last accessed on January 26, 2009.
- Zinoviev, A.E. (2005). Using GLONASS in Combined GNSS Receivers: Current Status. *ION GNSS 2005*, Long Beach, CA, September 13-16, 2005, pp.1046-1057.
- Zumberge J.F., M.B. Heflin and D.C. Jefferson (1997). Precise Point Positioning for the Efficient and Robust Analysis of GPS Data from Large Networks. *Journal of Geophysical Research*, 1997, 102 (B3): pp.5005-5017.